ΕΘΝΙΚΟ ΜΕΤΣΟΒΙΟ ΠΟΛΥΤΕΧΝΕΙΟ
ΣΧΟΛΗ ΕΦΑΡΜΟΣΜΕΝΩΝ ΜΑΘΗΜΑΤΙΚΩΝ
ΚΑΙ ΦΥΣΙΚΩΝ ΕΠΙΣΤΗΜΩΝ
ΤΟΜΕΑΣ ΦΥΣΙΚΗΣ

Φωτοβολταϊκή Τεχνολογία Οργανικών Ημιαγωγών:

Μελέτη Καινοτόμων Οργανικών Ηλιακών Κυψελών Φθαλοκυανίνης Μολύβδου (PbPc) σε υποστρώματα GaAs με επιφανειακές αναδομήσεις β2(2x4) και c(4x4)

ΔΙΠΛΩΜΑΤΙΚΗ ΕΡΓΑΣΙΑ

Κωνσταντίνα Θ. Ρούσση

Επιβλέπουσα: Επικ. Καθηγήτρια ΕΜΠ. Δρ. Δήμητρα Παπαδημητρίου

Συνεπιβλέποντες:
Καθηγ. Δρ. W. Richter (εκλιπών 2013), Technische Universität Berlin & Università degli Studi di Roma "Tor Vergata"
Καθηγ. Δρ. M. De Crescenzi, Università degli Studi di Roma "Tor Vergata"

Εξεταστική Επιτροπή:
Επικ. Καθηγ. Δρ. Δ. Παπαδημητρίου (Επιβλέπουσα)
Αναπλ. Καθηγ. Κ. Παρασκευαΐδης
Επικ. Καθηγ. ΣΜΜΜ Η. Χατζηθεοδωρίδης

ΕΜΠ, ακαδημαϊκό έτος 2013-14

NATIONAL **T**ECHNICAL **U**NIVERSITY OF **A**THENS

FACULTY OF APPLIED MATHEMATIC AND PHYSICAL SCIENCES

DEPARTMENT OF PHYSICS

Organic Semiconductor Photovoltaic Technology:

Study of Innovative Organic Solar Cells of Lead-Phthalocyanine (PbPc) grown on surface reconstructed GaAs β2(2x4) and c(4x4) substrates

DIPLOMA-THESIS

Konstantina Roussi

Supervisor: **Assistant Professor Dr. Dimitra Papadimitriou, National Technical University of Athens**

Co- supervisor: Professor Dr. Wolfgang Richter (deceased 2013), Technische Universität Berlin &
Università degli Studi di Roma "Tor Vergata"
Professor Dr. Maurizio De Crescenzi
Università degli Studi di Roma "Tor Vergata"

Academic year 2013-14

Ευχαριστίες

Η διπλωματική μου εργασία αποτελεί την ολοκλήρωση των σπουδών μου στο Εθνικό Μετσόβιο Πολυτεχνείο της Σχολής Εφαρμοσμένων Μαθηματικών και Φυσικών Επιστημών. Πάνω από όλα ευχαριστώ τους γονείς μου Μαρία Μπακάλου-Ρούσση, φιλόλογο, και Θεόδωρο Ρούσση, ιατρό, για την υποστήριξη, τη βοήθεια, την κατανόηση και την περίσσεια αγάπη τους κατά τη διάρκεια των σπουδών μου.

Ιδιαίτερα, θα ήθελα να ευχαριστήσω την Καθηγήτρια Δήμητρα Παπαδημητρίου, Επιβλέπουσα της διπλωματικής μου εργασίας, που μου έδωσε την επιστημονική, αλλά και την οικονομική υποστήριξη με υποτροφία του προγράμματος Erasmus, ώστε να ταξιδέψω και να δουλέψω τη διπλωματική μου εργασία στο Πανεπιστήμιο Tor Vergata, στη Ρώμη. Η μελέτη και ο χαρακτηρισμός Φωτοβολταϊκών Στοιχείων (Ηλιακών Κυψελών Φθαλοκυανίνης Μολύβδου) πραγματοποιήθηκαν στο εργαστήριο του ομότιμου καθηγητή του Πολυτεχνείου του Βερολίνου Wolfgang Richter με συνεργαζόμενο καθηγητή τον Maurizio De Crescenzi και ερευνητές τους Δρ. Linda Riele και Δρ. Luca Camilli. Με τη βοήθεια και την καθοδήγηση των καθηγητών Δ. Παπαδημητρίου, W. Richter, και M. De Crescenzi στάθηκε δυνατή η εκπαίδευση μου σε ενδιαφέροντες επιστημονικούς τομείς και η ολοκλήρωση της διπλωματικής μου εργασίας στην Τεχνολογία Οργανικών Φωτοβολταϊκών. Οι καθηγητές και οι συνεργάτες τους με βοήθησαν τόσο στην κατανόηση της λειτουργίας και το χαρακτηρισμό των ηλιακών κυψελών ως προς την απόδοσή τους, όσο και στη συγγραφή της εργασίας μου.

Επίσης, θα ήθελα να ευχαριστήσω τους διδάσκοντες της Σχολής ΕΜΦΕ του ΕΜΠ που προσφέρουν άριστο επίπεδο μόρφωσης.

Ακόμα, θέλω να ευχαριστήσω τους φίλους και τις φίλες συναδέλφους και μη, που μου κάνανε όμορφα τα φοιτητικά μου χρόνια. Το συνεχές ενδιαφέρον συγγενών και φίλων από τον ευρύτερο κοινωνικό κύκλο αποτελούσε πάντα κίνητρο για τη συνέχιση των προσπαθειών μου και τους ευχαριστώ θερμά.

Η ολοκλήρωση αυτή των σπουδών μου αποτελεί εφόδιο ζωής, τόσο από τις γνώσεις που απέκτησα όσο και από την επιστημονική μέθοδο που διδάχτηκα. Η συνεχής αναζήτηση της γνώσης και της δημιουργικότητας σε επιστημονικά θέματα, καθώς και η συνεργασιμότητα με τους σπουδαίους ανθρώπους – φίλους που απέκτησα στον Πολυτεχνειακό και τον ευρύτερο επιστημονικό χώρο αποτελούν μόνιμο στόχο μου. Το επιστέγασμα των προσπαθειών μου είναι η απόκτηση του Διπλώματός μου ως Φυσικού Εφαρμογών ΕΜΠ. Αποτελεί τιμή αλλά και υποχρέωση μου προς την Πολυτεχνειακή κοινότητα και την κοινωνία να σταθώ σαν ολοκληρωμένος άνθρωπος και επιστήμονας προς όφελος της κοινωνίας.

Ringraziamenti

La mia tesi di Diploma è il completamento dei miei studi presso l' Università Tecnica Nazionale di Atene, al Dipartimento di Matematica Applicata e Scienze Naturali. Soprattutto, ringrazio i miei genitori Maria Bakalou Roussi , insegnante della lingua Greca, e Theodore Roussi, dottore per loro sostegno, l'assistenza, la comprensione e l'amore in eccesso durante i miei studi .

In particolare, vorrei ringraziare la Professoressa Dimitra Papadimitriou, Supervisora della mia tesi, per l'opportunità scientifico e finanziario aiuto di studio con il programma Erasmus di viaggiare e lavorare la mia tesi all'univercita Tor Vergata, a Roma. Lo studio e la caratterizzazione di celle fotovoltaiche eseguite nel Laboratorio di Professore Emerito di valutazione internazionale Wolfgang Richter cooperando con il professor Maurizio De Crescenzi e ricercatori Drs. Linda Riele e Dr. Luca Camilli. Con l'aiuto e la guida degli professori D. Papadimitriou, W. Richter e M. De Crescenzi era possibile la mia formazione in settori scientifici interessanti e il completamento della mia tesi in Tecnologia fotovoltaico organico. Gli professori e collaboratori mi hanno aiutato a capire il funzionamento delle celle solari e la caratterizzazione della loro efficienza e anche di scrivere la mia tesi durante i miei studi lì.

Ancora vorrei ringraziare i professori della facoltà Applicata Scienze Matematiche e Fisiche di NTUA Scuola che offre un eccellente livello di istruzione.

Anch' io voglio ringraziare i miei amici e colleghi chi sono soprattutto persone eccezionali e che hanno fatto piacevolmente i miei anni di studio. Il continuo interesse di parenti ed amici è sempre stata una motivazione per il proseguimento dei miei sforzi e li ringrazio calorosamente.

Questa integrazione dei miei studi è un buon ed importante asset della vita sia della conoscenza acquisita e il metodo scientifico insegnato. La costante ricerca della conoscenza e la creatività in questioni scientifiche e cooperatività con grandi persone - amici che ho guadagnato in NTUA e scientifico più ampio sono permanenti mio obiettivo. Il culmine dei miei sforzi è un diploma e un onore e il mio dovere verso la comunità NTUA e la società a presentarsi come un uomo compiuto e scienziato per il bene della società .

Acknowledgements

My diploma thesis is the completion of my studies at the National Technical University of Athens, at the Department of Applied Mathematics and Natural Sciences. Above all, I thank my mother Maria Bakalou Roussi, philologist, and my father Theodore Roussis, medical scientist, for their support, assistance, understanding, and their love during my studies .

I am grateful to Professor Dimitra Papadimitriou, Supervisor of my Diploma-thesis, for her valuable scientific support and for giving me the opportunity to travel and elaborate my diploma thesis at the Tor-Vergata University, in Rome, with a scholarship from the Erasmus Programme. The studies within the present Diploma-thesis, in particular, the structural and electrical characterization of photovoltaic cells (Lead-Phthalocyanine organic solar cells) were performed at the Laboratory of worldwide respected Professor Emeritus of the Technical University of Berlin Wolfgang Richter in close cooperation with Professor Maurizio De Crescenzi and the scientific research assistants Dr. Linda Riele and Dr. Luca Camilli. With the help and guidance of the thesis Supervisor, Prof. D. Papadimitriou, and the Co-Supervisors, Prof. W. Richter and Prof. M. De Crescenzi, it has been possible to attain knowledge in interesting scientific fields and elaborate my thesis in Organic Photovoltaic Technology. Professors and associates helped me to understand the operation of solar cells in terms of their performance and evaluate their efficiency, and also to write a scientific text.

Furthermore, I would like to thank the members of the faculty of NTUA School of Applied Mathematics and Physics that offers excellent level of education and knowledge.

In addition, I would like to thank my friends and colleagues, who are exceptional people and they accompanied me during my years of study. The continued interest of relatives and friends has always been a motivation for the continuation of my efforts and I thank them warmly.

The achievement of my studies is an asset for life through the knowledge gained and the scientific method taught. The constant pursuit of knowledge in scientific issues and creativity, and the cooperation with great people - friends I met at NTUA are my goals. The culmination of my efforts in a diploma degree is an honour and a duty to the NTUA community and society and stands for the benefit of the society.

Contents

A. Introduction- Motivation

In this work, organic solar cells based on lead phthalocyanine (PbPc) grown on two different surface reconstructed Gallium Arsenide substrates GaAs(001), As-rich c(4x4) and stoichiometric β2(2x4), were structurally and electrically characterized. The PbPc-GaAs(001) c(4x4) and PbPc-GaAs(001) β2(2x4) bilayers were grown by Dr. P. Vogt (Workgroup Prof. Dr. M. Kneissl) at the Technical University of Berlin.

PbPc is an organic molecule with very good optoelectronic properties promising to be used in organic thin film solar cells or combination of organic and inorganic thin film solar cells [1]-[4]. Different substrates are exploited, because changes in the behavior of phthalocyanines and different molecule qualities have been reported in dependence of the substrate surface-structure [5]-[7]. In particular, PbPc belongs to the category of metal phthalocyanines that change their molecular ranking when they are deposited on different substrates by taking the orientation of the substrate surface-reconstruction, which means that they change their absorption properties. The experimental research and the results we gain can show us, which sample is efficient in absorbing solar radiation and can thus be used as solar energy converter. Understanding the material properties is important for potential applications and improvements in view of their use as molecular solar cells and their use as thin film interlayer to improve the electronic properties of optoelectronic devices. It is also important to study the interaction between the molecules and the substrate as this interaction can be strong, leading to the formation of chemical bonds between them. This interaction can also alter the chemical bonds of the molecules and, therefore, their structure. For this reason, the growth (usually epitaxial) of organic molecules on inorganic substrates is an actual and intensive research topic.

The electrical conductivity of lead phthalocyanine (PbPc), studied in this work, and that of metal phthalocyanines, in general, depends on the orientation of the molecules. Many parameters[1] are important to consider for the orientation and the arrangement of the organic molecules in a layer, but the research is focused on the interaction of the organic layer with the substrate and the arrangements of the organic molecules in the first monolayer of the interface of the organic layer-substrate (inorganic–bio mainly).

RAMAN Spectroscopy has been applied for the structural characterization of PbPc on GaAs substates within this diploma-thesis. Since PbPc was deposited on GaAs substates

[1] Important parameters for the control of the ordering of the molecules are the substrate temperature, evaporation rate and post evaporation annealing.

from the vapor phase, the Raman spectrum of PbPc in-vapor-phase has been studied. In these experiments, the organic molecules are formed following the crystalline ordering of the substrates they lay on. Raman scattering is a non-invasive experimental method[2] that detects the vibration of a molecule and identifies its characteristic spectral pattern (fingerprint). Samples can be examined in the solid-, liquid- or vapor-phase, in hot or cold states, in the bulk, as microscopic particles, and as surface layers.
The sample used for the Raman study was powder of lead phthalocyanine in glass container that was heated to produce PbPc free molecules in vapor phase. The study of PbPc in vapor phase was important as PbPc in the electrically characterized solar cells was deposited after being vaporized. The information of structural characterization of PbPc in vapor phase that is given by its Raman spectrum is considerable, since it provides us with information before the electrical characterization of the solar cells (PbPc on GaAs substrates). The spectral pattern of PbPc in vapor phase was initially recorded and the vibration modes of PbPc free molecules were extensively analyzed and presented within the frame of the doctoral thesis of L. Riele [6]. Assignment of the vibrational modes of PbPc powder was then at that time already known, since it has been reported by Dr. V. Stamelou in her doctoral thesis [7]. Apart from the experimental work referred, there are theoretical calculations of density functional theory (DFT) on the mode vibrations of PbPc molecules published by Yuexing Zhang and Xianxi Zhang [8] and by I.M. Kupchak in Ref. [6] which seem to be in agreement, when referring to mode vibrations and mode frequencies.

In the present diploma thesis, the Raman spectrum of PbPc in-vapor phase has been re-evaluated. Mode vibrations have been re-assigned by taking into account theoretical and experimental results known from the Literature. This new interpretation is in accordance with the results of DFT calculations reported in Ref. [8] and the Raman analysis of PbPc powder in Refs. [6]-[7]. For PbPc in-vapor, however, a mode-shift has been added in the evaluation of Raman-spectra by L. Riele [6] to account for additional motion (degrees of freedom) of vaporized molecules. On the contrary, the present evaluation is based on the fact that the molecule vibrations are drastically constrained by the presence of the heavy metal atom. Bearing in mind that the protruding lead cation (Pb^{2+}) is responsible for the spatial distribution and the asymmetry of the molecule, it is assumed that it is also, to a great extend, responsible for the molecule vibrations and that mode-frequencies are not significantly altered in both, the solid (PbPc powder) and the vapor phase (PbPc in vapor).
In the following, the I-V characteristics of PbPc-GaAs(001) c(4x4) and PbPc-GaAs(001) β2(2x4) solar cells and the Raman-spectrum of PbPc in-vapor-phase, as “start” material for the solar absorber, will be presented and discussed inclusive the basic principles of operation of photovoltaic cells and the principles of Raman scattering as the main material characterization technique. In addition, the instrumentation of the laboratory will be presented in the Experimental part so far it has been used in the referred experimental measurements.

[2] Raman scattering may lead to sample degradation and fluoresce although the recent advances in the instrumentation have limited these defects.

B. Photovoltaic technology and Physical principles

1.1 Photovoltaic Technology

Photovoltaic technology is the technology that generates electrical power from semiconductors when they are illuminated by light. Electricity is important to humanity (unfortunately not yet acquired by the third world) as it provides us with services such as electric light, radio, television, telecommunications, health services, clean water, cooling and heating, electromechanical energy etc.

Photovoltaic technology is of great importance as it uses solar energy for the production of electricity and/or heat (electrical plants and/or electrical thermal plants). The rising of photovoltaic technology coincides with the 70s when the oil fuel crisis started[3]. The demand for alternative sources of energy grew continuously and the research in this field increased enormously. Another factor that has driven humanity towards the study of environmentally friendly forms of energy is the severe pollution of the environment during this century such as global warming. The concern for global warming was declared by 191 countries, all members of the European Union, in the Kyoto protocol[4] (December 1997, Japan). Greece was among those countries. The universal interest has turned then to environmentally friendly forms of energy.

Even today, in the 21st century, one third of humanity does not have access to electricity and hence to a large number of electricity-based services and commodities. Millions of people die every year from drinking polluted water, while others suffer from the lack of basic medical services. Illiteracy denies millions of people any possibility of gaining access to ideas for a better living. Electricity properly applied could help resolve many of these ailments of society; photovoltaic systems may be the best solution for rural electricity so as to ameliorate the life of the third world countries.

[3] The 1973 oil crisis started in October 1973, when the members of Organization of Arab Petroleum Exporting Countries proclaimed an oil embargo to NATO.

[4] Kyoto protocol is one the protocols of Rio Conference, held in 1992, that have been signed by countries universal for the protection of the environment and have global strength. Especially, Kyoto protocol declares the global interest to reduce the Greenhouse gases: Carbon dioxide (CO_2), Methane (CH_4), Nitrous oxide (N_2O), Hydrofluorocarbons (HFCs), Perfluorocarbons (PFCs) and Sulphur hexafluoride (SF_6).

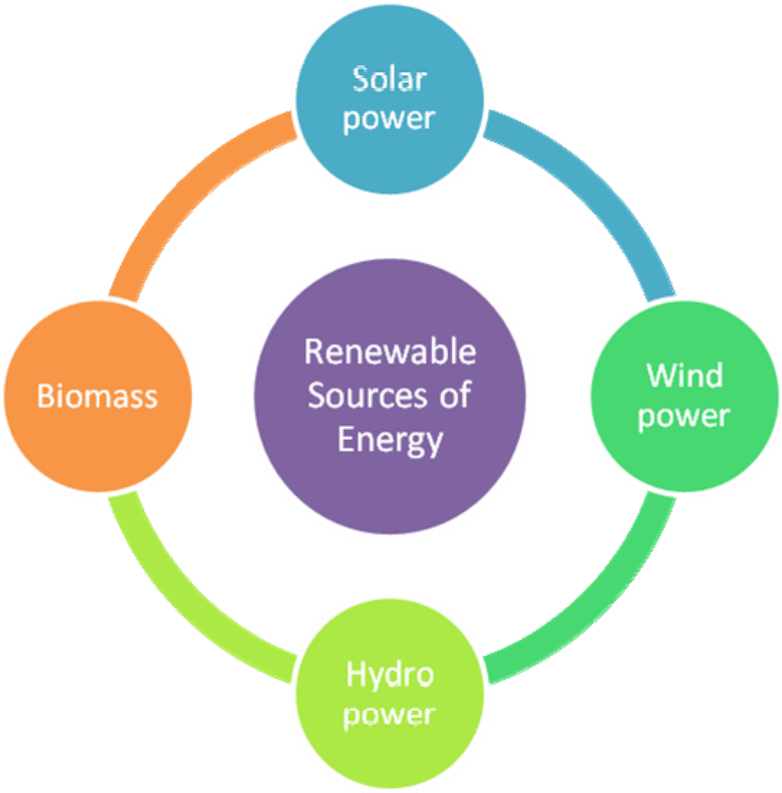

Figure 1.1 Environmentally friendly sources of energy

1.2 Solar Energy

Solar energy is renewable, ecologically friendly, and non-polluting energy supply contrary to fossil fuel that produced the green house effect or nuclear energy that has led to tremendous disaster sparked by accident in Chernobyl (Ukraine, 1986) and Fukushima (Japan, 2010) nuclear plants. In addition, solar energy is more prosperous than the other green energy sources (wind, biomass, hydropower, and geothermal) as the technical knowledge is broader and it can provide us with sufficient energy.

Photovoltaic (PV) technology has a range of terrestrial and space applications nowadays, such as power supply of satellites (since 1958) for telecommunication systems, remote sensing and navigation, cladding of buildings, grid-connected and autonome PV-plants for the supply of electricity, etc. Main advantages of photovoltaic applications are: low operational and service costs, long lasting efficient operation for 20-30 years, easy integration in facades and roofs of buildings, and embodiment in constructions with simultaneous cost reduction. Another advantage of the photovoltaic systems is that they can be integrated in the current grid of electricity power to an extra price per-kWh “feed-in-tariff” by offering long-term contracts to solar energy producers. The possibility of the creation of solar energy farms in deserts is also under consideration. Solar energy converted into electricity meets high expectations for the future in the field of renewables that can also be the solution for rural and remote areas supplies.

Figure 1.2. The 25.7 MW Lauingen Energy Park in Bavarian Swabia, Germany.

The disadvantages of the solar cells are their considerably high cost of production (PVs cost more than the usual forms of energy e.g. coal) and the technical difficulties in fabrication of large area cells.

Countries that have turned to solar energy and have photovoltaic considerable power stations are USA, Germany, Canada, France, India, China, Italy, Spain, Portugal, Ukraine, Thailand, Czech Republic and Bulgaria.

Our country Greece, although it has a lot of sun has not exploited this technology so much until now due to economic reasons, private households, and lack of space. On the other hand, it is worth to be mentioned that there are 6 PV parks: a 10 MWp park by Selective Volt located in Larissa, a park by Infoquest in Beiotia (7.5 MWp), in Peloponnese (6 MWp) by EDF, two 5 MWp, one in Thebes and another one in Drama, and the last one at Eleutherios Venizelos airport with 8 MWp power.

The following figure shows the cost of electricity by energy source. It is clearly depicted that solar energy is much more expensive than the other forms of energy supply. This is one major reason, why it is not sufficiently used, although it is beneficial compared to other sources.

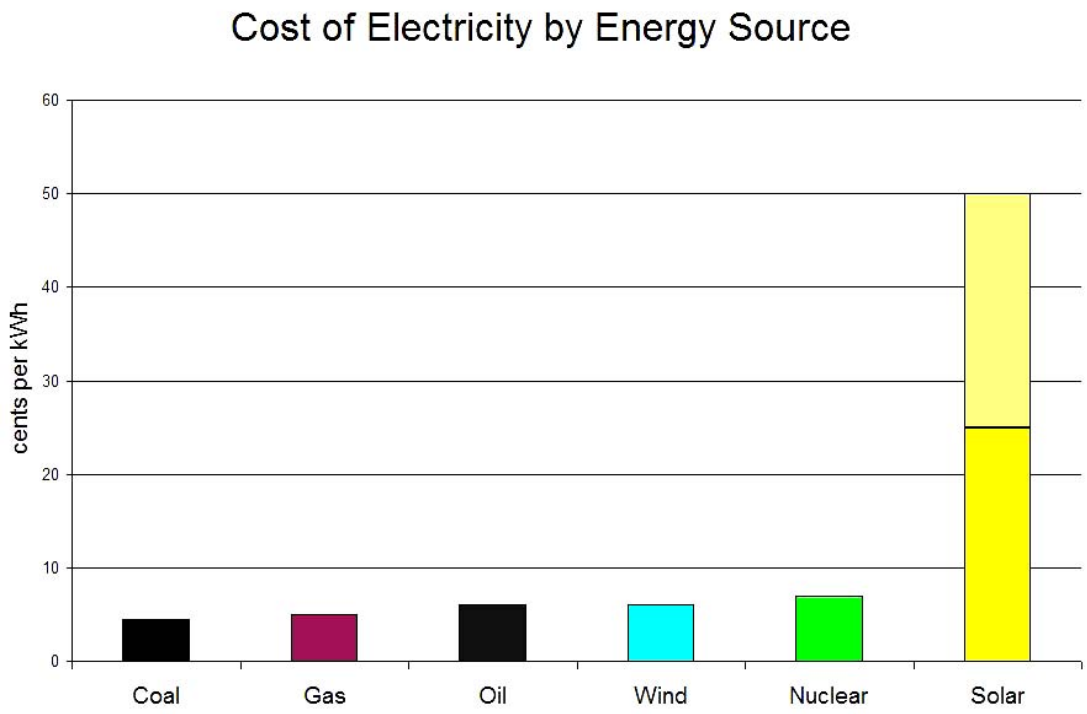

Figure 1.3 A bar chart of the cost of electricity by production source. Note that solar energy bar reflects the fact that such energy can cost between 25¢ and 50¢ per kWh, depending on the technology used and the estimated lifetimes of the cells [13].

1.3 Photovoltaic Effect

The photovoltaic effect converts solar energy to electricity [9]-[13]. It was first reported by Edmund Bequerel, in 1839, when he observed that the action of light on a silver coated platinum electrode immersed in electrolyte produced an electric current. The term "photovoltaic" comes from the Greek φῶς (*phōs*) meaning "light", and from "volt", the unit of electro-motive force, the volt, which in turn comes from the last name of the Italian physicist Alessandro Volta (Alessandro Giuseppe Antonio Anastasio Volta (18 February 1745 – 5 March 1827), inventor of the battery (electrochemical cell) in 1800. The term "photo-voltaic" has been in use in English since 1849.

Solar radiation consists of photons, the particles of light, each with quantized energy. The photons of the solar radiation with a sufficient energy are absorbed by proper semi-conducting materials and their transfer of energy creates an exciton, e.g. an electron-hole pair. The energy of photons $E(\gamma)=h\nu$ must be higher than the energy gap of the semiconductor E_G so as to be absorbed. In a photovoltaic device, however, there is some built-in asymmetry which pulls the excited electrons away, before they can relax, and feeds them to an external circuit. The extra energy of the excited electrons generates a potential difference or electromotive force. Electrons are driven to the negative (n) region of the semiconducting material and holes (a theoretical assumption which

determines the lack of the electron) are driven to the positively (p) charged region of the semiconductor. Then the electrons pass to an external circuit with an application of a voltage through a selective contact where they produce electricity. Figure 1.4 describes the physical basis of the photovoltaic effect in a solar cell: a photovoltaic panel with p- and n-type silicon layers is depicted.

For the p-type layer, silicon (Si) was doped with electron acceptors (Al, B), while, for the n-type layer, it was doped with electron donors (P, As). The p-n junction, where the photovoltaic effect occurs, is built between them. Photons of energy equal or higher than the band gap energy of the solar absorber (Si) transfer their energy to its atoms; each photon causes an electron to move from the valence to the conduction band leaving behind a hole also able to move across the junction, thus giving rise to charge carrier generation.

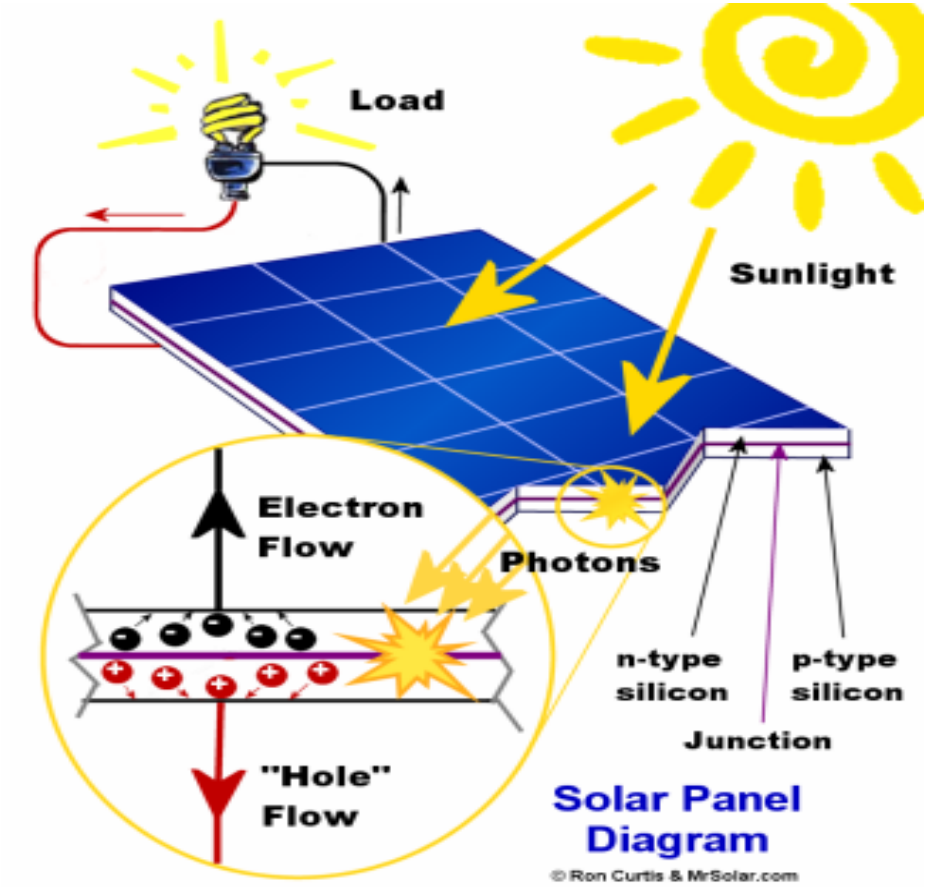

Figure 1.4. Description of the photovoltaic effect in a solar cell

When a load is positioned at the cell's terminals, electrons will pass through the external circuit, produce electricity, lose their energy and circulate back to the holes of the p-region.

2.1 P-N Junction

The physics behind a solar cell are explained in this part, as the p-n junction is the central region, where the PV effect takes place. Mathematical formulas [10] are used for in depth physical understanding of the phenomenon and of the reaction in a solar cell. The p-n junction, where the phenomenon occurs, is of great importance so as to refer to the electrostatics related to it. In thermal equilibrium, there is no net current flow and by definition the Fermi energy must be independent of position.

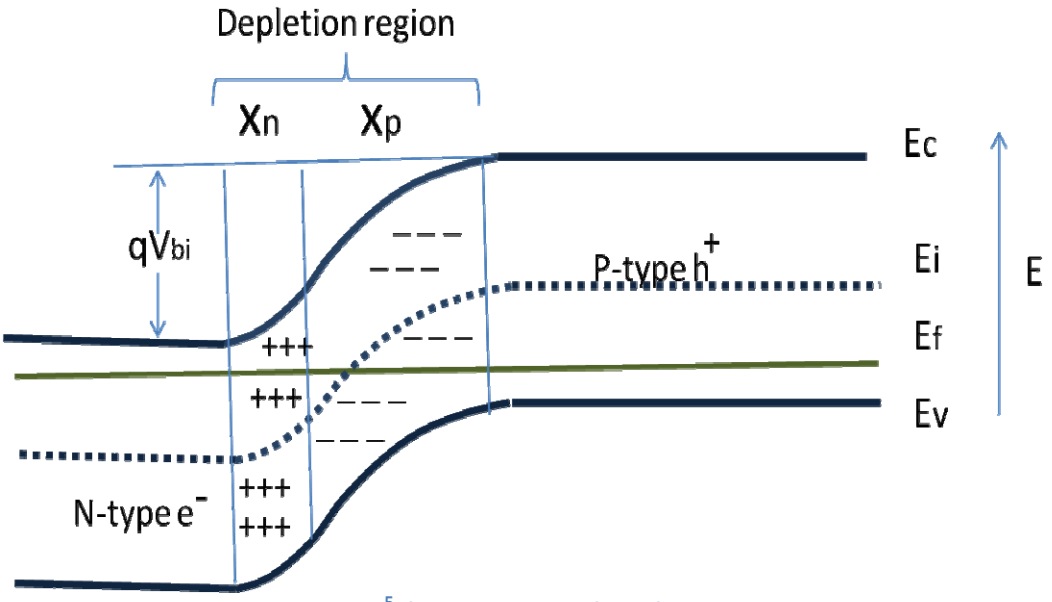

[5]Figure 2.1.a P-N junction

In figure 2.1.a, a simple solar cell structure used to analyze the operation of a solar cell is shown. Free carriers diffused across the junction (x=0) leaving a space-charge or depletion region practically devoid of any free or mobile charges. The fixed charges in the depletion region are due to ionized donors on the n-side and ionized acceptors on the p-side of the junction. The photovoltaic effect, as discussed previously, takes place in the p-n junction of the semiconductor. When the p-doped region (N_A) with an electron deficit is brought into contact with the n-doped region (N_D) with an electron excess, the e- diffuse from the n material to p. At a length x_p and x_n the region becomes negatively charged, at the p-region, and positively charged, at the n-region, respectively. The space-charge region or depletion region is created. An electric field (electrostatic potential difference) is thus set up between them tending to force electrons back to the

[5] Valence band is the highest band that would be filled at 0K while the next highest seperated by a bandgap of forbidden energies is the conduction band. The conduction band is mostly empty so the electrons that are in it can move relatively easily.

n-region and holes to the p-region. The electrostatic potential difference resulting from the junction formation is called the built-in voltage V_{bi} . A junction is now set up. By placing metallic contacts on the p and n region a diode is obtained. A diode permits the current flow only to one direction and it resembles a solar cell in the dark.

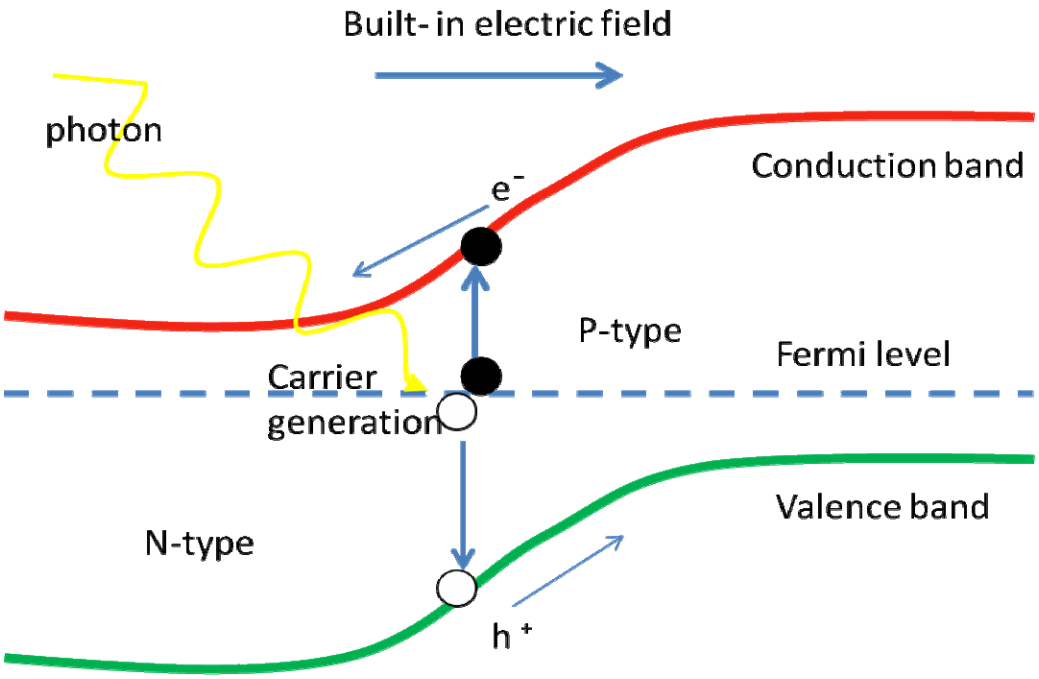

Figure 2.1.b Absorption of a photon at the Fermi level, carrier generation, paths of electrons, in the conduction band, and holes, in the valence band, and build-in electric field created by the diffusion of carriers.

One of the cornerstones of electrostatics is the set-up and solving the problems that are described by the Poisson equation. Finding ϕ for some given f is an important practical problem, since this is the usual way to find the electric potential for a given charge distribution described by the density function. The electrostatics of this situation (assuming a single acceptor and a single donor level) are governed by

$$\text{Poisson's equation} \quad \left(\nabla^2\phi = \frac{q}{\varepsilon(n_0 - p_0 - N_A^-)} - N_D^+ \right) \quad (2.1.1)$$

ϕ is the electrostatic potential, q is magnitude of the electron charge, ε is the electric permittivity of the semiconductor, p_0 is the equilibrium hole concentration, n_0 is the equilibrium electron concentration, N_A^- is the ionized acceptor concentration, and N_D^+ is the ionized donor concentration.

Within the depletion region, defined by $-x_N < x < x_P$, it can be assumed that p_0 and n_0 are both negligible compared to $|N_A - N_D|$ so that equation (1) can be simplified to

$$\begin{cases} \nabla^2\phi = -q\varepsilon N_D, \text{ for } -x_n < x < 0 & (2.5.2) \\ \nabla^2\phi = q\varepsilon N_A, \text{ for } 0 < x < x_p & (2.5.3) \end{cases}$$

Outside the depletion region, charge neutrality is assumed

$$\nabla^2\phi = 0, \text{ for } x < -x_n \text{ and } x \geq x_p \quad (2.5.4)$$

This is commonly referred to as “the depletion approximation”. The regions on either side of the depletion regions are the quasi-neutral regions.

The electrostatic potential difference across the junction is the built-in voltage V_{bi} and can be obtained by integrating the electric field,

$$E = -\nabla\phi \quad (2.5.5) \Leftrightarrow$$

$$\int_{-X_N}^{X_P} E dx = -\int_{-X_N}^{X_P} \frac{d\phi}{dx} = \int_{V(x_N)}^{V(x_p)} d\phi = \phi(-x_N) - \phi(x_P) = V_{bi} \quad (2.5.6)$$

Another type of a junction diode, except from the p-n, is the Schottky junction formed by a metal and a semiconductor. The total charge at either side of the depletion region balances and, therefore, the depletion region extends furthest into the more lightly doped side, as depicted by the equation

$$x_N N_D = x_P N_A \quad (2.5.7)$$

N_D, N_A are the densities of donors and acceptors (number of atoms/cm^3). The depletion width W_D under equilibrium conditions (at a constant temperature with no external injection or generation of carriers) is

$$W_D = x_n + x_p = \sqrt{\frac{2\varepsilon}{q}\frac{(N_A + N_D)}{N_A N_D} V_{bi}} \quad (2.5.8)$$

Under non-equilibrium conditions, the electrostatic potential difference across the junction is modified by the applied voltage V.

$$W_D = x_n + x_p = \sqrt{\frac{2\varepsilon}{q}\frac{(N_A + N_D)}{N_A N_D}(V_{bi} - V)} \quad (2.5.9)$$

$$\text{and } V_{bi}=\frac{kT}{q}\ln\left[\frac{N_A N_D}{n_i^2}\right] \quad (2.5.10)$$

The Fermi function determines the ratio of filled states to available states at each energy at thermal equilibrium (i.e. at a constant temperature with no external injection or generation of carriers) and is given by

$$f(E)=\frac{1}{1+e^{(E-E_F)/kT}} \quad (2.5.11),$$

Where E_F is the Fermi energy, k is Boltzmann's constant, and T is the temperature in Kelvin. At absolute zero, it is a step function and all the states below E_F are filled with electrons and those above E_F are completely empty. As the temperature increases, thermal excitation will leave some states below E_F empty and the corresponding number of states above E_F will be filled with the excited electrons.

When the Fermi energy, E_F, is sufficiently far (>3 kT) from either band edge, the carrier concentrations can be approximated (to within 2%) as

$$n_0 = N_C e^{(E_F - E_C)/kT} \quad (2.5.12), \quad p_0 = N_V e^{(E_v - E_F)/kT} \quad (2.5.13)$$

and the semiconductor is said to be non-degenerate. In non-degenerate semiconductors, the product of the equilibrium electron and hole concentrations is independent of the location of the Fermi energy and is just

$$p_0 n_0 = n_i^2 = N_C N_V e^{(E_V - E_C)/kT} \quad (2.5.14)$$

$$E_V - E_C = -E_G \quad (2.5.15)$$

The conduction-band and valence-band effective densities of state (cm^{-3}), are the N_C and N_V, respectively.

The Fermi energy $E_i = E_F$, in an intrinsic semiconductor, is

$$E_i = \frac{E_V + E_C}{2} + \frac{kT}{2}\ln\left(\frac{N_V}{N_C}\right) \quad (2.5.16)$$

The intrinsic carrier concentration is typically very small compared to the densities of states and typical doping densities and intrinsic semiconductors behave very much like

insulators; that is, they are not very useful as conductors of electricity. The number of electrons and holes in their respective bands, and hence the conductivity of the semiconductor, can be controlled through the introduction of specific impurities, or dopants, called donors-electrons and acceptors-holes. Generally, the donors and acceptors are assumed to be completely ionized, so that $n_0=N_D$ in n-type material and $p_0=N_A$ in p-type material.

The photoelectric effect takes place when the incident light interacts with the electron in the medium with sufficient energy to unbound the electron from the medium (higher energy than the binding energy of the electron) [9]-[13].

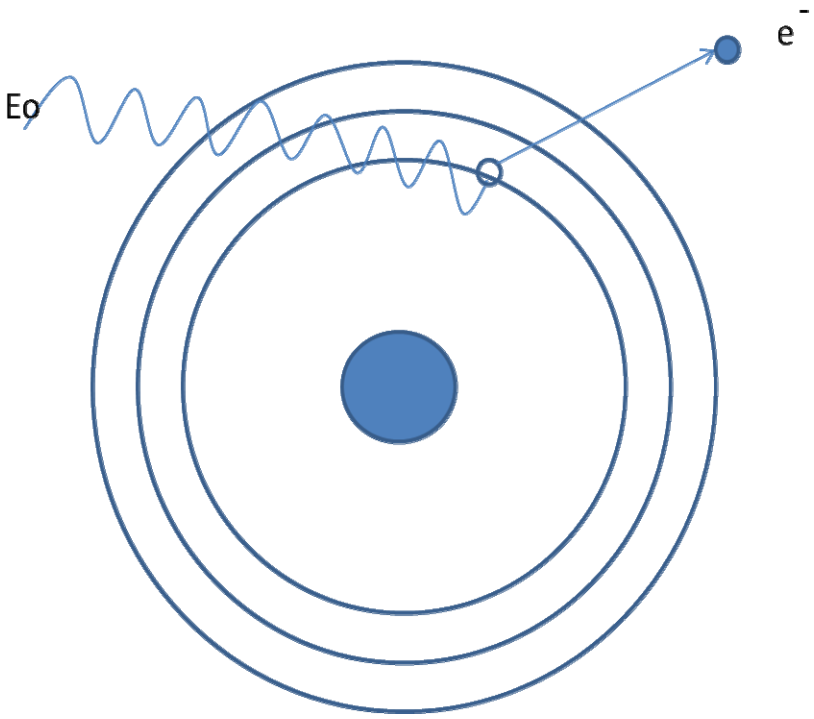

Figure 2.1.c Photoelectic effect

The Work Function Φ is another important quantity. It is the minimum energy with which an electron is bound to the metal and it is characteristic of every metal. It is of the order of a few electron volts. $\Phi=h*f_0$, where f_0 is the threshold frequency of the metal and Planck's constant $h=6,626*10^{-34}$ J*s.

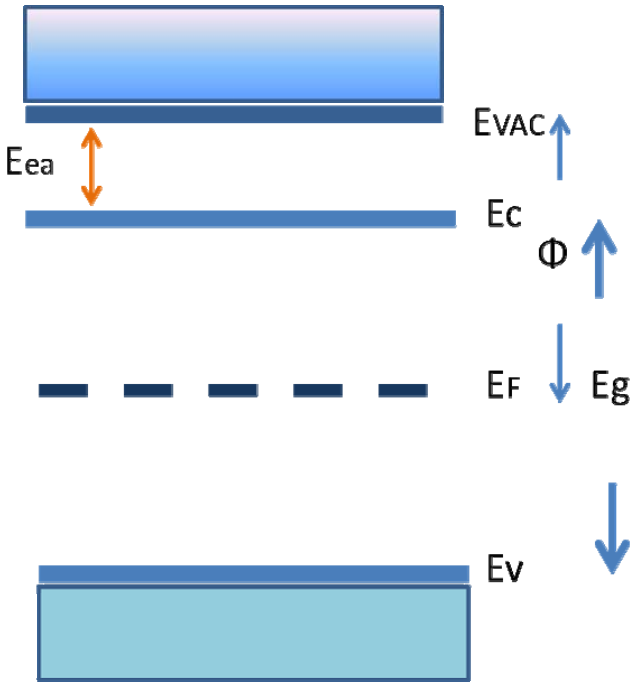

Figure 2.1.d Energy bands and work function of a metal

2.2 Solar Cell

A solar cell is a device that converts the energy of the sun into electrical energy. This device is usually a semiconductor that has the capacity to absorb light and to deliver a portion of the energy of the absorbed photons to the carriers of the electrical current: electrons and holes. A semiconductor diode separates and collects the carriers and conducts the generated electrical current preferentially in a specific direction. A schematic of a simple conventional solar cell is depicted below. Sunlight is incident from the top on the front of the solar cell. A metallic grid forms one of the electrical contacts of the diode and allows light to fall on the semiconductor in between the grid lines and thus be absorbed and converted into electrical energy. An antireflective layer between the grid lines increases the amount of light transmitted to the semiconductor. The metal grids are the electrodes that collect the electrons and lead them to the external circuit. They are more than two so that the collection of electrons is sufficient and they do not recombine with holes.

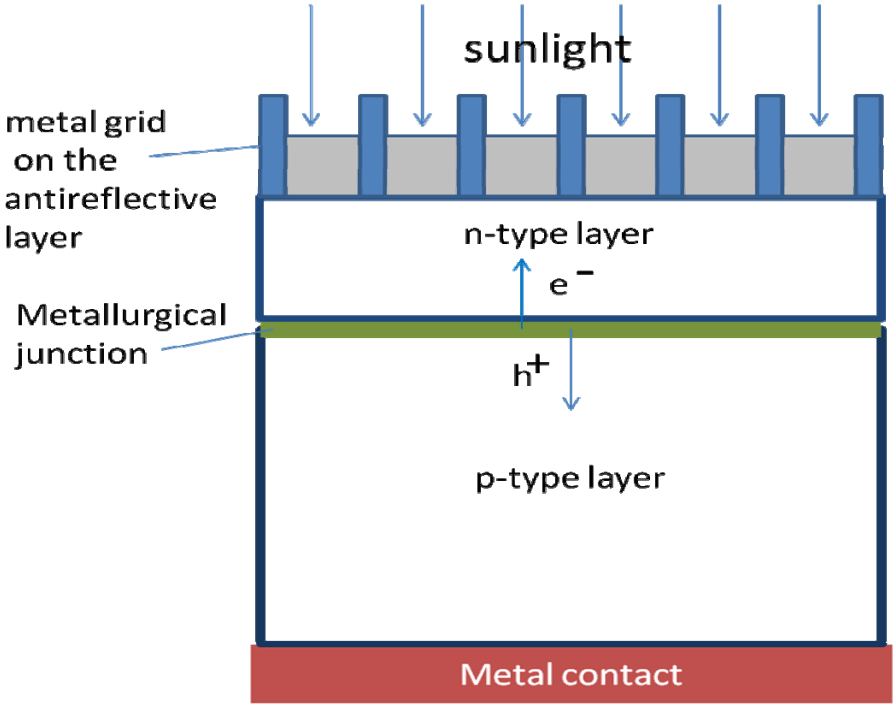

Figure 2.2.1. A solar cell with the following layers: metal contact at the bottom, p-doped region, n-doped region, an antireflective layer and metal grids. The creation of an electron and a hole pair takes place, between the p-n junction, with the absorption of the sunlight.

The semiconductor diode is fashioned when an n-type semiconductor and a p-type semiconductor are brought together to form a metallurgical junction. This is typically achieved through diffusion or implantation of specific impurities (dopants) or via a deposition process. The other electrical contact of the diode is formed by a metallic layer on the back of the solar cell.

Photovoltaic cells require an extended sequence of successful photophysical processes in order to efficiently convert sunlight into electrical energy. As already mentioned, the fundamental sequence is as follows: light absorption generates an electronically excited state. The excited state must either appear at or migrate to an interface or heterojunction, where an electron transfer can take place, since the oxidized and reduced species (holes and electrons) must be able to migrate to opposite sides of the cell where they can be collected as electrical energy. A typical solar cell thus needs at least three key components: a light-absorber, a hole-transport agent, and an electron-transport agent.

Sometimes one component is forced into multiple duties, as in a typical silicon cell, where silicon is the absorber and with different doping also serves as either a hole-transport (p-type) or electron-transport (n-type) agent. Many organic solar cells apply a similar approach using light-absorbing dyes as charge-transport agents, but other approaches separate all three functions to different materials.

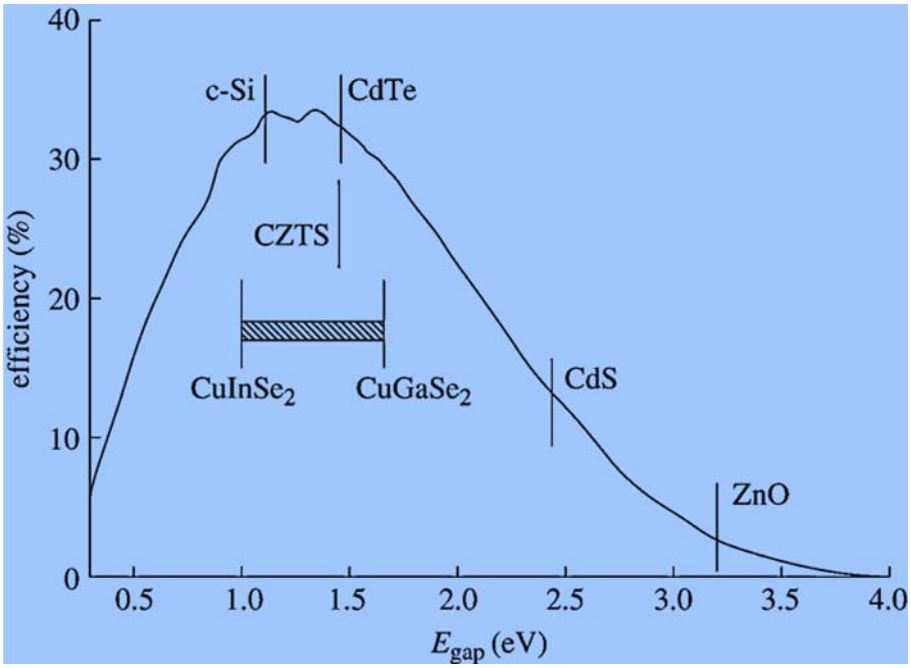

Figure 2.2.2 Maximum theoretical efficiency (Shockley–Queisser limit) for solar cells under AM1.5 illumination without concentration. The bandgaps of absorber materials (c-Si- monocrystalline Si, CdTe, CIGS, CZTS- Copper zinc tin sulfide) and (CdS, ZnO) are shown for comparison.

Harvesting of a significant fraction of the solar spectrum, that can happen at wavelengths below the 700nm, is important as almost the half of the energy of sunlight appears in this region of the spectrum. Additional absorption, at longer wavelengths, can gain additional efficiencies up to a point. The theoretical optimum band gap is at about 1.1 eV (1100 nm) and the maximum efficiency is 33.7% (single-junction cells). The maximum efficiency of 34% for single junction solar cells is a limit calculated theoretically by **William Shockley** and **Hans Queisser** at **Shockley Semiconductor**, in 1961, and it is therefore called Shockley-Queisser limit [14]. This is very important for solar cells as these two scientists have taken in consideration many of the parameters that determine the efficiency of a solar cell. These are the blackbody radiation, the phenomenon of radiative recombination, the spectrum losses and the limited mobility. Although a smaller band gap (at longer wavelengths) allows for harvesting a larger fraction of the solar spectrum, there are diminishing returns caused by the effect of degrading higher-energy photons to the level of the decreasing band gap. Thus an ideal solar absorber would appear black – absorbing all the ultraviolet and visible and into the near infrared. Silicon is indeed tough competition, with a broad absorption out past 900 nm.

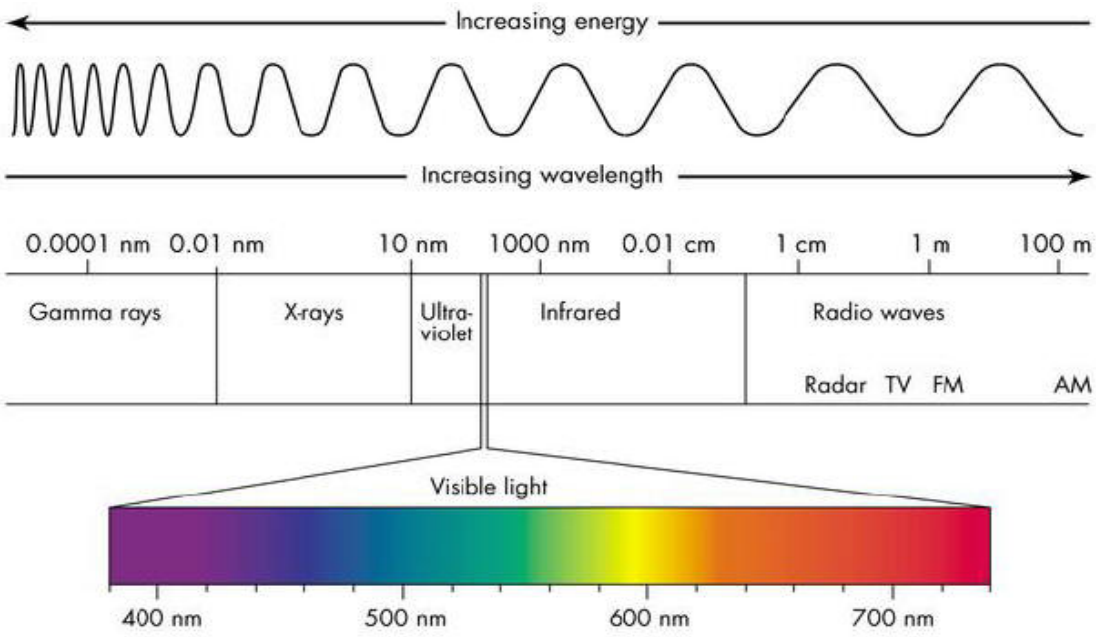

Figure 2.2.3 Electromagnetic spectrum

Following solar light harvesting, charge separation is the next essential step. Typically, this requires an interface or heterojunction involving differently charged materials. The excited states generated upon light absorption must transfer an electron (either oxidatively or reductively) in order to generate opposite charges. The energetic requirement is that the two different materials must have offset energy levels suitable for an electron transfer rapid enough to compete with deactivation of the excited state (typically nanoseconds). The physical requirement is that the two different materials must be close enough for this reaction to be that rapid.

Finally, the separated charges (oxidized and reduced equivalents, or holes and electrons) must be able to migrate substantial distances (typically a few micrometers at least) to be collected at the opposite electrodes. However, getting charges through organic material that is being studied in the following chapter is rather problematic. Electron and hole mobilities are low for most organic compounds. Hence conductive polymers are of particular interest. For example, polythiophenes and poly(phenylenevinylenes) are common constituents of BHJ cells (Bulk heterojunction, the analysis of this form of cell is given in chapter 3.2.A).

2.3 I-V characteristic graph

This characteristic graph is very important for the characterization of a solar cell. The photovoltaic characterization of a solar cell provides information on the efficiency of the cell. This information is mainly given by the I-V graph.

Solar efficiency can be measured as a quantum yield, ϕ (number of electron/hole pairs collected per absorbed photon, sometimes called internal quantum efficiency, IQE) or as an incident-photon-to-current efficiency (IPCE, number of electron/hole pairs collected per incident solar photon, sometimes called external quantum efficiency, EQE).

A more comprehensive efficiency measure is the overall power conversion efficiency (η), sometimes called PCE (power cell efficiency), which compares the total electrical energy output with the total energy contained in the solar irradiance. A standard solar irradiance is typically taken as the integrated solar spectrum as it reaches Earth's surface after traversal of 1.5 atmosphere thickness (AM1.5 Global standard).

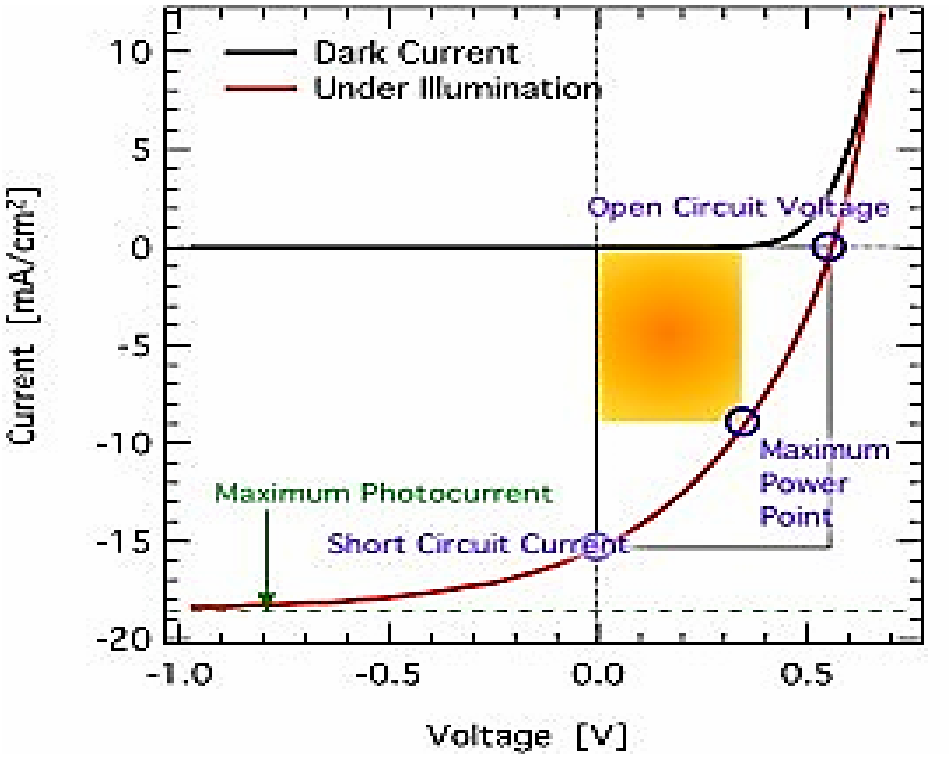

Figure 2.3.a I-V characteristic graph of a solar cell[6]

Experimentally, the output of a photovoltaic cell is given by a photocurrent voltage (I-V) curve (Fig. 2.3.a). The photocurrent is generally the most sensitive measure of the performance of a photovoltaic cell. It depends on the light-harvesting efficiency (the absorption spectrum), the quantum efficiency of charge separation, and the avoidance of undesirable back reactions (effectively representing short circuits). Photovoltage is primarily determined by the choice of materials and their relative energy levels, although kinetic factors can also diminish photovoltage. A comparable curve is also determined in the dark, typically showing simple diode behavior – zero current at applied voltages until a breakdown potential is reached.

[6] Figure from http://blog.disorderedmatter.eu

The main formulas that describe the efficiency and the characteristics of a solar cell [9]-[11] as well as the characteristic I-V graph of a solar cell in dark (the curve passes from zero) and under illumination (the curve has the short circuit current under illumination with zero voltage) are presented in the next page. The important parameters of every cell are

- V_{OC} is the Open Circuit Voltage,
- I_{SC} is the Short Circuit Current,
- P_{max} or MPP is the maximum power point of the solar cell under illumination.

In Fig. 2.3.a, maximum power is given by the yellow parallelepiped and is the multiplication of the respective current (I) and voltage (V).

The fill factor of the cell is given by $FF=\frac{P_{max}}{I_{SC}V_{OC}}$ and it describes the percentage of the P_{max} to the ideal power obtained by the two maximum characteristics of the solar cell. It is the characteristic of the ideality of the solar cell.

The overall solar energy conversion efficiency is the maximum power extracted compared to the incident solar power and it is measured by the following formulas: $\eta=FF\frac{I_{SC}V_{OC}}{P_S}$ or $\eta=\frac{P_{max}}{P_S}$, P_S = power of the source.

Optimizing the output of a typical photovoltaic cell requires maximizing the short-circuit photocurrent, the open-circuit photovoltage, and the fill factor so as to achieve the maximum possible efficiency [12].

The fill factor is governed primarily by cell resistances: internal shunt (parallel) resistances and series resistances. In an ideal cell, parallel resistances would be infinite (no shunts) and series resistances would be negligible. Such a cell would be an ideal diode, for which the IV plot would follow an exponential curve and would have a fill factor of 0.89.

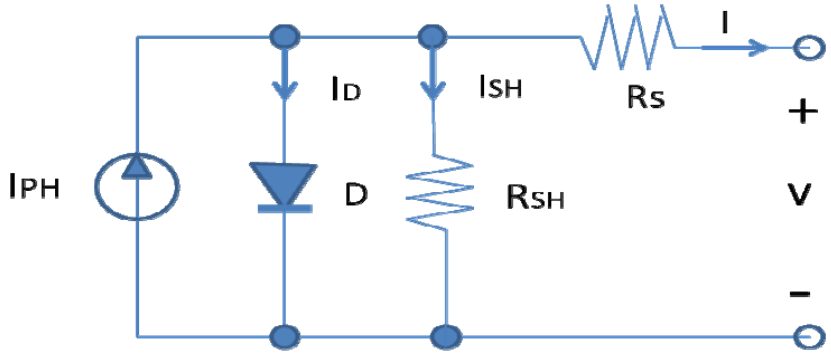

Figure 2.3.b The circuit is a model for a solar cell. R_S is the series resistance and RSH is the shunt resistance. I_L is the current from the photovoltaic effect.

3.1 Materials in photovoltaic technology

Semiconductors are the most appropriate materials in optoelectronics and solar cells. They have weakly bonded electrons occupying the valence band. When absorbed energy of a photon exceeds the band gap energy of the semiconductor, the electron from the valence goes to the conduction band where it can "conduct" electricity through the material. Then, electrons are driven through the circuit to the valence band.

The most used material in current technology of solar cells is silicon (Si), covering 90% of the market. It is an abundant element on earth as it can be found in sand, second to oxygen. It is available in non-crystalline form as amorphous Si (a-Si) and in the crystalline form (c-Si). The latter covers the following material types: monocrystalline, polycrystalline, microcrystalline, and ribbon. It is environmentally friendly in disposal and recycling. Silicon is a semiconductor with an indirect band gap of 1,12 eV which allows the material to absorb photons in the infra-red region of light. It belongs to the first generation of solar cells and it is relative expensive to produce, but it has the highest reported single-junction cell efficiency in comparison with the second and third generation solar cells described below. The first generation silicon solar cells were developed in Bell laboratories, in 1954, with an efficiency of 6%. This was the first inorganic solar cell ever developed. Nowadays, the efficiency of single-crystal Si solar cells has reached 27,6%.

The second generation solar cells are thin film solar cells made from direct energy gap semiconducting materials. The materials used are gallium arsenide (GaAs, Eg=1,43eV), indium gallium phosphide (InGaP), copper indium (gallium) (di)selenide CI(G)S and copper indium (di)selenide CIS which are chalcopyrite absorbers and cadmium telluride (CdTe). CdTe, GaAs, and copper indium gallium (di)selenide (CIGS) have been widely studied, but do not have large market shares. Among them, chalcopyrite absorber (CIS and CIGS) based solar cells are lower in production costs and compete currently with the

most efficient Si solar cells (record efficiencies of CIGS cells 20,8% [15]). Polycrystalline silicon solar cells (poly-Si) have efficiencies up to 20%, while the most advanced GaAs cells tend above 40%. GaAs failed to be widely commercialized (outside of niche markets like space) mostly because of its high production costs. Environmental issues (toxicity of cadmium) and lower efficiencies have limited the chances of CdTe solar cells for competition.

Another category of solar cells known as the third generation solar cells are the multiple-junction or tandem solar cells with three or four p-n junctions each tuned to a different wavelength of light so that their efficiency may strongly increase and reach in case of GaAs cells 86%. Because of their high efficiencies and high costs, they are applied in ex-terrestrial use only (satellites). Dye sensitized solar cells DSSCs (a combination of organic and inorganic materials) belong also to the third generation solar cells and are cheaper, but with the lowest efficiencies until now. Promising new materials have been also developed [16]-[20], as for example the molecular organic semiconductors embedded in organic solar cells with efficiency up to 12% [20].

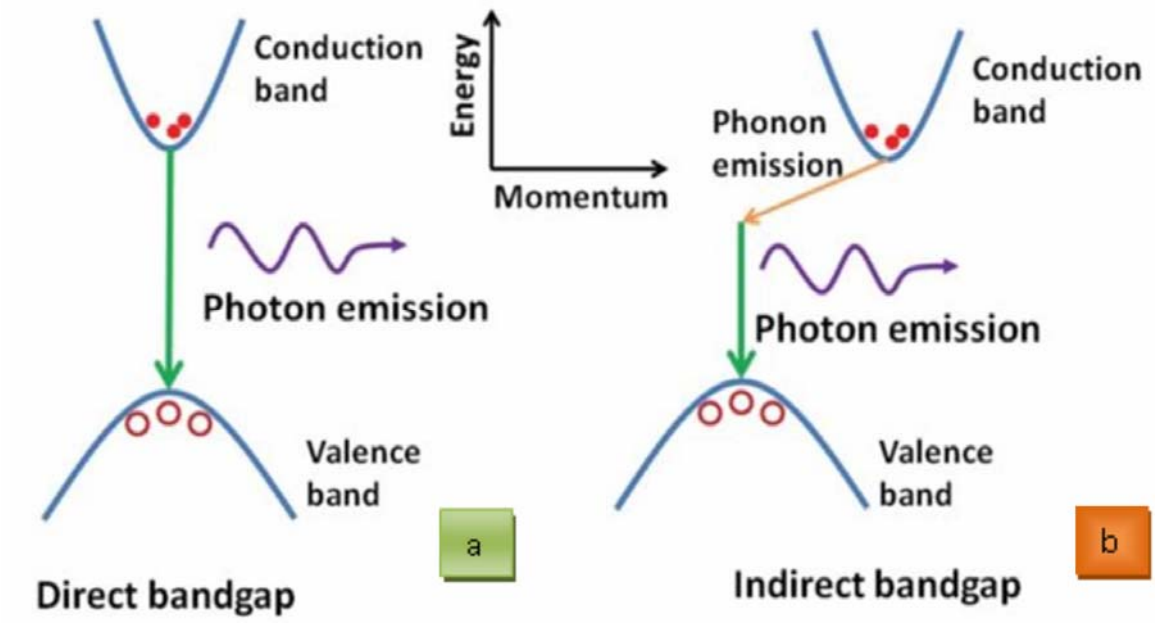

Figure 3.1. Direct gap as GaAs and Indirect gap as Si

An indirect band gap occurs when the valence and conduction band edges are not aligned in *k* space. *k* space is a coordinate system, which is used for counting quantum states and describing band gaps. When the momentum (k-x axis) is the same at the valence and conduction band, the band gap is direct and an electron can directly emit a photon, otherwise it is an indirect band gap and an intermediate state is needed, e.g. the electron has to pass through an intermediate state and transfer momentum to the crystal lattice assisted by a phonon. The physical laws govern these two transitions are (1) the energy conservation and (2) the momentum conservation.

3.2.A Organic films –Organic solar cells

From the early 50's onwards, scientific and industrial laboratories are searching for new materials (organic compounds containing carbon[7]) for photovoltaic technology. The photovoltaic effect was first observed on an organic material in the 60s after it was discovered that some common dyes had semiconducting properties. The breakthrough in the field came in 1986 due to Tang's patent of creating a heterojunction solar cell. In 1991, Gratzel created the first dye-sensitized solar cell with an efficiency of 11% [21], the greatest reported until now in organic solar cells. Common materials for organic solar cells are phthalocyanines (especially metal-phthalocyanines as p-type materials), porphyrins, chlorins and close to those tree macrocycles [22]-[29]. The first requirement is the harvesting of a significant fraction of the solar spectrum. Almost half of the total energy of sunlight appears at wavelengths below 700 nm, a region typically covered well by the porphyrin and phthalocyanine families. Porphyrins and related derivatives having extended conjugation are a common approach to extending the range of the absorption spectrum into the near infrared [25].

A problem that arises in organic materials is to collect electric carriers (electrons and holes) with the electrodes. Electron and hole mobilities are low for most organic compounds. Hence, conductive polymers are of particular interest. Polythiophenes and poly(phenylenevinylenes) are two of them. In addition, porphyrins and their derivatives organized as liquid crystals or as conductive nanostructured polymers have been studied as improved charge carrier materials for solar cells.

Organic films deposited on semiconductor surfaces have gained interest due to their semi-conductive properties which make them candidates for optoelectronic and electronic devices such as organic field effect transistors (OFETs), organic light emitting diodes (OLEDs), chemical sensors, and organic solar cells. Another important factor of the heterostructures of organic films on semi-conductive materials is their modification in terms of their optoelectronic and electronic properties by changing the assembly of the molecules or the semi-conductive surfaces they are absorbed in.

Organic solar cell research has been developed during the past 30 years; especially in the last decade, it has attracted scientific and economic interest triggered by a rapid increase of power conversion efficiencies. This was achieved by the introduction of new materials, improved materials engineering, and more sophisticated device structures. Today, enhanced conversion efficiencies have been accomplished with several device concepts [16]-[21], [25]. Commercial efficiencies usually reach 6%-7%. Generally, efficiencies of these thin-film organic devices have not yet reached those of their inorganic counterparts ($\eta \approx 10–20\%$), but the perspective of cheap production employing roll-to-roll processes drives the development of organic photovoltaic devices further in a dynamic way. The organic solar cells in the market have the schematic of the figure below. The materials vary having from one central to three layers organic.

[7] Of the 2000 compounds known, approximately 90% are organic.

One of the principle difficulties when trying to fabricate an organic solar cell is the instability of most cell materials in ambient conditions. Most of the cells presented in the literature are fabricated and characterized without ever being exposed to air. They also have very short lifetimes making them useless in any real application without some type of encapsulation that adds cost and difficulty of manufacture. These disadvantages need more research to be solved.

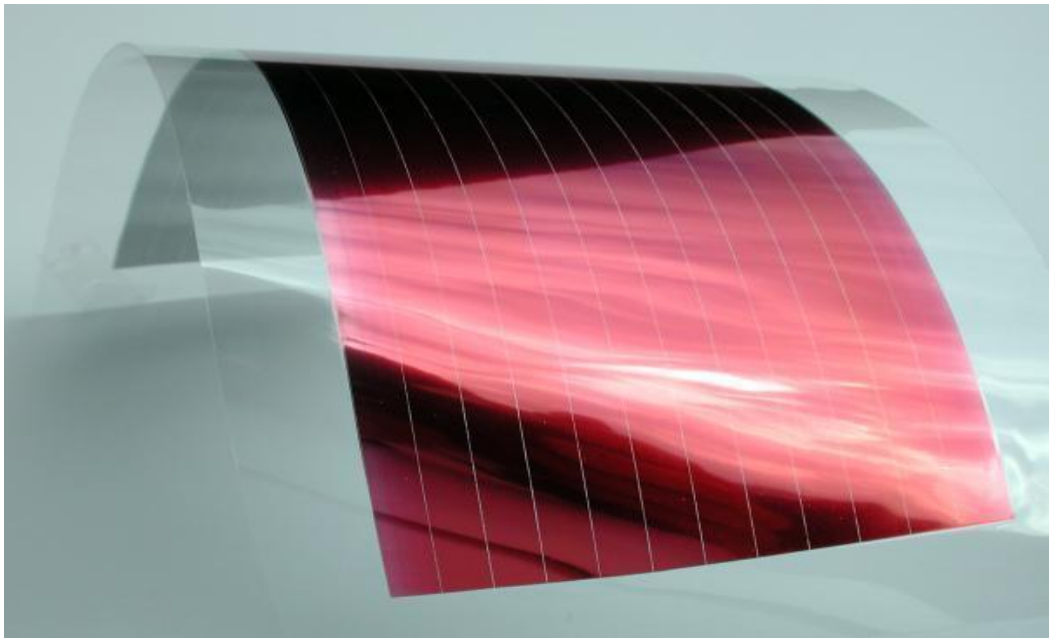

Figure 3.2.A1 Thin film organic solar cell (Fraunhofer ISE)

As it is mentioned above, the first report on the development of an organic solar cell was published by Tang, in 1986. It is an organic solar cell composed of Cu-phthalocyanine and a perylene derivative. Since then, the field expanded rapidly and now includes a wide variety of "small" molecule solar cells containing phthalocyanines or porphyrins as dyes, conjugated polymers as the p-type donor phase, and C_{60} or perylene derivatives as the acceptor phase [23]-[25]. Phthalocyanine is a p-type, hole conducting material that works as electron donor, whereas perylene and its derivatives show an n-type, electron conducting behavior and serve as electron-acceptor material. Research on organic solar cells – OPVs (organic photovoltaics) generally focuses either on solution processable organic semiconducting molecules/polymers or on vacuum-deposited small-molecular materials.

In general, organic semiconductors can be regarded as "intrinsic wide band gap semiconductors"[8] (band gaps above 1.4 eV) down to "insulators" (band gaps above 3 eV) with a negligibly low intrinsic charge carrier density at room temperature, in the dark. Chemical, photochemical, or electrochemical doping is used to introduce extrinsic charge carriers into organic semiconductors. For example, photo-induced electron transfer from a donor to an acceptor-type organic semiconductor film introduces free charge carriers (positive charge carriers on the donor layer, i.e., p-type, and negative charge carriers on the acceptor layer, i.e., n-type). Donor-acceptor-type bi-layer devices can thus work like classical p-n junctions. Chemical doping of a semiconductor matrix by introducing small concentrations of reagents (dopants) has also been reported[9].

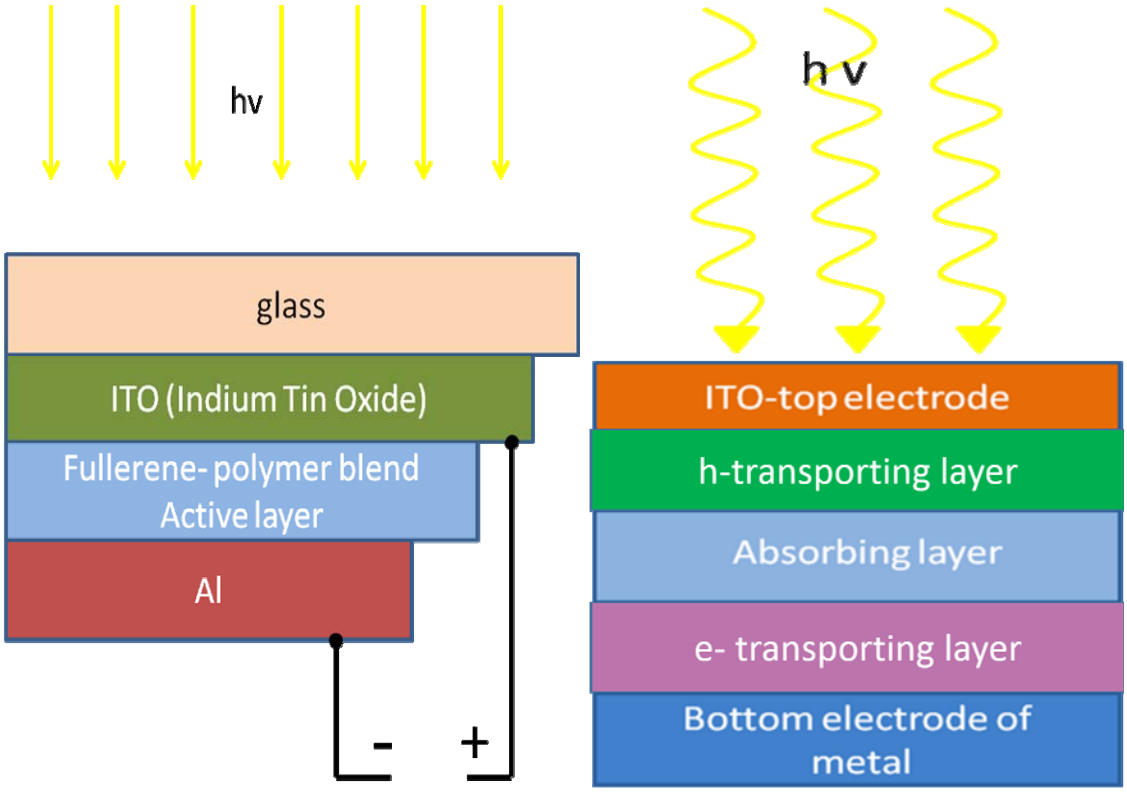

Figure 3.2.A2 Schematic layouts of organic bulk heterojunction solar cells.

Other materials used to create organic solar modules are the fullerene/polymer blends created by solution-based technologies.

Some more specific studied combinations of the materials used in organic solar cells found in literature are presented in the following:

[8] The band-gaps of organic semiconductors are between 1,4 eV and 2,5 eV.

[9] Al, Ca, Ag that are used as back electrode have work function Φ more positive than ITO.

1. Evaporated films – phthalocyanine (donor) / fullerene[10]- C_{60} (acceptor) solar cells.

   - Copper Pc (CuPc)
   - Palladium Pc (PdPc) } mettaloPcs / C_{60}
   - Zinc Pc (ZnPc)/
   - Tin Pc (SnPc) / C_{60}
   - Alluminum Phthalocyanine Chloride (ClAlPc) /C_{60}
   - Boron Subphthalocyanine Chloride/C_{60}

2. Thin porphyrin or phthalocyanine films with electron acceptor C_{60} or PCBM[11] (a fullerene derivative of C_{60})
3. Tandem organic solar cells with the combination of (1),(2)
4. Porphyrins or phthalocyanines incorporated into polymer solar cells.

Many other forms and chemical types of polymers, fullerenes, porphyrins, and phthalocyanines and combinations of them have been studied.

Another material that replaces ITO[12] (transparent conductive glass), or is combined with it, is PEDOT:PSS that serves to make efficient electrical contact to the organic photoactive layer. The PEDOT:PSS also serves to smooth out the extremely thin active layers (10-200 nm), can often serve as a contact point for a short-circuit in a solar cell device. The photoactive layers are evaporated, printed, or solution cast onto the ITO/PEDOT: PSS electrode.

OPVs can be divided into three categories: 1. Dye Sensitized Solar Cells, 2. small molecular organic solar cells, 3. Polymer solar cells (or else called plastic cells). A question is raised for their stability as their lifetime stability in commercial use (glass encapsulated modules from Konarka) is of 3-4 years by now, whereas that of the commercial solar cells of inorganic compounds is of 25-30 years.

Dye-Sensitized Solar Cells were initially reported in 1991 by the researchers O'Regan and Grätzel. Generally, the components of the cells are inexpensive and the overall efficiency can be up to 11%, therefore, it can be a low-cost alternative to standard silicon photovoltaics.

---

[10] Fullerene is any molecule composed entirely of carbon. C_{60} was the first fullerene molecule prepared and discovered in 1985 by Richard Smalley, Robert Curl, James Heath, Sean O'Brien, and Harold Kroto at Rice University. Generally, fullerene molecules occur in nature.

[11] PCBM is the common abbreviation for the fullerene derivative [6,6]-phenyl-C_{61}-butyric acid methyl ester. It is being investigated in organic solar cells. It was first synthesized in the 1990s by Fred Wudl's group. It is an electron acceptor material and is often used in plastic solar cells or flexible electronics in conjunction with electron donor materials such as P3HT or other polymers. It is also a highly cost derivative for commercial application.

[12] Indium Tin Oxide

The most common implementation of the DSSC uses ($_{44}$Ru) ruthenium-based dyes. Unfortunately, ruthenium is not an earth-abundant element, and it is unlikely that the supply and/or cost of ruthenium will allow such DSSCs to be as widely adopted as needed for a true solar-based economy. In order to solve this problem extensive research has and is being done to replace the ruthenium sensitizer with a dye that can achieve the same or better efficiency while remaining inexpensive and easy to synthesize. Porphyrinoid molecules have received a great deal of attention in that regard because of their versatility, ease of construction, long-term stability, and relation to natural photosynthesis. The report of a porphyrin solar cell with 11% efficiency clearly shows that these compounds can match up with the best of sensitizers for DSSCs. The five main tetrapyrrole structures that have been used in DSSCs are porphyrins, chlorins, bacteriochlorins, phthalocyanines, and corroles.

The usual organic photovoltaic device architectures are:

1. Bilayer devices
2. Bulk heterojunction devices (BHJ)

In a bilayer heterojunction device, p-type and n-type semiconductors are sequentially stacked on top of each other. Such bilayer devices using organic semiconductors were realized for many different material combinations. In such devices, only excitons created within the distance of 10-20 nm from the interface can reach the heterojunction interface. This leads to the loss of absorbed photons further away from the interface and results in low quantum efficiencies. The efficiency of bilayer solar cells is limited by the charge generation 10-20 nm around the donor-acceptor interface. Using thicker films creates optical filter effects of the absorbing material before the light gets to the interface, resulting in a minimum photocurrent at the maximum of the optical absorption spectrum. Also, the film thicknesses have to be optimized for the interference effects in the multiple stacked thin film structure.

Bulk heterojunction (BHJ) is a blend of the donor and acceptor components in a bulk volume. It exhibits a donor-acceptor phase separation in a 10-20 nm length scale. In such a nanoscale interpenetrating network, each interface is within a distance less than the exciton diffusion length for the absorbing site. The bulk heterojunction concept has heavily increased (orders of magnitude) the interfacial area between the donor and acceptor phases and resulted in improved efficiency solar cells.

While in the bilayer heterojunction the donor and acceptor phases are completely separated from each other and can selectively contact the anode and cathode, in the bulk heterojunction both phases are intimately intermixed. This mixture has a priori no symmetry breaking in the volume. There is no preferred direction for the internal fields of separated charges, that is, the electrons and holes created within the volume have no net resulting direction they should move. A symmetry breaking condition (like using different work-function electrodes) is thus essential in bulk heterojunctions. Otherwise, only concentration gradient (diffusion) can act as driving force. Furthermore, separated charges require various pathways for the hole and electron transporting phases to the contacts. In other words, the donor and acceptor phases have to form a nanoscale,

bicontinuous, and interpenetrating network. Therefore, the bulk heterojunction devices are much more sensitive to the nanoscale morphology in the blend, which will be discussed in more detail below. Bulk heterojunctions can be achieved by co-deposition of donor and acceptor pigments or solution casting of either polymer/polymer, polymer/molecule or molecule/molecule donor-acceptor blends.

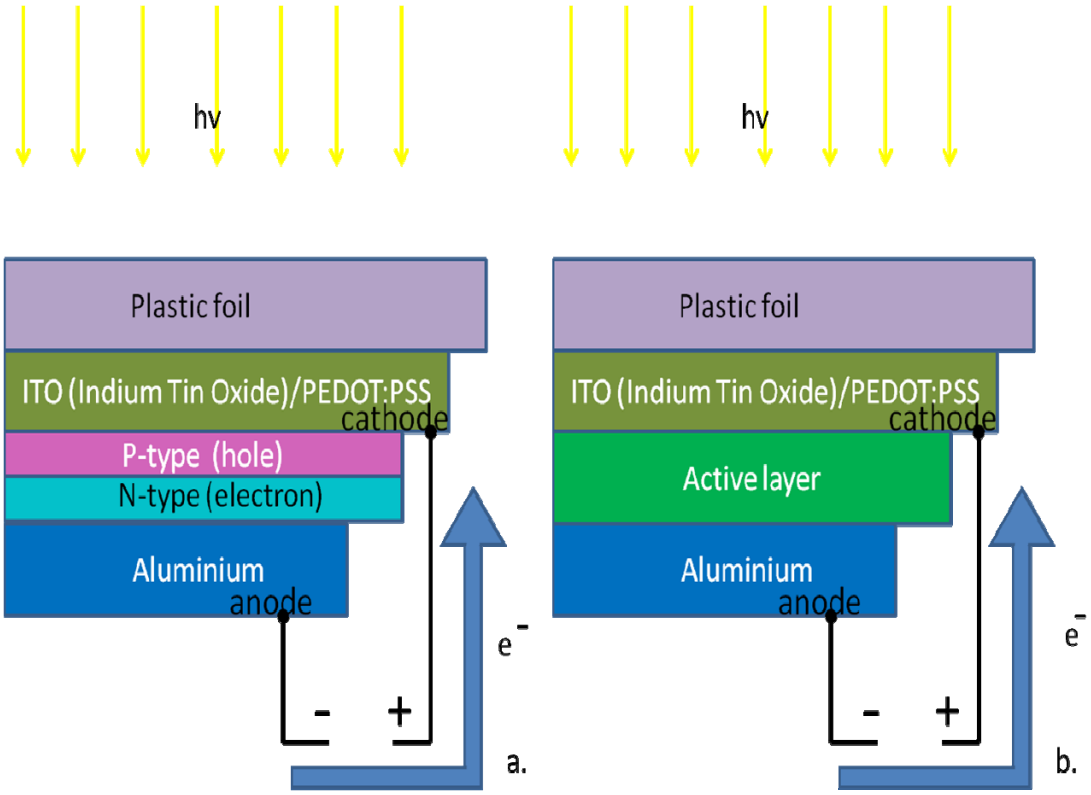

Figure 3.2.A3 Bilayer configuration in organic solar cell, 2. Bulk heterojunction configuration in organic solar cell.

As it was mentioned before, PEDOT-PSS (poly(3,4-ethylendioxythiohene)-polystyrene-para-sulfonic acid) improves the surface quality of the ITO electrode (reducing the probability of shorts) as well as facilitates the hole injection/extraction.

To conclude: with organic solar cells, it is advisable to refer to their structure. The general structure used for organic solar cells is similar to the organic light emitting diodes LEDs. The devices are fabricated in sandwich geometry. As substrates, transparent conducting electrodes (for example, glass or plastic covered with ITO) are used. ITO (indium tin oxide) electrodes are transparent and conductive, but expensive.

3.2.B Optical excitations in organic semiconductors

In organic donor-acceptor (D-A) heterojunctions the nature of optical excitations is different from that of the inorganic semiconductors. In inorganic semiconductors, the absorbed photons instantly generate free electrons and holes at room temperature (25 degrees Celsius or 298 degrees Kelvin). Organic semiconductors have a lower dielectric constant than the inorganic semiconductors (~3 in contrast to ~12 in Si) and thus less electric field screening. Hence, the absorbed photons generate tightly bound singlet (spin=0) excitons.

Exciton is the consideration of an electronic excitation as a quasi-principle, capable of migration. It is also a bound electron–hole pair which is chargeless in its unity. Such excitons, so called Frenkel excitons named after Yakov Frenkel[13], are typical in organic materials and have a small diffusion length of the order of 5-10 nm and their binding energies are in the order of ~ 1eV which is several times more than the thermal energy at room temperature kT (~1/40 eV).

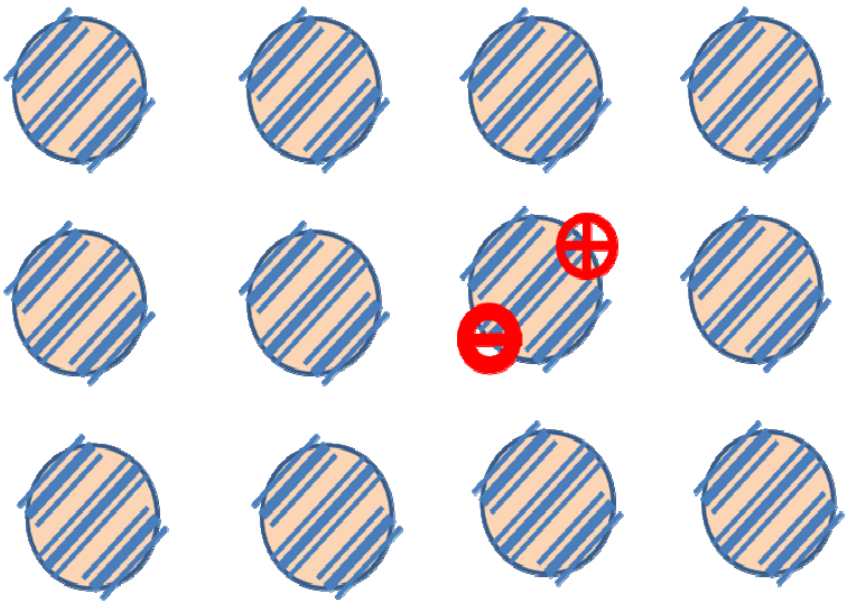

Figure 3.2.B1 Molecular picture of Frenkel excitons in organic material of crystalline order.

[13] Yakov Frenkel, Russian (10 Feb. 1894, Rostov-on-Don - 23 Jan. 1952, Leningrad) was a Soviet physicist renowned for his works in the field of condensed matter physics.

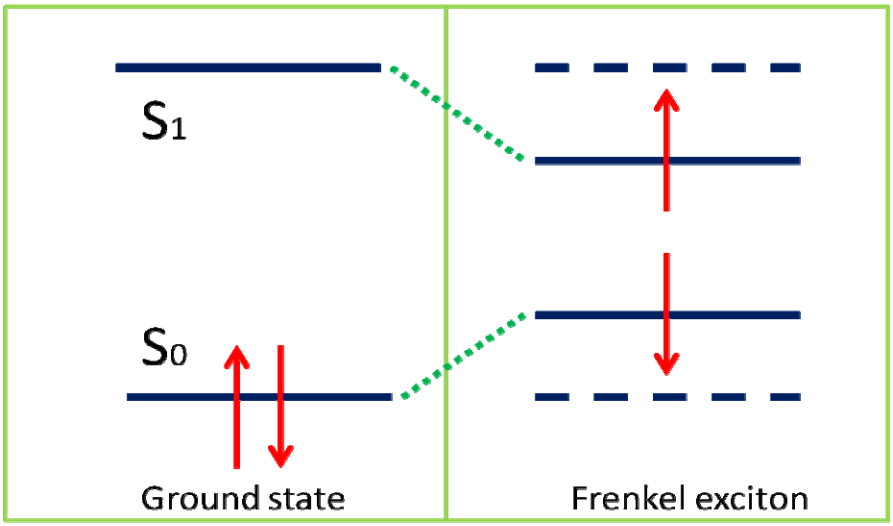

Figure 3.2.B2 exciton generation

The absorbed photons generate a singlet exciton (tightly bound electron-hole pair) in the material, the donor or the acceptor. The singlet exciton, a neutral quasi particle, will diffuse into the junction. The energy level difference between the HOMO (Highest Occupied Molecular Orbital) levels of the donor and acceptor will cause the electron to dissociate into a negative polaron (an electron charge coupled with a cloud of photons at the acceptor side), and a positive polaron at the donor side. The negative and the positive carriers will stay bound at the interface. To separate them, an external electric field is needed. The external electric field arises from the metal junctions' field and the PV field. For most organic polymers and molecular structures, the energy required to separate an exciton into a hole and an electron must be larger than the Coulomb attraction between hole and electron, typically around 0.3–0.4 eV.

The free positive and negative charges will transport by hopping across the donor and acceptor material, respectively. From the point of view of the system chemistry, what happens is a photon induced redox reaction, where electron and holes hop through a series of chemical reactants after the singlet exciton is dissociated at the donor-acceptor interface.

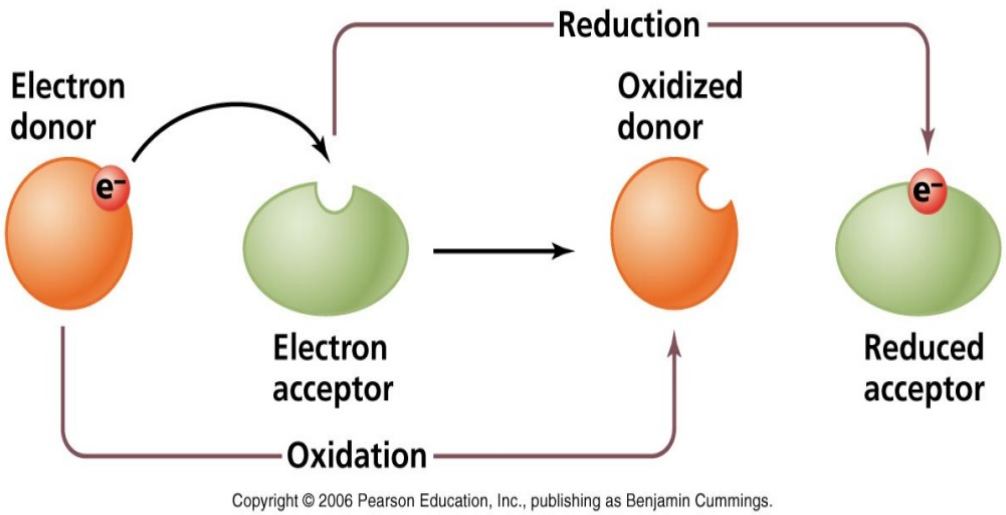

Figure 3.2.B3 Schematic drawing of a Redox (reduction-oxidation) reaction: Oxidation occurs with the loss of an electron (here), hydrogen, or a gain of oxygen. Reduction is the inverse process.

Increasing the solar spectral response of the photoactive layer is an important goal for organic solar cells, especially when utilizing porphyrins and phthalocyanines whose visible light absorbance onset is usually at 650 nm for porphyrins and at 750 nm for metallophthalocyanines (Cu, Zn, Pd) [23], [25].

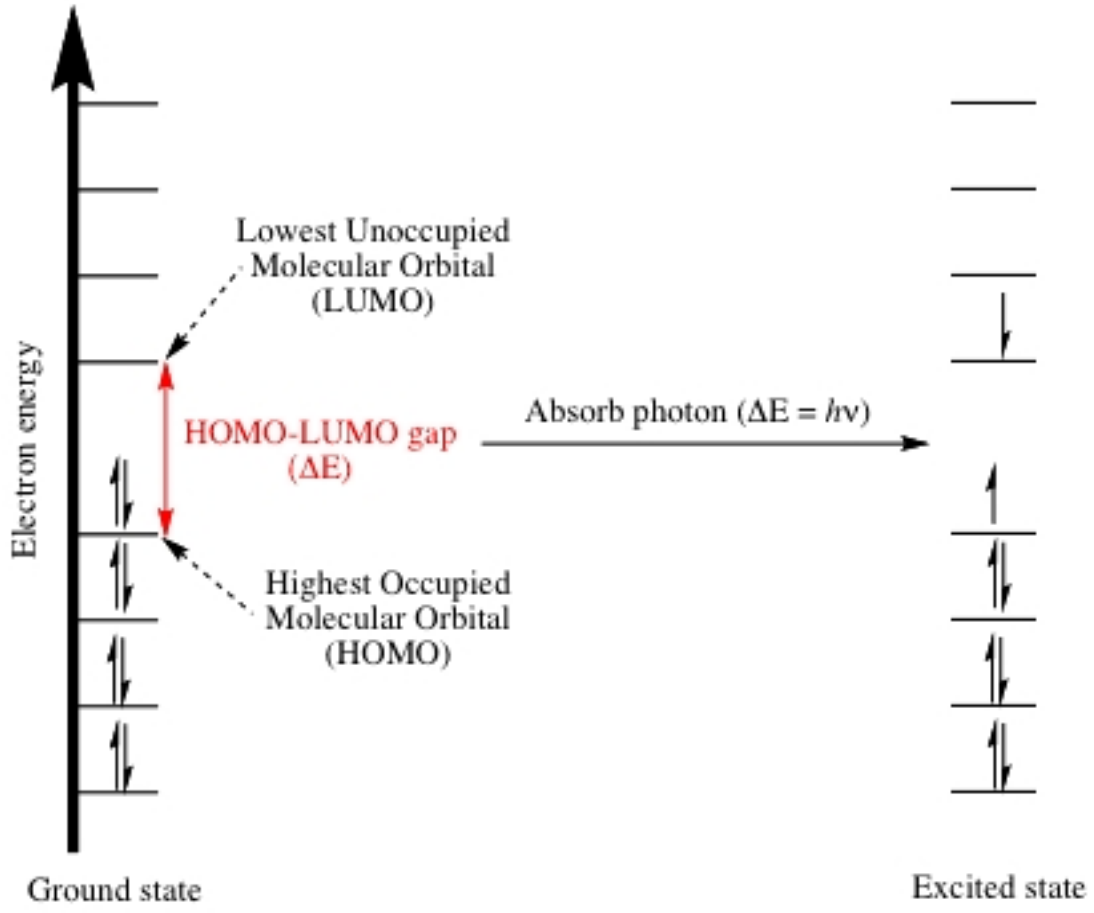

Figure 3.2.B4[14] HOMO – LUMO molecural orbitals in the ground state and, with the absoption of a photon, in an excited state.

HOMO is the highest occupied molecular (HOMO) level of the donor (quasi Fermi level of the holes) and LUMO is the lowest unoccupied molecular orbital (LUMO) level of the acceptor (quasi Fermi level of the electrons).

The following figure 3.2.B5 shows the optical transition in a typical organic solar cell in which the photoactive layer consists of two materials: an electron donor (such as a conjugated polymer) and an electron acceptor (such as fullerene derivatives). As we can see in the figure below a difference in energy level between polymer donor and acceptor is essential for efficient exciton creation (1) and electron transfer (2).

[14] Figure from http://www.chem.ucla.edu/harding/IGOC/H/homo_lumo_gap.html

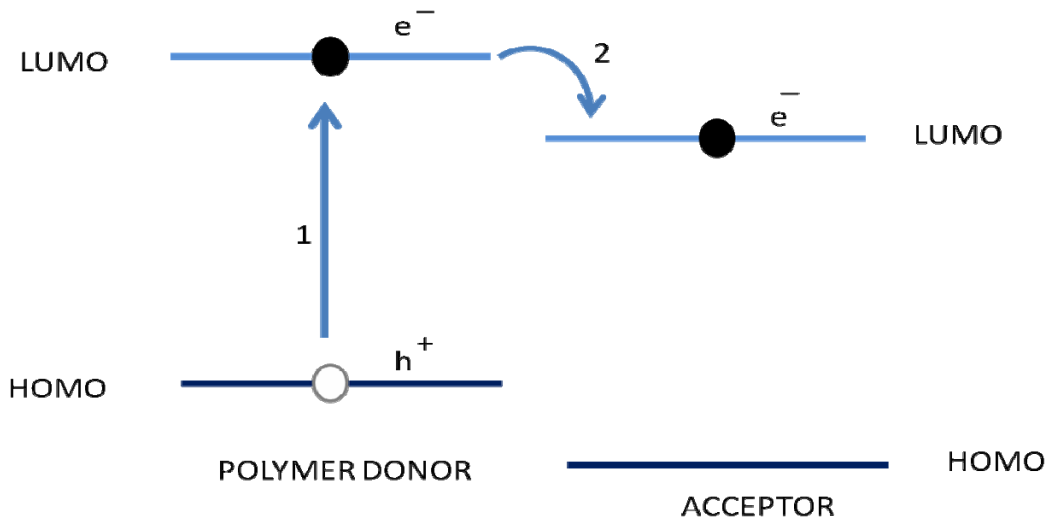

Figure 3.2.B5 Generation of free carriers (electron and hole) and transfer of electron to the acceptor material which is in less energy level.

3.3 Phthalocyanines

The family of phthalocyanines (Pcs) represents one of the most promising candidates for organic thin films as these systems offer excellent film growth properties as well as possessing advantageous optoelectronic properties and chemical stability, low cost, flexibility in functional group substitution and high tendency of self organization [22]-[29]. Pcs are particularly prominent in molecular solar cells. They have been used as important dyes and pigments since their synthesis at the beginning of the last century. In recent years, phthalocyanine derivatives have been used as charge carriers in photocopiers and laser printers and materials for optical storage. The semiconducting properties of single phthalocyanines have been studied since the 60's and in recent years there has been a renewed interest in small molecular films, their growth and electrical properties. Phthalocyanines are also used in Dye- sensitized solar cells. In addition, the fact that Pc's have similar structural relationship to chlorophyll, which performs the sunlight harvesting for the ultimate solar energy conversion process "photosynthesis", gives further encouragement to their use in solar cells.

Phthalocyanine (Pc) is a symmetrical 18 p-electron aromatic macrocycle of four iminoisondole units, closely related to the naturally occuring porphyrins. Like the porphyrins, the Pc macrocycle can play host to over seventy different metal ions in its central cavity and the choice of central metal cation can strongly influence its physical properties. Especially, the central cavity of phthalocyanines is known to be capable of accomodating 63 different elemental ions, including hydrogens (metal-free phthalocyanine, H_2-PC). A phthalocyanine containing one or two metal ions is called a metal phthalocyanine (M-PC). In the last decade, as a result of their high electron transfer abilities, M-PCs have been utilized in many fields such as molecular electronics, optoelectronics and photonics. More recently they have been employed in several 'hi-tech' applications such as the photoconducting material in laser printers and the light absorbing layer in recordable CDs. They are also used as photosensitisers in laser cancer

therapy, as nonlinear optical materials and as industrial catalysts. In photodynamic therapy of cancer they have been used as they have strong absorption in the infrared region (650-800nm). The name was conceived by the researcher Linstead[15] as a combination of the prefix phthal, originally from the Greek naphtha (rock oil) to emphasize the association with its various phthalic-acid- derived precursors and the Greek cyanine, blue. Their use as industrial colorants started in 1935 (manufacture of copper Pc), then Pcs are not found in nature. Another great application of phthalocyanines[16] is in molecular physics due to their stability. Therefore, for many new experimental techniques, they have bridged the gap between crystalline inorganic materials (e.g. metals and ionic crystals), originally used to develop the technique, and molecular materials.

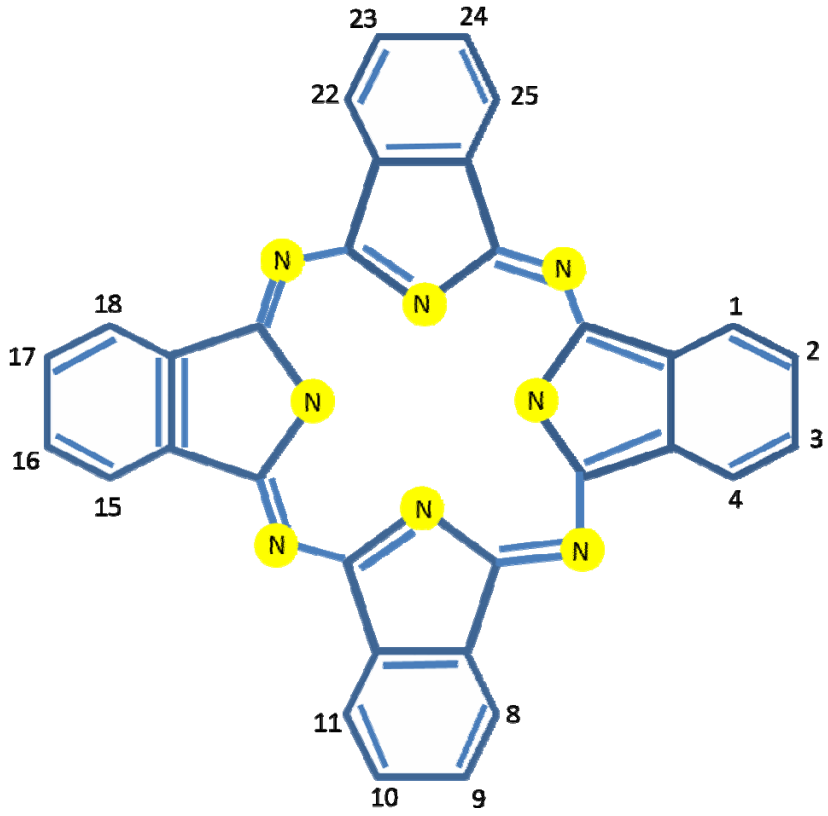

Figure 3.3.1 The structure of phthalocyanine with sixteen possible sites for macrocycle substitution at the benzo-positions: The 2,3,9,10,16,17,23,24 carbon atoms are termed the (p) peripheral sites and the 1,4,8,11,15,18,22,25 are denoted the non-peripheral sites (np).

[15] Researcher at the Imperial College Reginald P. Linstead (1902-1966).

[16] Pcs were accidentally found (1907 and 1927); research began after J. Monteath Robertson reported the first single-crystal structures of phthalocyanine complexes in 1935.

Phthalocyanine-based organometallic complexes used for DSSCs have reached conversion efficiencies of about 4% for monochromatic illumination. Metal Phthalocyanines MPcs are semiconductors with a band gap that depends on the metal bound in phthalocyanine molecule.

Some Metal Pcs are created with the following metals: Fe, Co, Ni, Cu, Zn, Mg and Pb [26]. The strongest absorption of M-PCs in the visible region, the so-called Q band, can be attributed to the allowed highest occupied molecular orbital (HOMO) → lowest unoccupied molecular orbital (LUMO) (π-π*) transition.

Pc materials are used in the two classical solar cell formations: p-n junction and semiconductor metal (Schottky) junction. The Schottky junction device of Pc are composed by a Pc film sandwiched between two electrodes. One of the metal electrodes with the relatively low work function Φ (its main characteristic is that it donates electrons readily) forms the Schottky junction. The other electrode with higher work function (gold-Au or Indium Tin Oxide) creates the Ohmic contact and serves to connect the device to an external circuit.

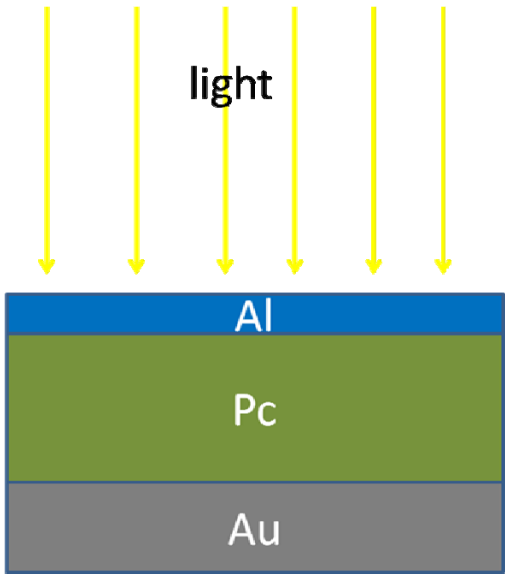

Figure 3.3.2 Schottky-junction of Pc film formed between the layers of Pc-Al and Pc-Au.

The creation of a p-n junction with organic compounds, most common Pc and perylene (Pe) derivatives as p-type and n-type semiconductors, respectively, produces greater light absorption over the entire solar spectrum. Phthalocyanine and perylene have common applications in thin film organic solar cells. Phthalocyanine is a p-type hole conducting material that works as electron donor, whereas perylene and its derivatives show a n-type, electron conducting behavior and serve as electron-acceptor material. In addition, phthalocyanines have advantages of using over porphyrins in a blended OPV. These are: wider spectral range, longer exciton diffusion lengths, and higher hole mobility.

3.4 Gallium Arsenide reconstructed surfaces

Gallium Arsenide substrates were used to deposit the lead phthalocyanine (PbPc) thin films and develop the solar cells studied in this work. Hence, it is important to refer to the reconstruction surfaces of GaAs [22], [30] and especially the two of them used for deposition.

GaAs is III-V semiconducting material and it is often used for the epitaxial growth of semiconductors. It has a direct band gap of 1,424eV at 300K which results in infrared emission at 870nm and its crystal structure is zinc-blende. Similar to Diamond (or Sphalerite), the zinc-blende structure consists of a face centered cubic (fcc) Bravais point lattice which contains two different atoms per lattice point. The distance between the two atoms equals one quarter of the body diagonal of the cube. Generally, the zinc-blende and the diamond structures are important because the majority of the semiconductors belong to these; for example, Si and Ge belong to diamond structure, while GaAs and ZnSe to the zinc-blende.

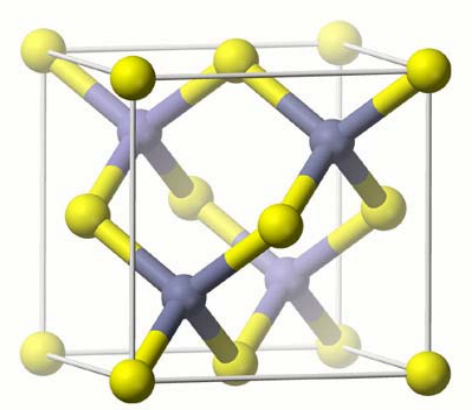

Figure 3.4.1 zinc-blende structure (yellow is Ga and purple As).

For the development of solar cells, in this work, we used GaAs (001) substrates; (001) are the direction indices - Miller's indices of GaAs.

The surfaces reconstructions of GaAs (100) we studied in our hybrid cells are:

- c(4x4) , As-anion rich surface
- β2(2x4), moderately As rich – stoichiometric surface

There are another 4 main reconstruction surfaces of GaAs (001):

- (2x6) , As rich
- α2(2x4) , moderately Ga rich
- ζ(4x2) , Ga rich
- mixed dimmer.

In Figure 3.4.5, the top views of GaAs (001) reconstruction surfaces used in the experiments as substrates are depicted. Empty (filled) circles represent Ga(As) respectively. Larger circles indicate the position of the atoms in the uppermost two atomic layers. Arsenides are toxic materials and possibly carcinogens.

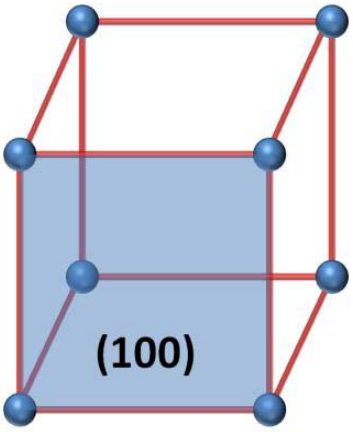

Figure 3.4.2 one of the three most important planes of a cubic cell (100)

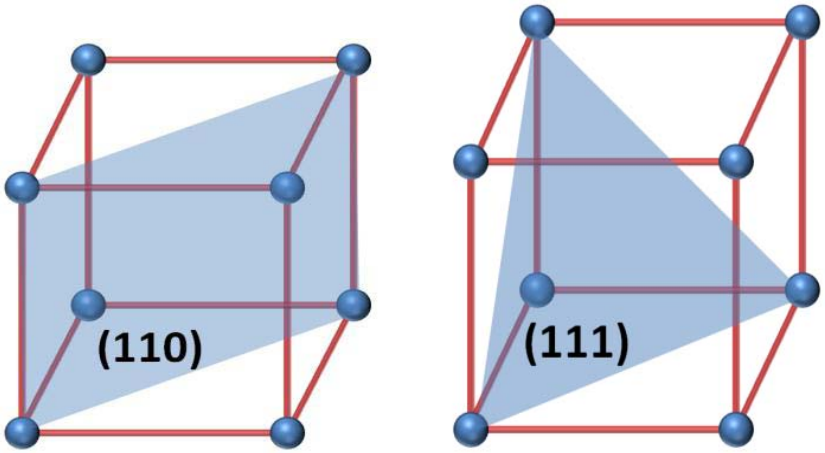

Figure 3.4.3 the other two important planes of a cubic cell (110) and (111)

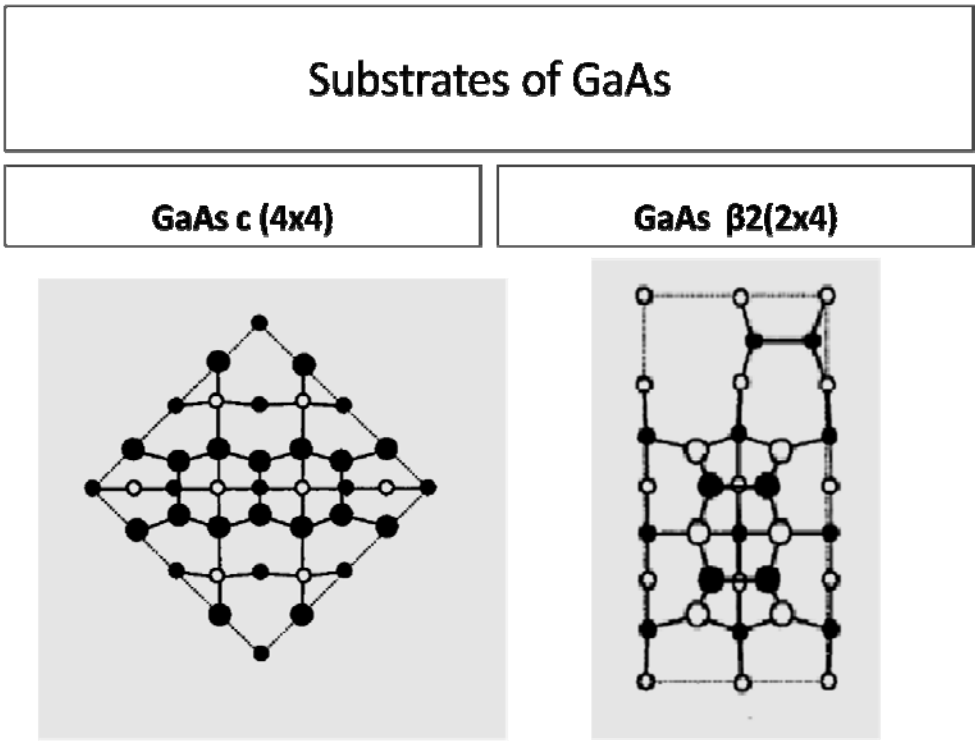

Figure 3.4.5 top views of GaAs (001) c(4x4) and β2(2x4)

C. Experiment

Electrical Characterization of PbPc/GaAs organic solar cells

4.1 Electrical Characterization set-up

The experimental set-up for the electrical characterization (I-V and EQE) of the two different solar cells of lead phthalocyanine ultra thin films of 20nm thickness deposited on two different reconstruction surfaces of GaAs, PbPc/GaAs(001)-c(4x4) and PbPc/GaAs(001)-β2(2x4), was operated in the laboratory of Professor Maurizio de Crescendi, in the Physics Department of the University of Rome "Tor Vergata". The efficiency of the developed solar cells was determined by measuring the photocurrent spectra. An optical set-up consisting of a Xenon spectral-lamp, a monochromator, focusing and collecting optics, a reflecting chopper, and lock-in electronics was used.

It is noted, that the spectrum of a Xe-lamp is very similar to that of the sun. The sun radiation can, therefore, be simulated to measure the solar cells.

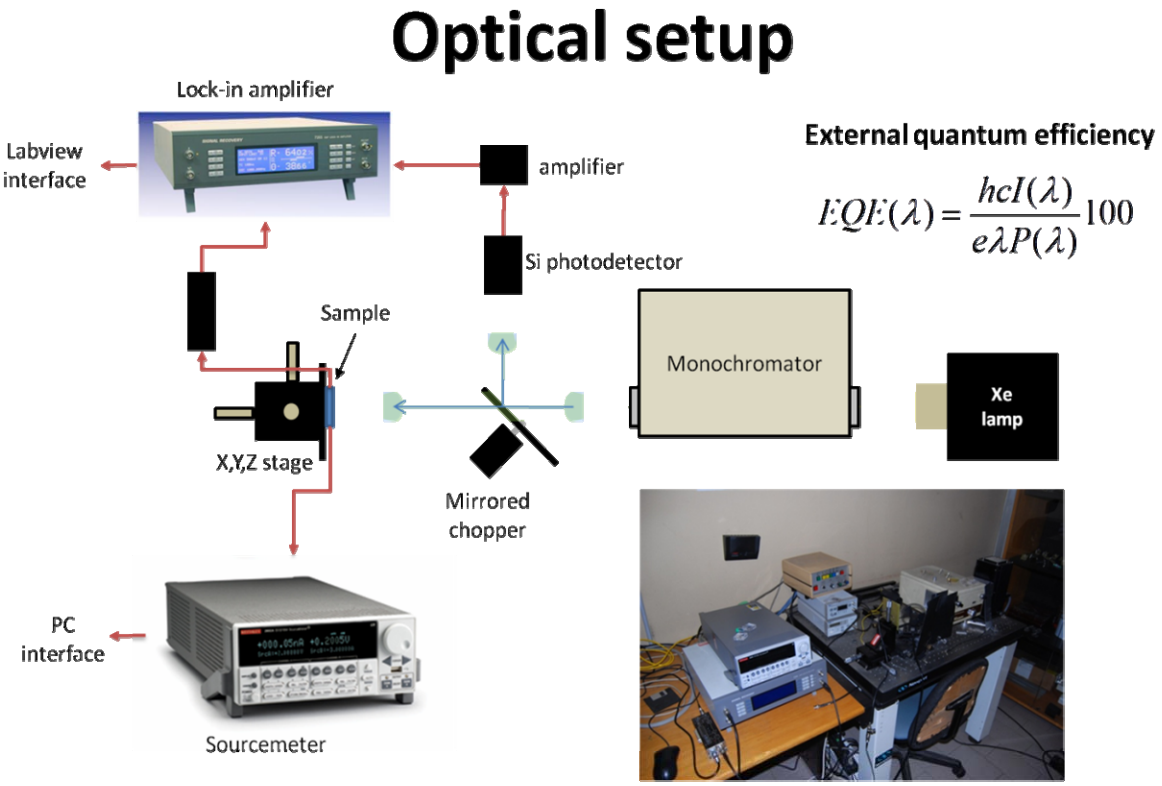

Figure 4.1.1 The experimental SET-UP used to determine the External Quantum Efficiency (EQE) of solar cells.

The operation-principle of a Xe spectral lamp is based on the excitation of the Xe gas atoms by an electrical discharge ignited by high voltage (1500V). The emitted light passes throught a monochromator scanning the entire wavelength range by a step of 5nm. After being monochromatized, the light is focused by a lens alternately, one time on the sample, and the next time on a silicon photodiode through the reflective chopper. Generally, a photodiode is a p-n junction that can convert light into current or voltage depending upon the operation. The Si-photodetector used (wavelength–range from 190nm to 1100nm) converts light into voltage. In this way, the reflective chopper, made from aluminium, allows the light one time to be focused on the Si-diode detector and amplified by lock-in electronics in order to measure the incident power and the other time to reach the sample. The light spot size on the sample was (0.5×3)mm^2. The sample absorbes the light and produces photovoltaic power. The photovoltage and the initially detected photodiode signal are compared and give the External Quantum Efficiency (EQE) of the sample. The equation of EQE is derived below. For allignment purposes, the sample holder is mounted on (x,y,z)-stage that can move the sample in all three directions.

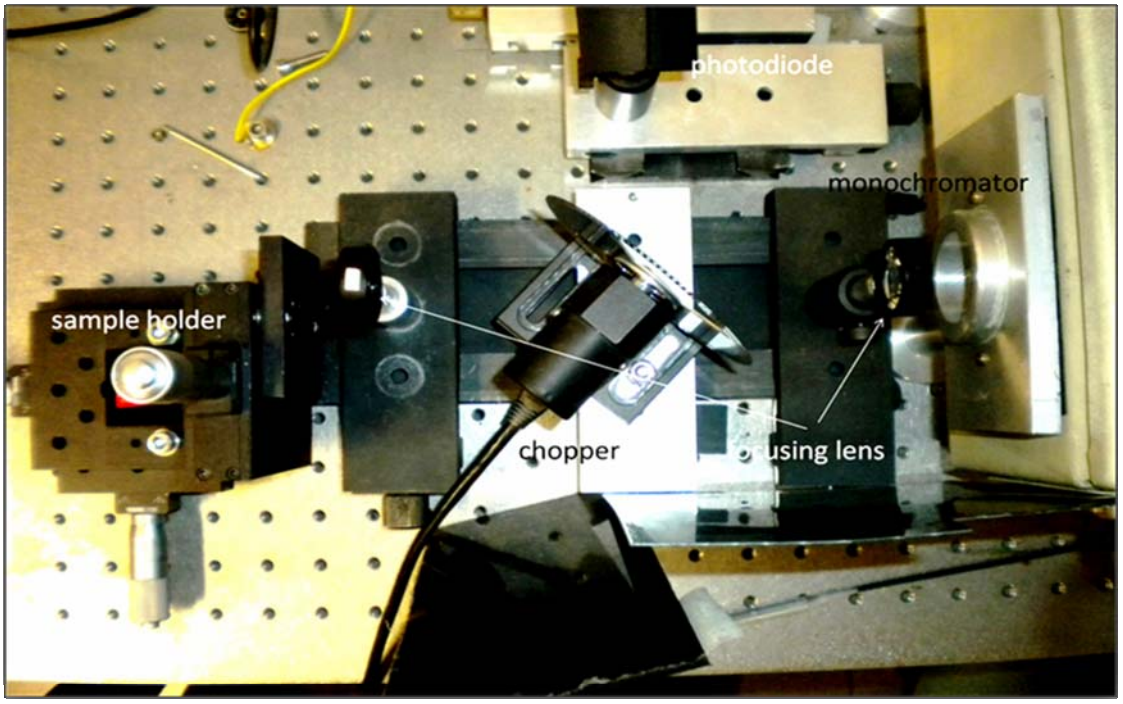

Figure 4.1.2 Detail of the experimental set-up of Figure 4.1.1 showing the two different paths of the Xe-lamp light: 1) focused by two lenses on the sample and 2) after the first focusing lens, it hits the reflective-chopper and is forwarded to photodiode detector.

The photocurrent generated by the sample was too small. A pre-amplifier was used to amplify it so that it could be measured by the lock-in electronics. The lock-in electronics eliminate the background steming from the diffuse light of the room (optical noise) and the electronics. The sourcemeter (Keithly Instruments) measures the I-V characteristic graphs. A low noise amplifier is needed in our experiment because of the low signal of our sample (micro amperes μA). In case of samples that give higher currents the low noise amplifier is not in use.

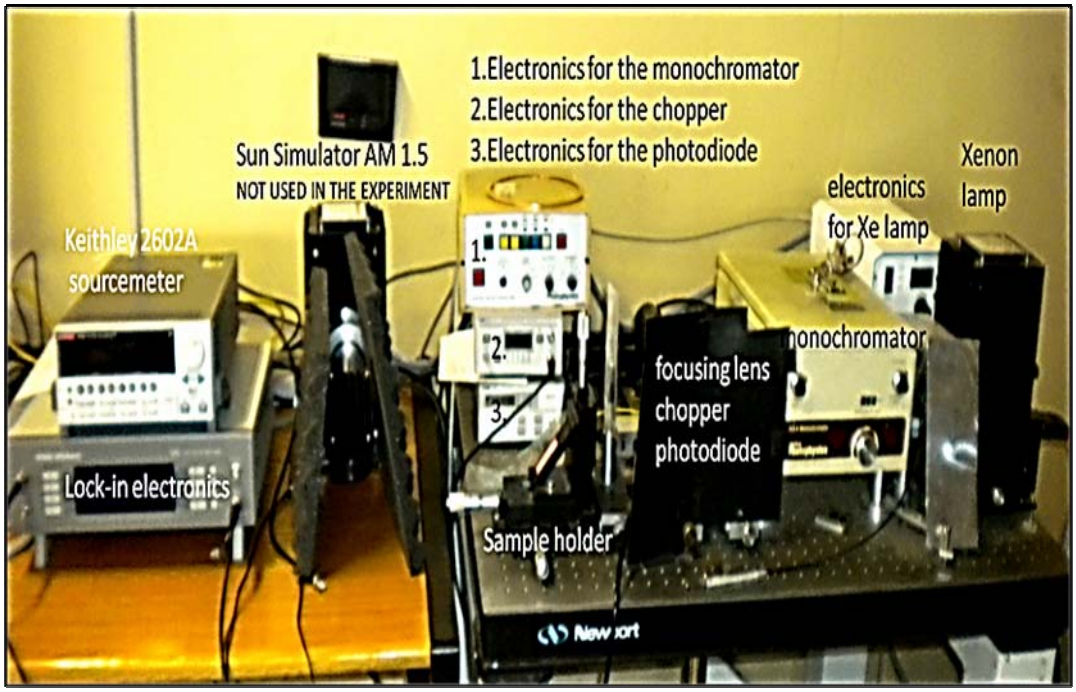

Figure 4.1.3 The experimental set–up used to measure the EQE of solar cells

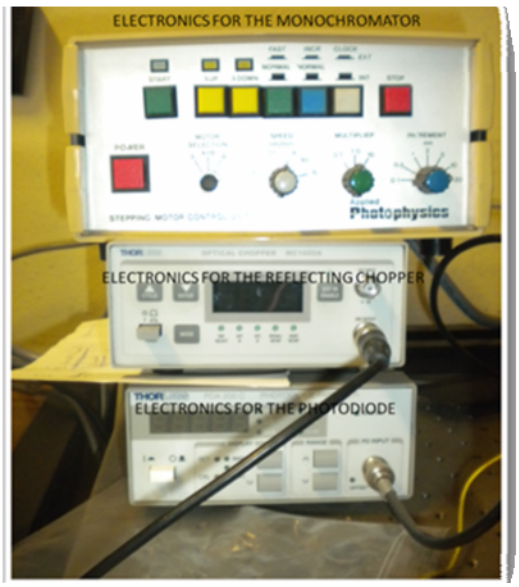

Figure 4.1.4 the electronics of the monochromator, the aluminum chopper, and the photodiode detector

Figure 4.1.5 lock-in electronics and source-meter

This instrumentation measures the I-V curves and the external quantum efficiency (EQE) of a solar cell. With EQE, the optical response of the sample for every wavelength is found, while with the I-V curves the following parameters of the solar cell are obtained:

1. short circuit current, Isc
2. open circuit voltage, Voc
3. maximum power point, MPP

Sample preparation

Electrodes from silver:

Metallic electrodes of silver (Ag) in solution (silver and solvent acetone which evaporated) were dropped on the sample PbPc/GaAs β2(2x4). Silver is used because it has good conductivity.

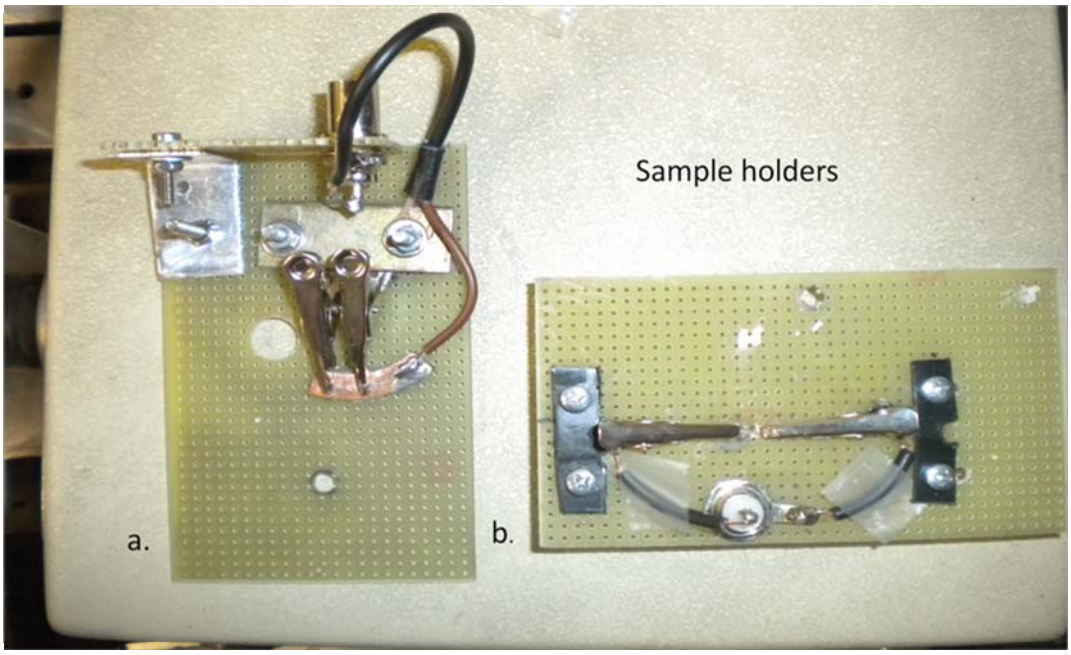

Figure 4.1.6 The first sample holder (a) is used for top- down configuration and the second (b) for planar configuration. These are the directions of current flow generated and are also designated in the following figures 4.1.7, 4.1.8.

The two different sample holders, in Figure 4.1.6, are used to measure different current flow in our samples. The sample holders are designed for measurements in two different configurations, e.g. perpedicular and parallel to the layer stack, as demonstrated in the following figures 4.1.7, 4.1.8: the top–down configuration and the planar configuration. Top–down configuration is when the current is collected form the bottom and the top electrodes at the same time, while in planar configuration, the current is collected from the top electrodes only. In these figures, the arrows point to the direction of the current flow. We study both configurations in order to extract, which configuration has better signal, and in accordance with that to optimize the way of harvesting solar energy.

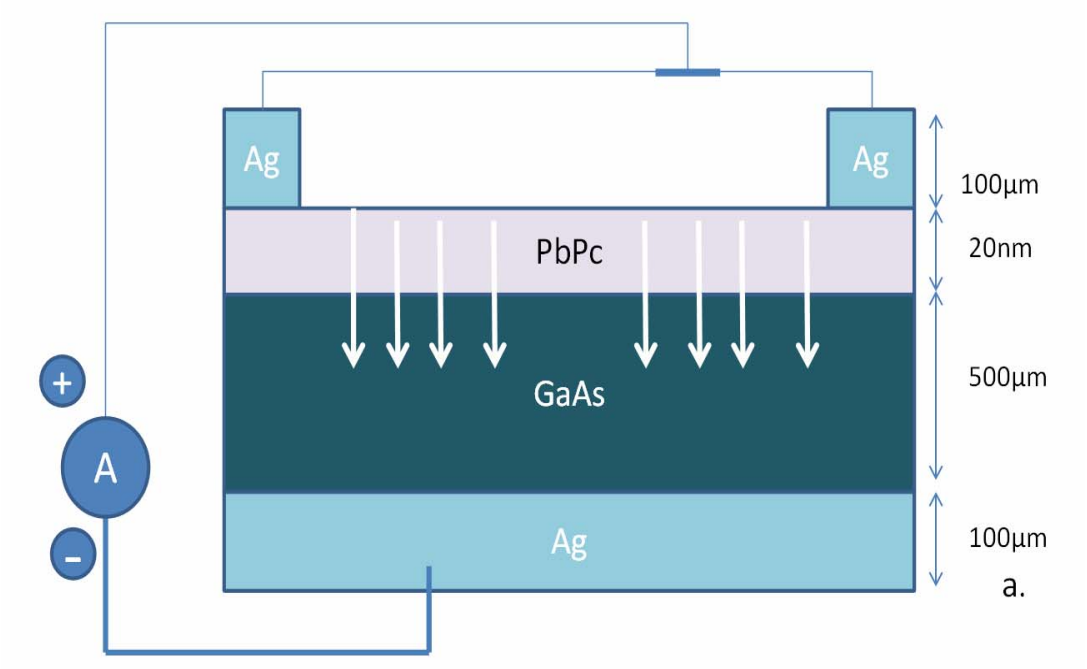

Figure 4.1.7 PbPc/GaAs solar cell in top-down configuration: GaAs is n-type (donor) and PbPc is p-type (acceptor). The front parts of Ag connected built the positive electrode and the bottom, the negative. In this configuration, the current flow is measured between the front and the bottom Ag-contact (white arrows depict the current flow).

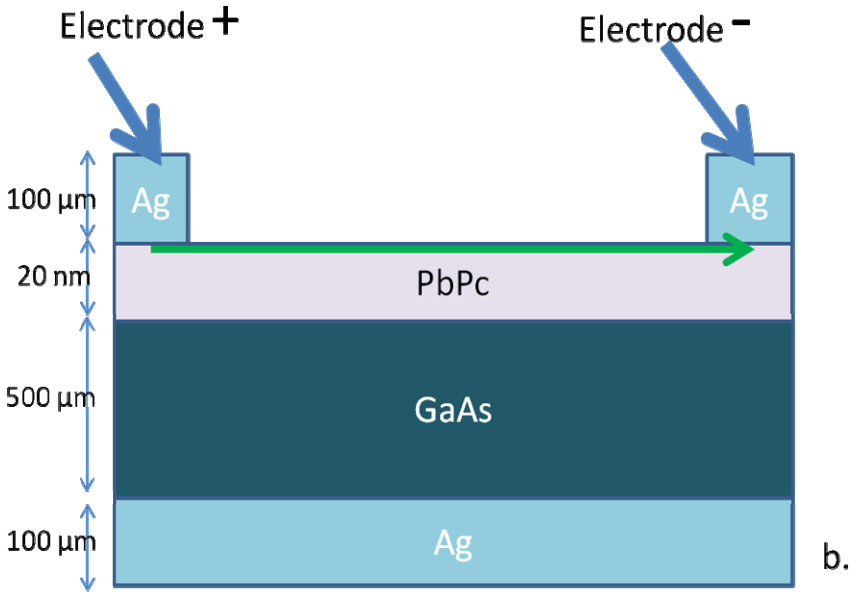

Figure 4.1.8 PbPc/GaAs solar cell in planar configuration. The direction of current flow through the layer of PbPc is depicted by the arrows. PbPc is the active layer for exciton generation; this layer contains the electrons that pass through the negative electrode to the external circuit and are collected back to recombine with the holes through the positive electrode.

The photocurrent density, I(λ), was measured under illumination as a function of the incident photon wavelength λ. The number of incident photons that contribute to current efficiency is defined as the fraction of the incident photons, N_{ph}, converted into photocurrent, i.e. the number of the generated $e^- - h^+$ pairs, $N_{e\text{-}h}$, multiplied by the electronic charge e^-. The number of the incident photons is then evaluated in terms of the power density of the Xe lamp, P(λ), since $N_{ph} = \frac{\lambda P(\lambda)}{hc}$. Therefore, the Incident Power Cell Efficiency (IPCE) is given by:

$$IPCE = (\%) = \frac{electrons}{photons} = \frac{100hc\, I(\lambda)}{\lambda P(\lambda)} \quad (4.1)$$

I(λ) was measured by modulating the light by an optical chopper and recovering the amplified current signal (converted to voltage) by a lock-in amplifier locked on the chopper frequency. The lamp power P(λ) was measured simultaneously in a similar way by a calibrated Si photodiode. The power density of the Xe-lamp ranges from 0,5 to 3 $mW\,cm^{-2}$ over the investigated spectral region. Using a Keithley 2602A source-meter, we recorded the current by focusing the light beam on several spots of the cell surface, at variable distance from the metallic contact electrode, at which the signal is measured and to which the bias can be applied both, in the dark and under illumination. In this way, we obtained the current–voltage curves. Generally, solar cells are measured in Standard Test Conditions (STC) which are: a temperature of 25 °C and an irradiance of 1000 W/m^2 with an air mass 1.5 (AM1.5) spectrum. These conditions correspond to a clear day with sunlight incident upon a sun-facing 37°-tilted surface with the sun at an angle of 41.81° above the horizon.

In addition, it is important to mention that many losses in the efficiency can be counted. These are:

1. Reflectance losses which are accounted for by the quantum efficiency value, as they affect "external quantum efficiency".
2. Recombination losses are accounted for by the quantum efficiency, V_{OC}, and fill factor values.
3. Resistive losses are predominantly accounted for by the fill factor value, but also contribute to the quantum efficiency and V_{OC} values.

4.2 Results

Current-Voltage (I-V) characteristics and External Quantum Efficiency (EQE)

Gallium Arsenide (GaAs) was measured in order to compare the photoresponce of the PbPc/GaAs with that of the GaAs substrate without coverage. The response was low as expected for the substrate. The substrate forms a Schottky junction due to the contact of Ag and GaAs. For this reason no linear dependence is observed with increasing negative voltage. In solar cells, Ohmic (instead of Schottky junction) should be warranted at the metal-semiconductor interface, so as the photocurrent should flow without resistance. The maximum power of the substrate was found to be 0,341nW. I-Vs of PbPc/GaAs β2(2x4) and PbPc/GaAs c(4x4) will be compared with the I-V of the bare GaAs-substrate and thus estimate how efficient our solar cells are and how much PbPc layers have ameliorate their efficiency.

a. GaAs (gallium arsenide) substrate graphs of dark current & under illumination

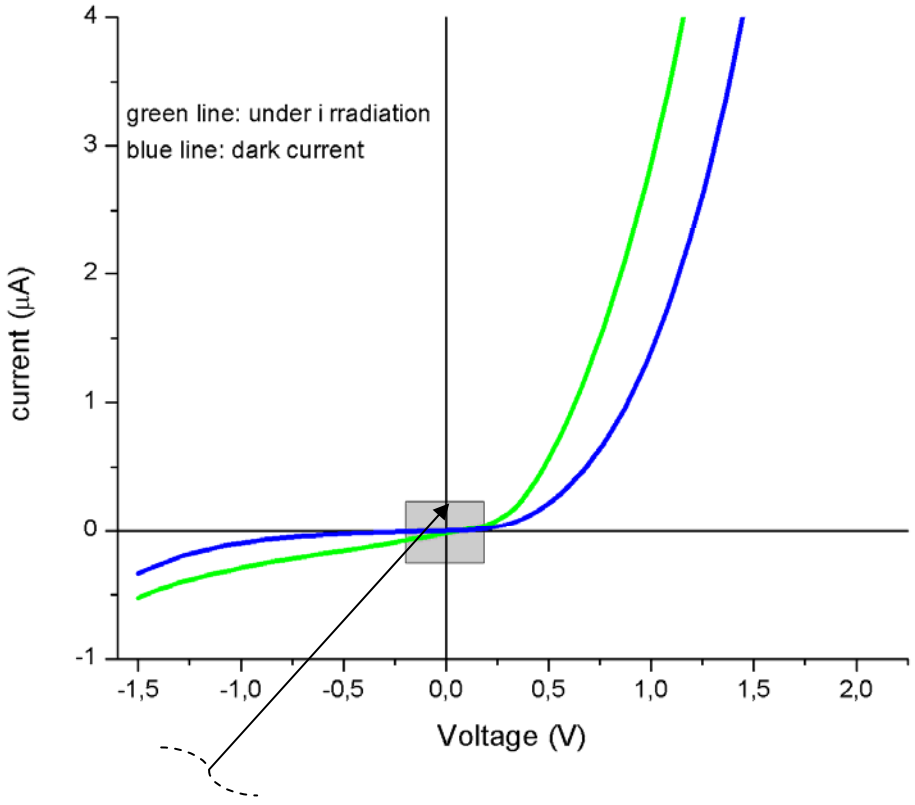

Graph 1. I-V of GaAs substrate in the dark and under illumination

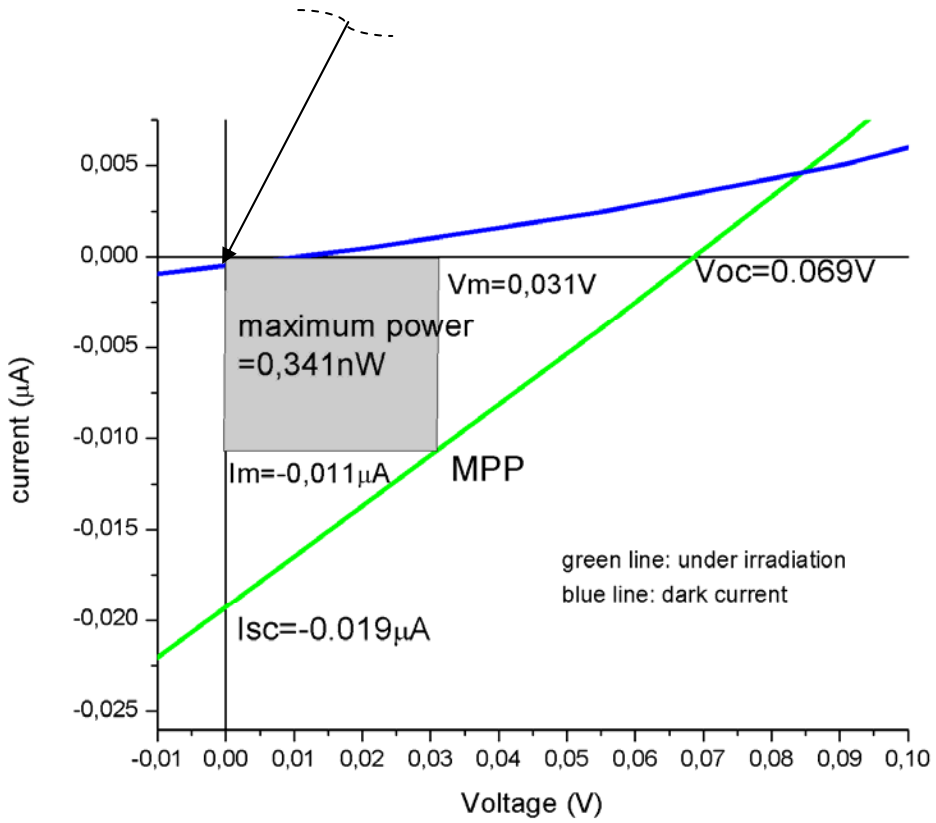

Graph 2. Details of the I-V of GaAs substrate in the dark and under illumination

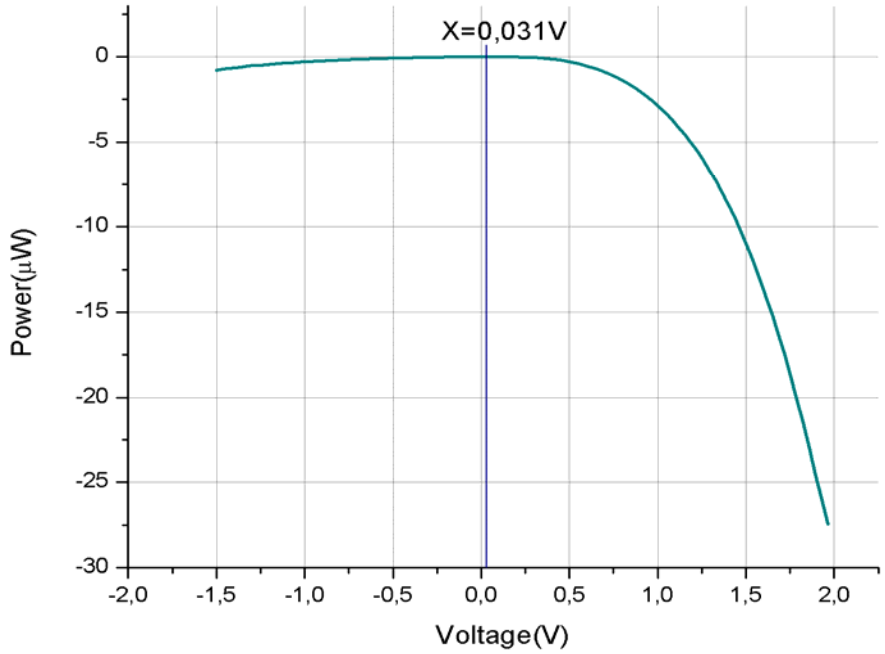

Graph 3. Power – Voltage of GaAs substrate: Vm=0,031V for the maximum power point

b. PbPc/GaAs β2 (2x4) graphs of dark current and under illumination

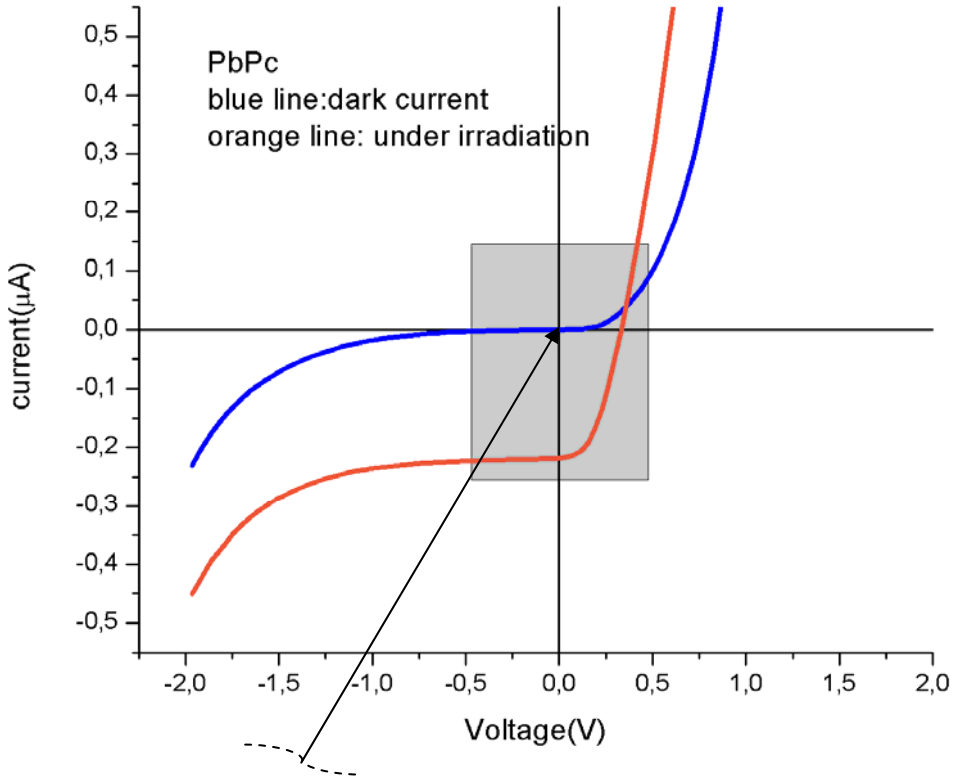

Graph 4. I-V of PbPc/GaAs β2 (2x4) in the dark and under illumination

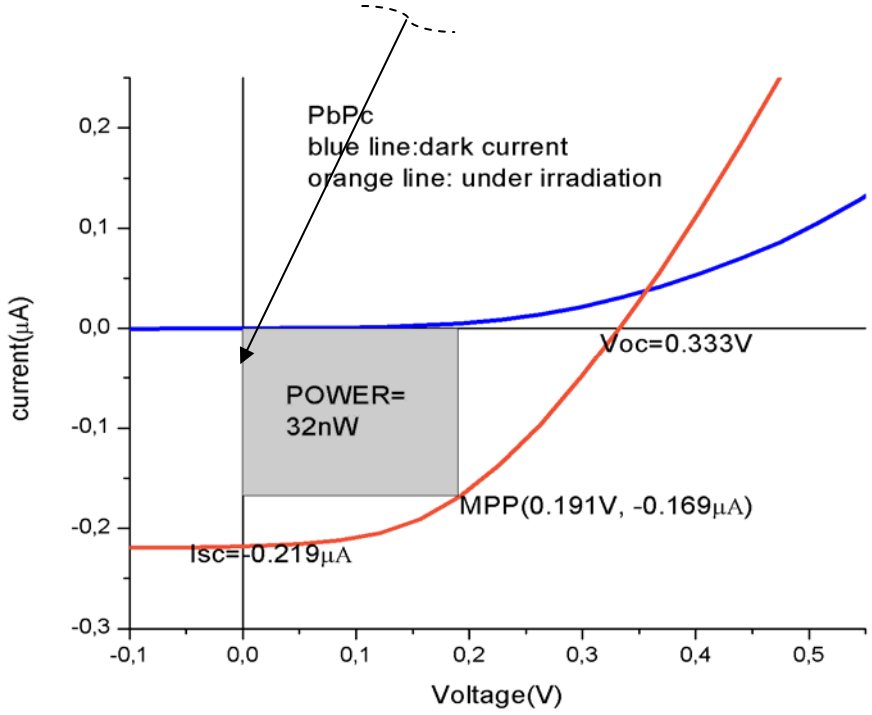

Graph 5 Details of the I-V of PbPc/GaAs β2 (2x4) in the dark and under illumination

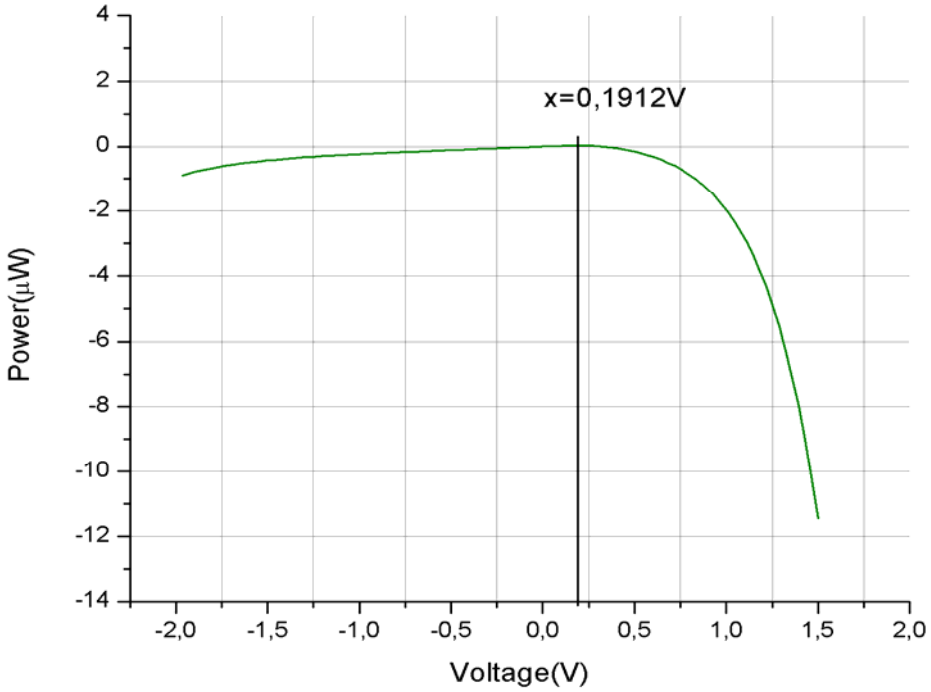

Graph 6 Power-Voltage of PbPc/GaAs β2(2x4): Vm=0,1912V at the maximum power point

Discussion of the graphs of PbPc/GaAs β2(2x4) top-down configuration

Graphs 4-6 depict the I-V curve of sample PbPc/GaAs (001)-β2(2x4). Measurements were performed in the dark (the blue curve), without illumination, and under illumination (the orange curve). For clarity purposes, the voltage region that provides information about the cell activity appears enlarged in Graph 5. The dark current curves pass through zero, while the I-V curve under illumination, at zero voltage, measures the short circuit current (I_{SC}). Short circuit current and open circuit voltage are two parameters that describe a solar cell and are marked in Graph 5. The area of the rectangle, in Graph 5, represents the maximum power. The respective current and voltage of the Maximum Power Point can then be obtained. For evaluation purposes, first, the power-in-relation-to-voltage characteristic curve is drawn to find the maximum power point, then the maximum power rectangle, and, at the end, I_{sc} and V_{oc} are estimated. The voltage at which we found the maximum power is Vm=0,1559V. The maximum power of the substrate is 0,341nW, while the maximum power of PbPc/GaAs β2(2x4) is 32nm (0,032μW), therefore, it is about two orders of magnitude higher than that of the bare GaAs substrate.

Graph 4 is indicative of a double diode behavior (see the figure below) as the exponential curves show the characteristics of a double diode behavior. This is due to the presence of another junction beyond the PbPc – GaAs Schottky junction. The other Schottky junction emerges between GaAs and Ag. Instead of an Ohmic junction, another Schottky junction is formed, especially in the top-down configuration. Generally, high performance solar cells have Ohmic junctions at all their electrodes and the I-V, at negative voltages, is parallel to the voltage-axis.

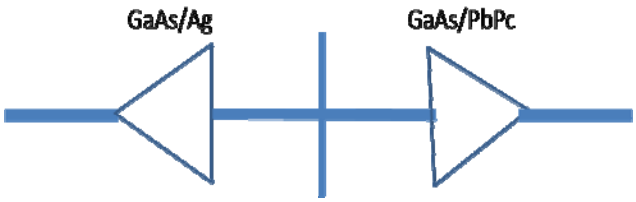

Figure 4.2.1 double diode behavior. The phenomenon of a double diode behavior is due to two continuous and different junctions.

c. PbPc/GaAs c(4x4) - Au graphs of dark current and under illumination

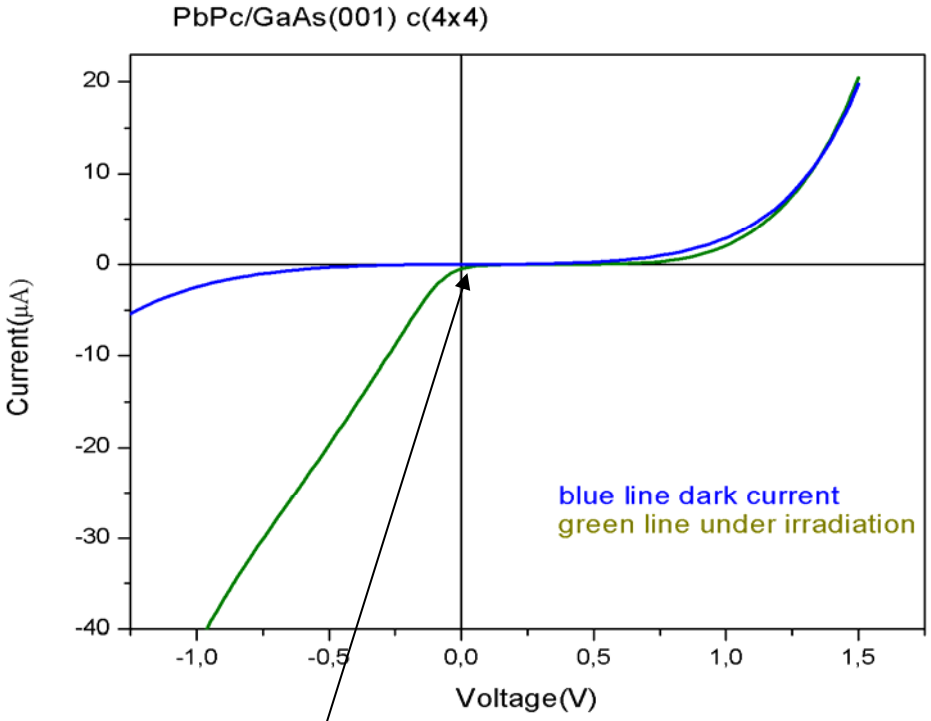

Graph 7 I-V of PbPc/GaAs c(4x4) – Au in the dark and under illumination

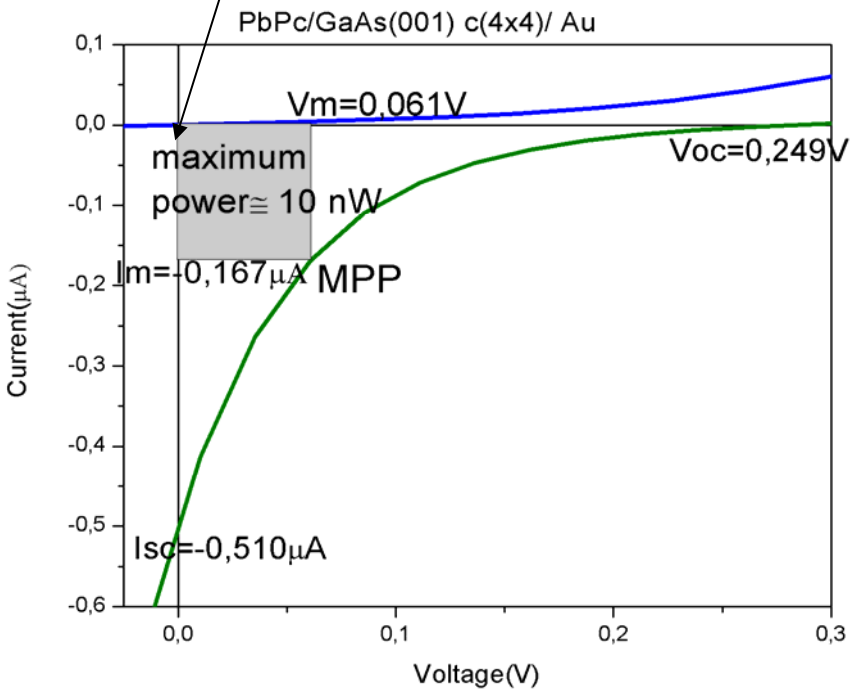

Graph 8 Details of the I-V of PbPc/GaAs c(4x4) – Au in the dark and under illumination

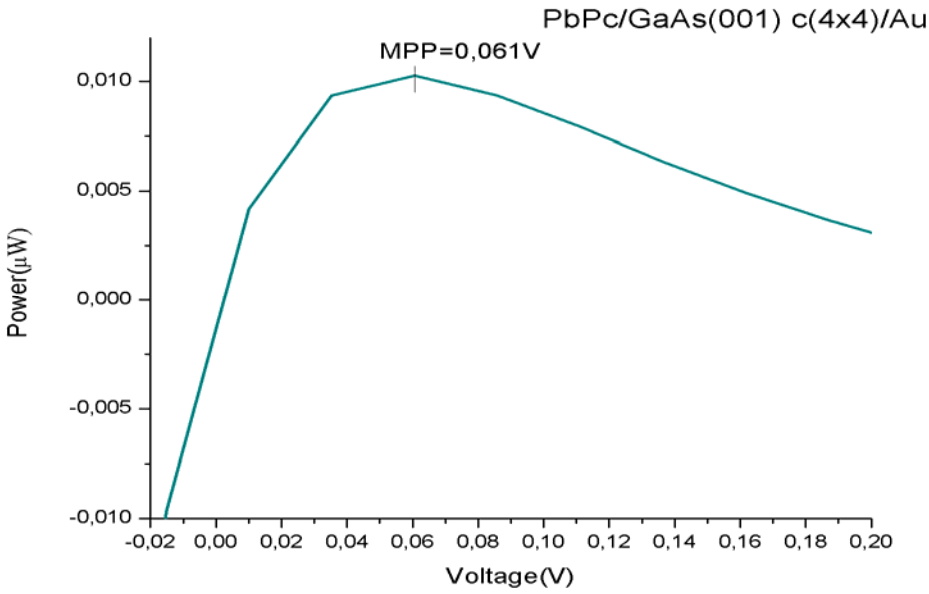

Graph 9 Power-Voltage of PbPc/GaAs c(4x4) – Au: Vm=0,061V at the maximum power point

Discussion of the graphs of PbPc/GaAs c(4x4) top-down configuration

Graphs 7-9 depict the I-V curves of sample PbPc/GaAs c(4x4) in the top-down configuration. Measurements were performed in the dark (the blue curve) and under illumination with white light (the green curve). Gold contacts were used to increase the conductivity of the sample; however, the evaporation of gold may have led to a short circuit, as can be seen with respect to the first curve (the blue one). In fact, the behavior of the sample, in the dark, is a line with very low current although a voltage of 1,5 V was applied.

On the other hand, the I-V under white light illumination (green curve) indicates a double diode behavior of the sample. This behavior leads to a small value of Fill Factor and, thus, a small value of cell efficiency η.

Summary: Calculation of efficiencies

The Fill Factor and the efficiency of GaAs, PbPc/GaAs β2(2x4), and PbPc/GaAs c(4x4) are calculated in the following. The formula are

$$FF=\frac{I_m V_m}{I_{SC} V_{OC}} \quad (4.2.1) \qquad \eta=FF\frac{I_{sc} V_{oc}}{P_S} \quad (4.2.2)$$

I_m and V_m are the current and the voltage of the maximum power point, MPP. Ps, the power of the source, is given for the Xenon lamp equal to 21mW.

Table 1. Fill Factor and Efficiency of GaAs, PbPc/GaAs β2(2x4), and PbPc/GaAs c(4x4)

Pinc=21mW *I(μA), V(V)*	*Fill Factor %*	*η (efficiency)%*
1.GaAs ***Im=-0,011 Vm=0,031*** ***Isc=-0,019 Voc=0,068***	***26,4***	***0,016*** **x10^{-4}**
2.PbPc/GaAs β2(2x4) ***Im=-0,191 Vm=0,169*** ***Isc=-0,219 Voc=0,333***	***44,3***	***1,537*** **x10^{-4}**
3.PbPc/GaAs c(4x4) ***Im=-0 ,167 Vm=0,061*** ***Isc=-0,510 Voc=0,249***	***8,0***	***0,485*** **x10^{-4}**

The calculations are rounded in the last digit. The results imply that the maximum Fill Factor and Efficiency are observed on the sample PbPb/GaAs β2(2x4).
The enhancement factor is given by the formula

$$\frac{f_2 - f_1}{f_1} 100 \quad (4.2.3)$$

f_2 relates to the parameters of the higher fill factor/efficiency sample and

f_1 to the parameters of the lower one.

Thus, comparing PbPb/GaAs β2(2x4) and GaAs substrate, we find that the Fill Factor enhancement is ***67,8 %*** and the efficiency enhancement is ***95,1 %***. The PbPc/GaAs has increased very much those factors compared to bare GaAs. The maximum efficiency of PbPc/GaAs β2(2x4) is ***1,537*** **x10^{-4} %**; it is very low compared to the less efficient polymer based organic solar cells with maximum efficiency 3,0%. It can be improved with the methods described in the following. By comparison of the two samples of PbPc on the two different substrates of GaAs(001), it is evident that PbPc on GaAs β2(2x4) is more efficient than PbPc on GaAs c(4x4). This is partially due to the layer of gold (Au) deposited on the sample that did not bring the expected results. On the contrary, it has probably produced a short circuit in our solar cells. The enhancement of the efficiency of sample 2 compared to sample 3 is more than double. We cannot directly compare PbPb/GaAs c(4x4) and GaAs substrate, as the deposition of gold (Au) affects mainly PbPc/GaAs c(4x4) - Au and not its substrate. It is advisable that more research is done on those combinations with stable parameters.

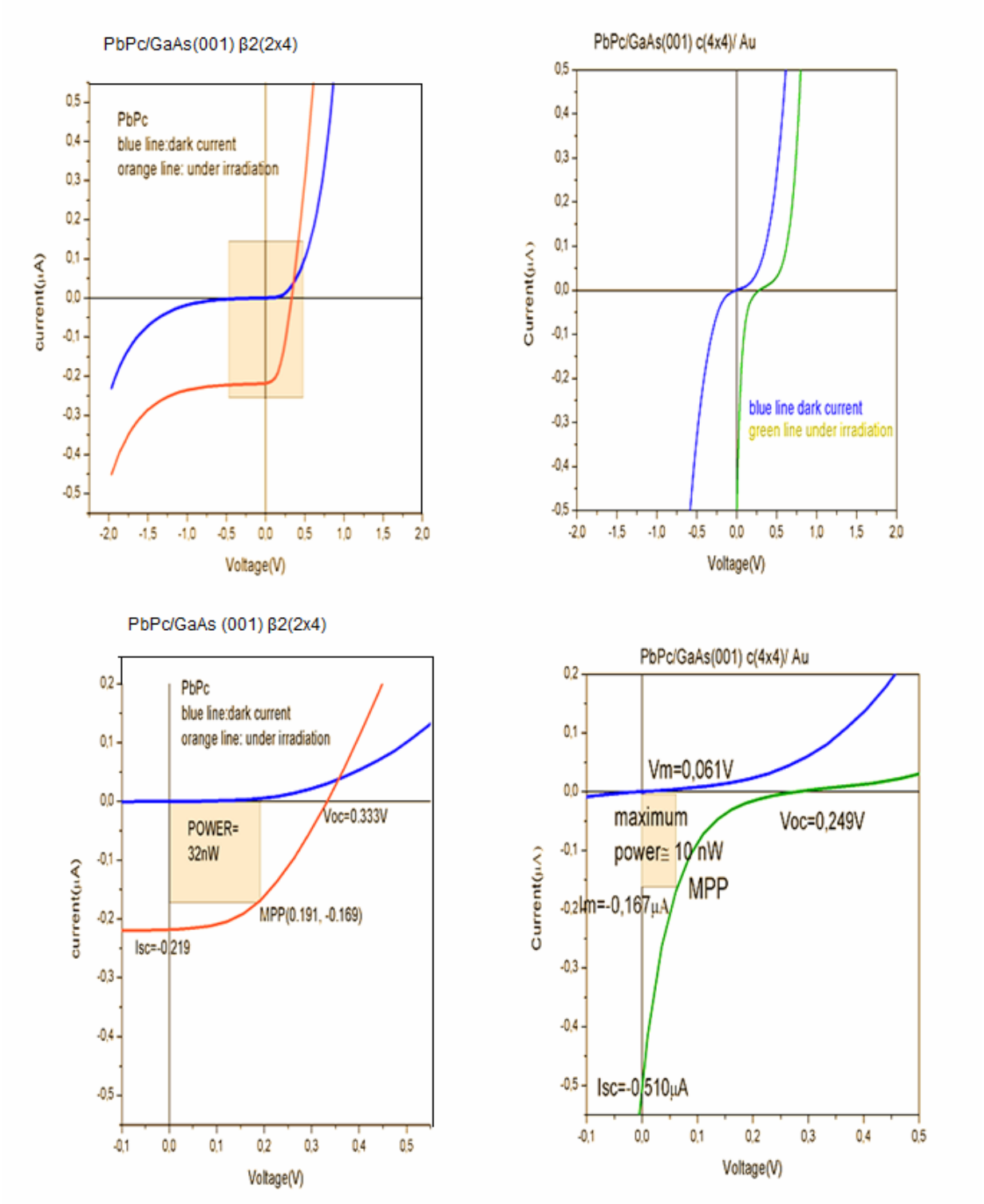

Graph 10. Comparison of the I-Vs of PbPc on GaAs β2(2x4) and PbPc on GaAs c(4x4)

d. External Quantum Efficiency of lead phthalocyanine layers on different reconstructions of gallium arsenide

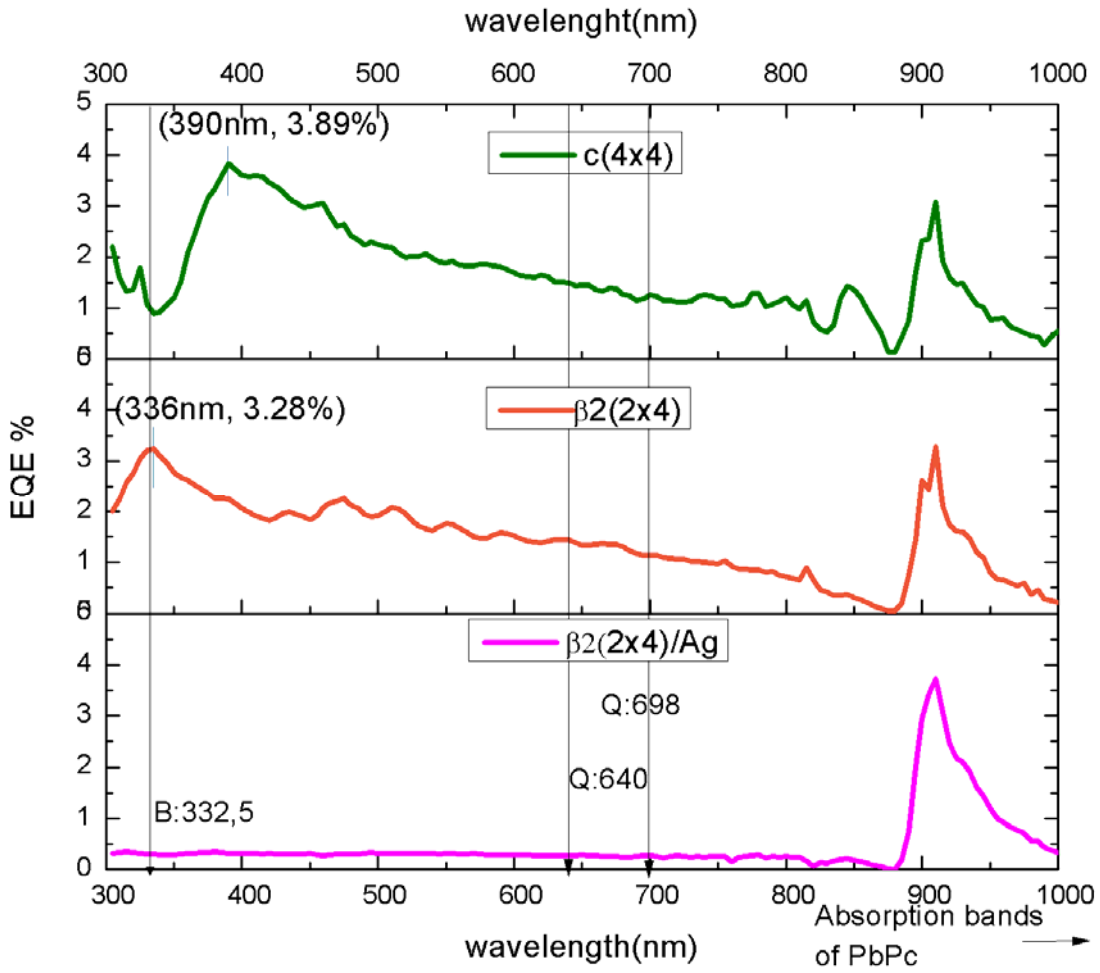

Graph 11. Spectral efficiency (EQE) of PbPc/GaAs c(4x4), PbPc/GaAs β2(2x4), and PbPc/GaAs β2(2x4)/Ag

The EQE gives the percentage of electrons generated in the sample by the incident photons.

$$EQE = \frac{number\ of\ e^-}{number\ of\ photons} 100 \quad (4.2.4)$$

The formula used for wavelength – energy conversions in the following are:

$$\text{Wavelength } (\mathring{A}) = \frac{12408}{E(eV)} \quad (4.2.5) \text{ and derives from } E=hv=\frac{hc}{\lambda} \quad (4.2.6),$$

$c=3*10^8$ m/s, $h=6{,}626\ 10^{-34}$ J*s=4,136 eV*s,

$$E= \frac{12{,}408 \bullet 10^{-7}}{\lambda(nm)} \quad (4.2.7)$$

The band at 900-1000nm (infrared λ>700nm) is an artifact induced by the Xenon lamp and appears in all three graphs.

The band gap energy of GaAs (E=1,424 eV at T=300K) is located at 870nm (871,34nm), which is observed in the first spectrum. In the other two spectra, EQE converges to zero at this wavelength.

In the ultraviolet and violet region, the phthalocyanine is the major contributor to the EQE, while, in visible, the EQE response is dominated by the absorption of GaAs.

In the first two spectra, it can be seen, how the substrate orientations change the photo-response of the sample. In fact, the maximum EQE for the sample with c(4x4) reconstruction surface is at 390nm (E= 3,18eV), while for the sample with β2(2x4) reconstruction surface is shifted towards the ultraviolet region λ<336nm. In the EQE spectrum of the sample with substrate orientation β2(2x4), the band 336 nm (E=3,69 eV) corresponds to the B band of the absorption spectrum of lead phthalocyanine. There are no peaks related to the Q band of lead phthalocyanine although the Q band is more intense than the B band, as shown in following Figure 4.2.2. In both samples, the maximum EQE is (3,5±0,5)%. The EQE analysis shows that both samples have almost the same photo-response and produce the same current.

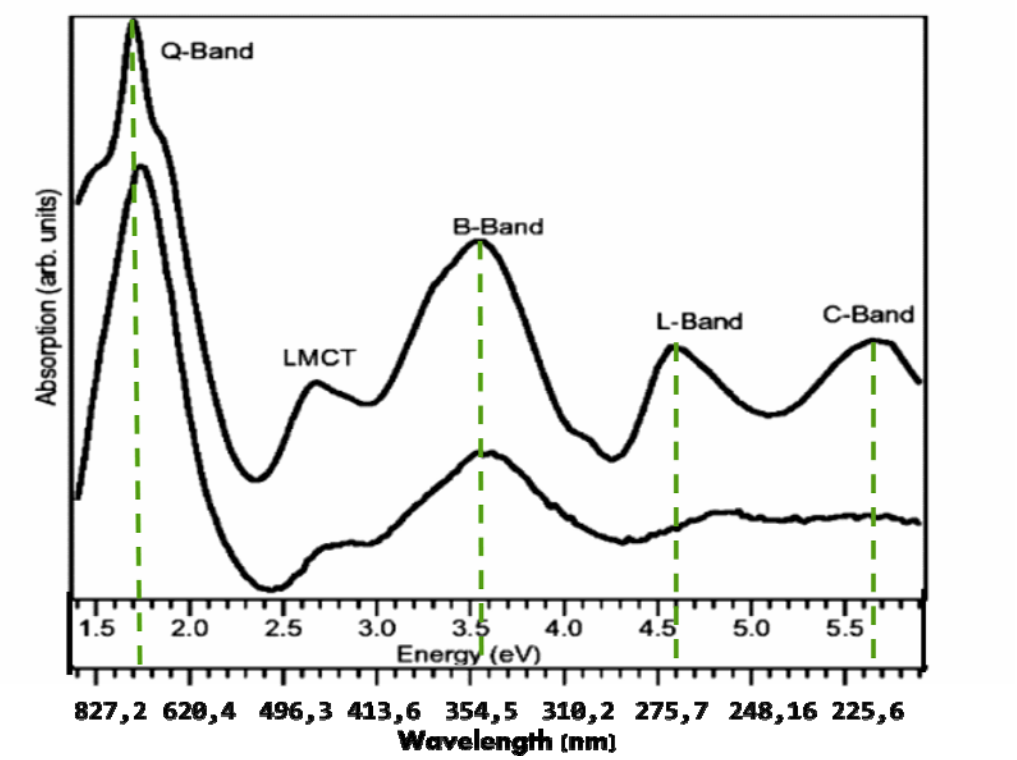

Figure 4.2.2 The upper curve is the UV-VIS absorption of the family of phthalocyanines. The second curve is the Low Energy loss Spectrum. This spectrum applies to the whole family of phthalocyanines except of the LMCT peak which is unique for every phthalocyanine.

Graph 11, includes also the EQE spectrum of the sample where more silver paint was deposited to improve the contact. There is no photocurrent generation due to the excess of the metal silver deposited. In fact, silver prevents the incident light to reach the photoactive junction between phthalocyanine and GaAs, because it reflects and/or absorbs the light. This “light attenuation” through silver does not produce photocurrent because excitonic lifetimes are too short to separate and collect electrons and holes.

In order to improve the solar cell efficiency we have to

1. *create an Ohmic contact at the bottom and top electrode.*
   This can be done with the usage of an intermediate material between GaAs and Ag with a work function similar to the work function of GaAs. Commercial solar cells have Ohmic junctions between their electrodes and the semi-conductive material. The double diode behavior, as demonstrated in Graph 4, is due to the failure to create an Ohmic junction. With an Ohmic junction, the I-V at negative voltages will be aligned parallel to the Voltage-axis.

2. *reduce the series resistance.*
   The reduction of series resistance will increase the power generated by the solar cell.
   a. More electrodes (in a grid-like structure) can be brought at the front to collect more electrons, as shown in the following figure 4.3.1. In this way, the path of an electron collected and transferred to the external circuit is smaller, therefore, the resistance too.
   b. Generally, the thickness of the phthalocyanine layer is 25nm-300nm. The thickness of this layer in our samples was 20 nm. Experiments can be done with thicker layers for the reduction of the resistance.

4.3 Improvements of the cell-structure

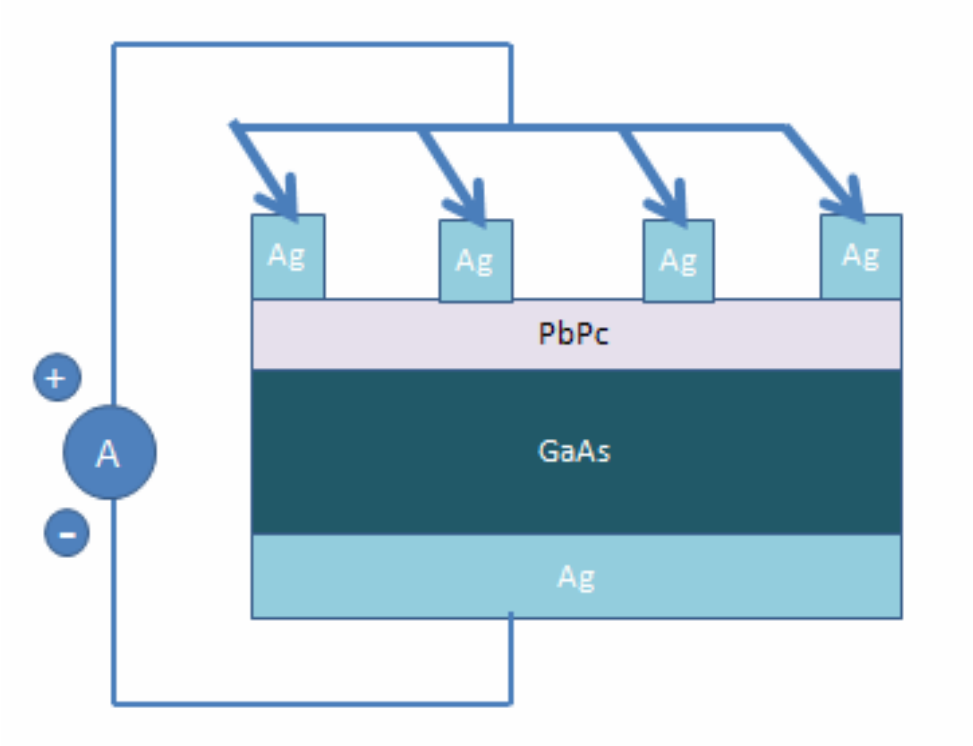

Figure 4.3.1 More electrodes can be used at the front contact (in a grid-like structure) to improve the efficiency of a solar cell

Generally, in our solar cell structure PbPc/GaAs(001), electrons from PbPc should be collected at the top Ag electrodes and electrons from GaAs at the bottom Ag layer. However, the top electrodes, we put, were in liquid phase and they may have penetrated the layer of PbPc creating a direct contact with the GaAs, therefore, result in a short circuit. This decreases the performance of our sample by reducing the Open Circuit Voltage. A possibility to avoid the short circuit is to put an intermediate layer between Ag and GaAs, as presented in the following Figure 4.3.2.

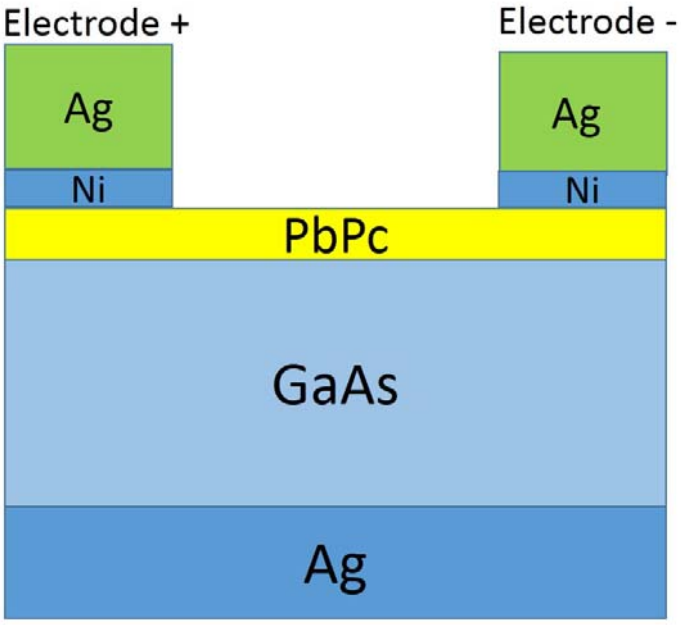

Figure 4.3.2 An intermediate layer (for example Ni) can be inserted between electrodes and PbPc to avoid the short circuit Ag-GaAs.

Conclusive Remarks

The samples of PbPc/GaAs(001) studied produced low efficiency in comparison with the lowest efficiency of 3% that organic solar cells usually exhibit. Further research with variation of the material and device parameters is required as the combinations we used are only start attempts for controlling the properties of organic solar cells through the substrate orientation.

D. Experiment

Optical characterization of PbPc free molecules – Raman spectroscopy

5.1 The Raman Effect

The Raman Effect is observed by the interaction of light and matter [32]-[33]. The scattering of light, as a result of its interaction with matter, can be classified as elastic (Rayleigh or Mie-Tyndall scattering) or inelastic (Raman or Brillouin scattering). In elastic scattering, the scattered light is observed at the same frequency as the incident light. In the second case of inelastically scattered light, this is detected at different frequencies of the incident light and constitutes the Raman or Brillouin spectrum of the sample.

The phenomenon of inelastic scattering of light was first predicted theoretically by Smekal[17] in 1923 and first observed experimentally (in liquids) by Raman[18] and Krishnan in 1928, therefore, it is referred as the Raman Effect since then. In the original experiment, sunlight was focused by a telescope onto a sample which was either a purified liquid or a dust free vapor. A second lens was placed after the sample to collect the scattered radiation. A system of optical filters was used to show the existence of scattered radiation with an altered frequency of the incident light, -the basic characteristic of Raman spectroscopy.

In molecules, Raman scattering deals with the interaction of vibrational and/or rotational motions of the molecules with the electromagnetic radiation. Brillouin scattering involves the translational motion of molecules and produces very small frequency shifts which have not yet yielded important applications.

In Raman inelastic scattering process, the two photons are not identical and there is a net change in the state of the molecule. When the created photon is less energetic than the annihilated one, the scattered light is observed at a lower frequency than the incident light. This is Raman-Stokes scattering. When the created photon is more energetic of the two, the Raman frequency will be higher than that of the laser and the anti-Stokes spectrum will be observed.

The scattering process described above is illustrated in Figure 5.1.

---

[17] Adolf Gustav Stephan Smekal (September 12, 1895, Vienna, Austria — March 7, 1959, Graz, Austria) was an Austrian theoretical physicist, with interests in solid state physics, known for the prediction of the inelastic scattering of photons.

[18] Sir Chandrasekhara Venkata Raman (7 November 1888 – 21 November 1970) was an Indian physicist whose ground breaking work in the field of light scattering earned him the 1930 Nobel Prize for Physics.

The laser excitation at a frequency ν_0 reappears as the relative strong Rayleigh line. The much weaker Raman 'sidebands' are the result of inelastic scattering by a molecular vibration ν_v. The efficiencies of these scattering processes are very low. In order of magnitude, the intensity of the Rayleigh line is about 10^{-3} with respect to the incident excitation, while Raman features are at least another factor 10^{-3} weaker.

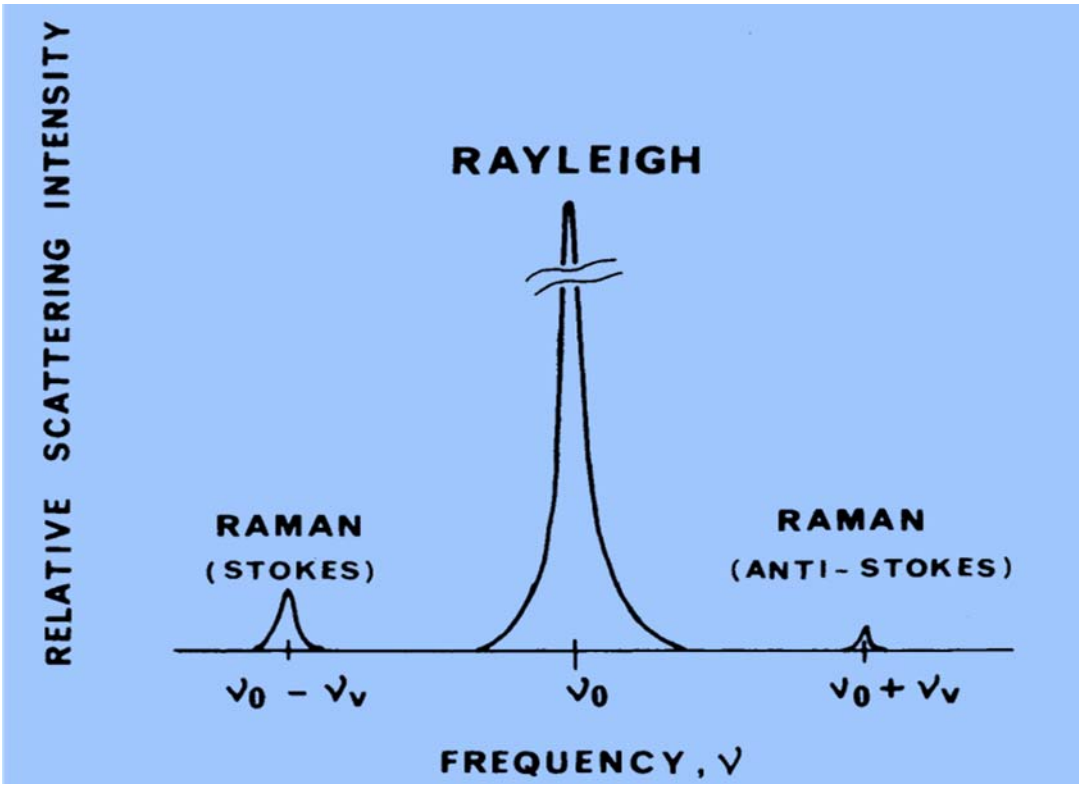

Figure 5.1 Raman and Rayleigh scattering of excitation at a frequency ν_0. A molecular vibration in the sample is of frequency ν_v.[19]

Raman scattering and infrared absorption are two of the main spectroscopic techniques to detect vibrations in molecules. They are used to provide information on chemical structure and physical properties, to identify substances from the characteristic spectral patterns (the 'Raman fingerprint'), and to determine quantitatively or semi-quantitatively the amount of a substance in a sample.

The important characteristics of Raman spectroscopy are related to two fundamental optical considerations: the focusing of the excitation laser beam on the sample and the collection of the scattered light. Raman spectroscopy uses a single frequency of radiation to irradiate the sample and the radiation scattered from the sample is detected shifted in energy with respect to the energy of the incident beam.

[19] Figure of the book 'Raman Microscopy' of George Turrell, first chapter 'Raman Effect'.

5.2 Raman spectroscopy- Theory

The theory of Raman spectroscopy will be further discussed in this chapter.

The interaction of light and matter can lead to the absorption or scattering of light. Light is absorbed, when the energy of the incident photon corresponds to the energy between the ground and the excited state of a molecule.

When a light wave interacts with a molecule, it distorts the cloud of electrons around the nuclei. This phenomenon differs from the phenomenon of absorption as it does not promote any electron to an excited state of the static molecule. The lifetime of the excited state is very short compared to most absorption processes. The entire process is completed within picoseconds or less. More specifically, while the light passes over the molecule, it polarizes the molecule and simultaneously it promotes the electrons in a higher energy state. At that instant, the energy present in the light wave is transferred into the molecule.

This interaction can be considered as the formation of a very short-lived 'complex' between the photons and the electrons in the molecule in which the nuclei do not have time to move appreciably. This results in a high energy form of the molecule with different electron geometry but without any large nuclei movement. This 'complex' between the light and the molecule is not stable and the light is released immediately as scattered radiation. It is often called the virtual state of the molecule, as we can see in the following figure 5.2.

Further, the actual shape of the distorted electron arrangement will depend on how much energy is transferred to the molecule and hence it depends on the frequency of the laser used. Thus, the laser defines the energy of the virtual state and the extent of the distortion. This virtual state is a real state of the transitory 'complex' formed. The radiation is scattered as a sphere and not lost by energy transfer within the molecule or emitted at a lower energy. In addition, there is a link between the polarization of the exciting and scattered photons which can be of value in assigning particular vibrations.

Raman and Rayleigh scattering are illustrated in figure 5.2. Rayleigh scattering is an elastic process (no change in the energy). When the electron cloud relaxes without nuclei movement, the scattered light retains its initial energy state. Rayleigh scattering is the most usual scattering of photons, therefore, it is so intense. Raman scattering, on the other hand, is a much rarer event which involves only one in 10^6 – 10^8 of the photons scattered. This occurs when the light and the electrons interact and the nuclei begin to move at the same time. Since the nuclei are much heavier than the electrons, there is an appreciable change in energy of the molecule to either lower or higher energy depending on whether the process starts with a molecule in the ground state (Stokes scattering) or from a molecule in an excited vibrational state (anti-Stokes scattering).

More specifically, Stokes scattering is observed, when a molecule in the ground vibrational state absorbs energy and is promoted to an excited vibrational state. Anti-stokes scattering is observed, when a molecule is at an excited vibrational state (probably due to thermal energy) and, by interaction with a photon, the molecule transfers part of its energy to the photon, and then rests at the ground state. At room temperature (27˚C or 300K), the majority of the molecules are in low energy states – ground vibrational states, therefore, the phenomenon of Anti-Stokes[20] scattering is rare.

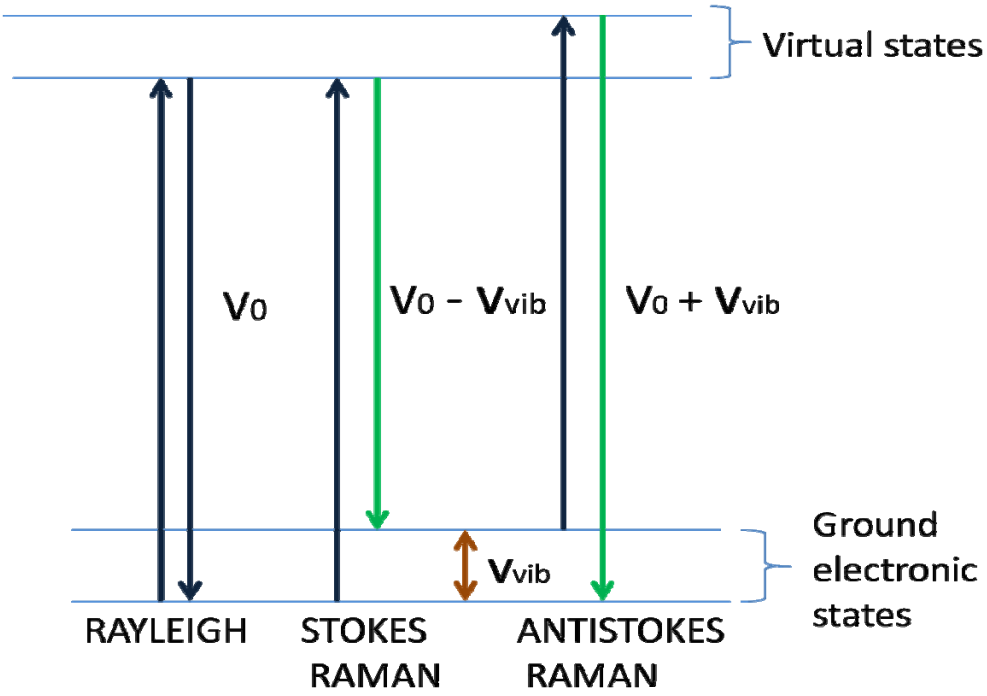

Figure 5.2 Raman and Rayleigh scattering

In Raman spectroscopy, radiation of light is used to excite the molecules and the difference in energy between the ground and the excited vibrational state of the molecule is measured by subtracting the energy of the scattered photon from that of the incident light beam [32]-[33].

Generally, Raman spectroscopy deals with the analysis of the inelastically scattered light from atoms, molecules, and solids. Due to the interaction of light and matter, absorption or emission of phonons[21] are possible processes leading to changes of the frequency of the incident light.

[20] As temperature increases, the Anti-Stokes scattering becomes more intense as more molecules acquire more energy and occupy excited vibrational states, while Stokes scattering becomes a little weaker.

[21] A phonon is a collective excitation in a periodic, elastic arrangement of atoms or molecules in condensed matter such as solids and some liquids.

The practical applications of Raman spectroscopy beyond pure science are:

- Raman gas analyzers used in medicine for real-time monitoring of anesthetic and respiratory gas mixtures during surgery.
- Spatially offset Raman spectroscopy (SORS), which is less sensitive to surface layers than conventional Raman, used to discover counterfeit drugs without opening their packaging and for non-invasive monitoring of biological tissue.
- Raman spectroscopy used to investigate the chemical composition of historical documents with a non-invasive way.

Raman techniques are applied mainly in physics and chemistry, apart from medicine and archeology mentioned above, as it can identify vibrational and rotational modes of a molecule by analyzing its Raman spectrum. In our experiment, we are searching for the 'fingerprint' (the rotational and vibrational modes) of gas lead phthalocyanine (PbPc) – free molecules.

PbPc contains 8 nitrogen atoms, 32 carbon atoms, 16 hydrogen atoms and one metal atom and its fundamental vibrational modes for Raman and infrared spectra are:

Γ_{vib} (PbPc)= $22A_1$ (IR, Ra) +$41E$ (IR, Ra) +$21B_1$ (Ra) + $21B_2$ (Ra)+ $19A_2$ [36],
A is the symmetrical breathing mode and B,E are the anti-symmetrical modes.

5.3 Experimental set-up of Raman spectrometer

The experimental set-up consists of an Ar^+-laser able to produce an intense beam, reflecting mirrors and lenses to guide, focus, and enhance the beam on the sample by aligning the beam to the focus point, a Dilor Charge-Coupled Diode (CCD), which is a very sensitive detector of light, cooled to minimize the background noise.

The sample container was tied around with a ribbon of glass fibers that inside had a wire of wolfram. The wire was connected to a power supply and the current flow raised the wire temperature. The temperature of the sample was measured by a thermocouple. The container was heated to evaporate the PbPc powder inside. It was important to reach the sublimation temperature of PbPc powder of 500°C, so that the PbPc molecules are in the gas phase and therefore free. Heating was done under conditions of high vacuum. In the vacuum chamber, where the PbPc powder was evaporated, a pressure of approximately $8*10^{-8}$ mbar was achieved. The spectrum of the molecules was recorded in vacuum.

The following figures show the experimental set-up, the light path, and the mirror-lens apparatus used to focus on the sample.

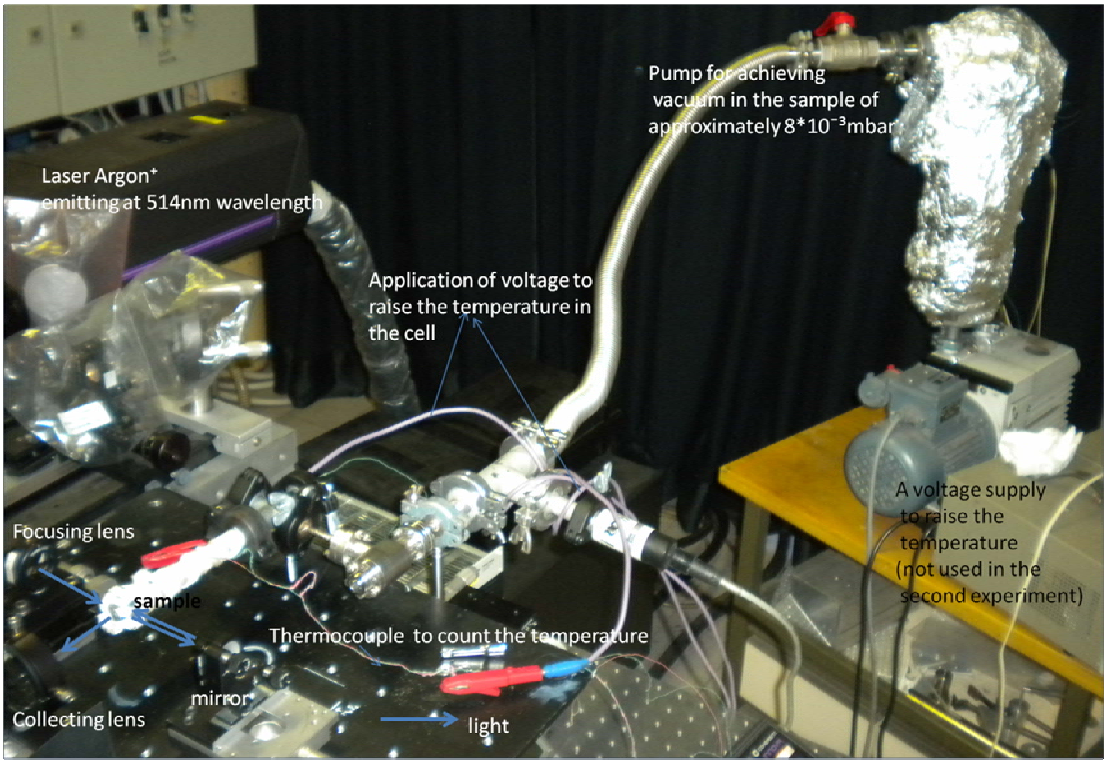

Figure 5.3.a Experimental set-up for sample preparation and measurements

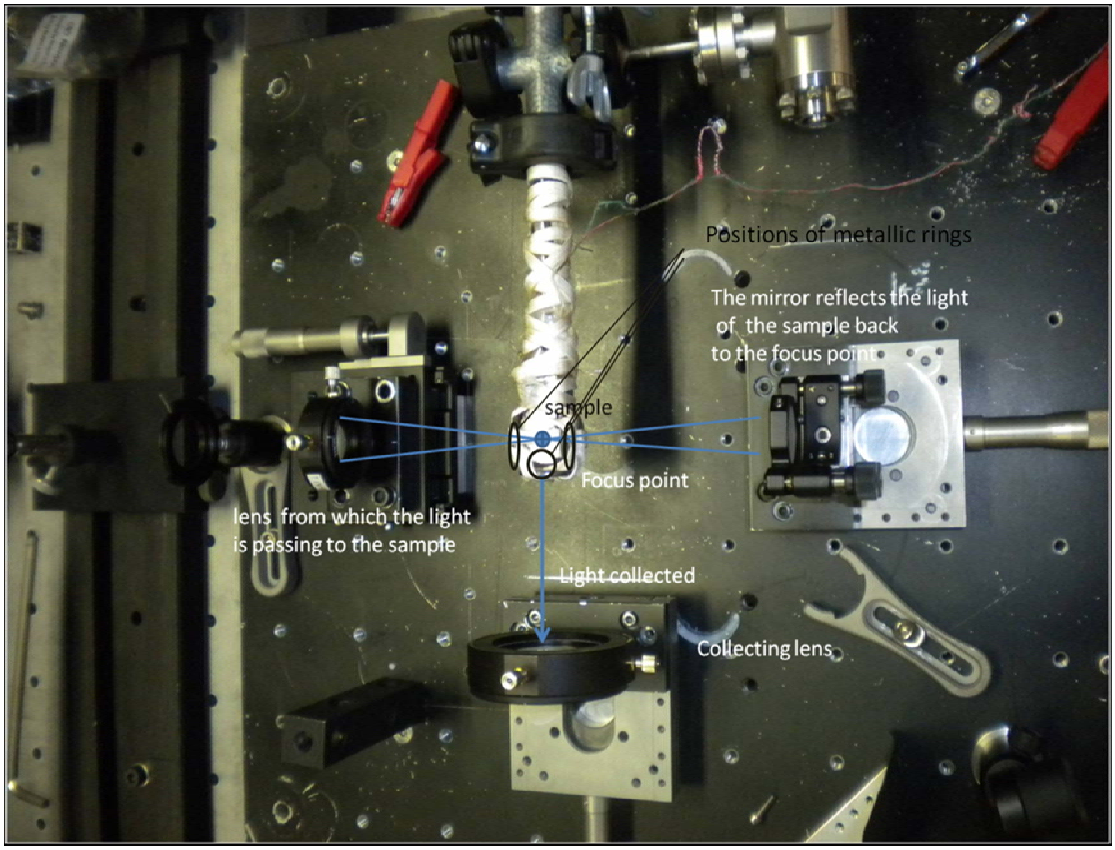

Figure 5.3.b Optical path with mirrors and lenses to guide the laser beam through the sample container; the metallic rings were used to raise the temperature at the windows for optical measurements.

The alignment of the Raman equipment and the pass through the glass container with the sample needed time and trials. Special care was taken to avoid contamination of the container and the sample inside it, since it may lead to false results; additionally, we were very careful with the lenses and the glass containers by using plastic gloves.

The Raman spectrometer used in the experiments is described in the following:

1. Ar^{+}-laser[22] operated at 514,5 nm (green). Generally, argon ion lasers emit at 13 different wavelengths from ultraviolet, through visible, and up to near-infrared spectrum: 351.1 nm, 363.8 nm, 454.6 nm, 457.9 nm, 465.8 nm, 476.5 nm, 488.0 nm, 496.5 nm, 501.7 nm, 514.5 nm, 528.7 nm, 1092.3 nm with the most prominent and most used wavelengths the 514.5 nm (green) and the 488.0 nm (blue-green) emission lines.
2. Lenses and mirrors to guide and focus the laser beam on the sample as well as to reflect back and re-focus the beam on the same sample spot (multi-pass) in order to increase the intensity of the scattered light which is low as the sample is in the gas phase (Figure 5.3.b).
3. Charge–Coupled Diode (CCD) detector cooled with liquid nitrogen. Raman scattering consists of a very low signal, therefore, the background noise of the instrumentation has to be minimized.

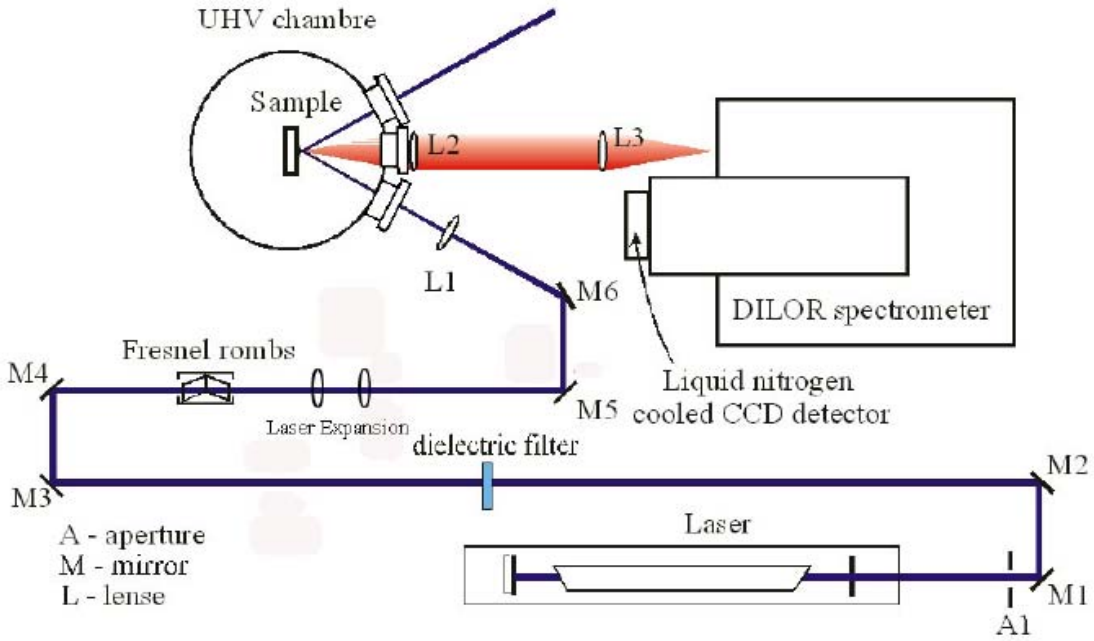

Figure 5.3.c Experimental set-up of Raman spectrometer inclusive sample container

[22] The Argon Ion laser was invented in 1964 by William Bridges at Hughes Aircraft and is one of an Ion-laser family that uses a noble gas as the active medium.

For the sample, we used two different glass containers. Glass (as water) is a strong absorber of infrared radiation and they are both weak scatterers, which makes them (and especially the glass container we used) suitable for Raman spectroscopy [23]. The purpose was to heat the PbPc powder to its sublimation temperature (500^{o}C) in order to establish an ensemble of free molecules in the gas phase and then record the Raman spectrum (the fingerprint) of the free PbPc molecules .

In the following, the accessories related to the sample are described in detail

1. Glass cell: in order to eliminate optical background interferences, one of the two glass cells, we used, was made of glass of very good optical quality.
2. Metallic rings in order to maintain high temperature at the optical windows and avoid sublimation of the molecules on these. Despite the use of metallic rings, it has not been possible to eliminate the phenomenon of sublimation on the windows. Heat gun has been also applied.
3. Heating of the sample: The wire of wolfram used as heater was twiddled (two wires), so that its resistance ($R=\rho L/A$) was lowered and the temperature was increased. A ribbon of glass fibers tied in grid surrounded the glass contained, so that the sample is heated homogeneously with the wolfram wire inside the ribbon. The power supply was programmed to raise the temperature of the sample up to 570°C, since the quartz glass container of the sample has a softening temperature of 580°C.
4. Thermocouple of nickel chrome and nickel aluminum.

We tried to heat the sample homogeneously using the glass ribbon with the wolfram wire inside, the metallic rings, and the heat gun, because it is very important, for the Raman measurements, that any focal point[24] produces the same results and the sample homogeneity means a lot. Since we were investigating the gas phase of PbPc, we needed a considerable number of molecules in the gas phase per unit volume and used a quite long glass container, as can be seen in the following figure 5.3.d. The glass container should be clean from fingerprints which may cause fluorescence. Besides, the sample should be tied carefully with the glass ribbon in grid, so that the cell is well covered in order to be heated homogenously. The current to the sample heater was applied with a small step in order to avoid huge and rapid differences in temperature, which might damage or break the glass container of the sample. The highest temperature reached was 565°C. At higher temperatures, the molecules of lead phthalocyanine could be destroyed (burnt). The main problem we faced was the sublimation of the molecules on the optical windows, which was difficult to avoid as the temperatures differences at these parts of the sample container forces the molecules to stack on them, so that the laser beam cannot pass through. As already mentioned, a solution for this problem was to use a heat gun for extra heating on these parts.

---

[23] Glass and water produce Raman spectra that need to be considered in case the Raman spectrum of the material studied is weak and shadowing by the interfering elements cannot be excluded.

[24] The focal point is essential, since the Raman data are collected from this point.

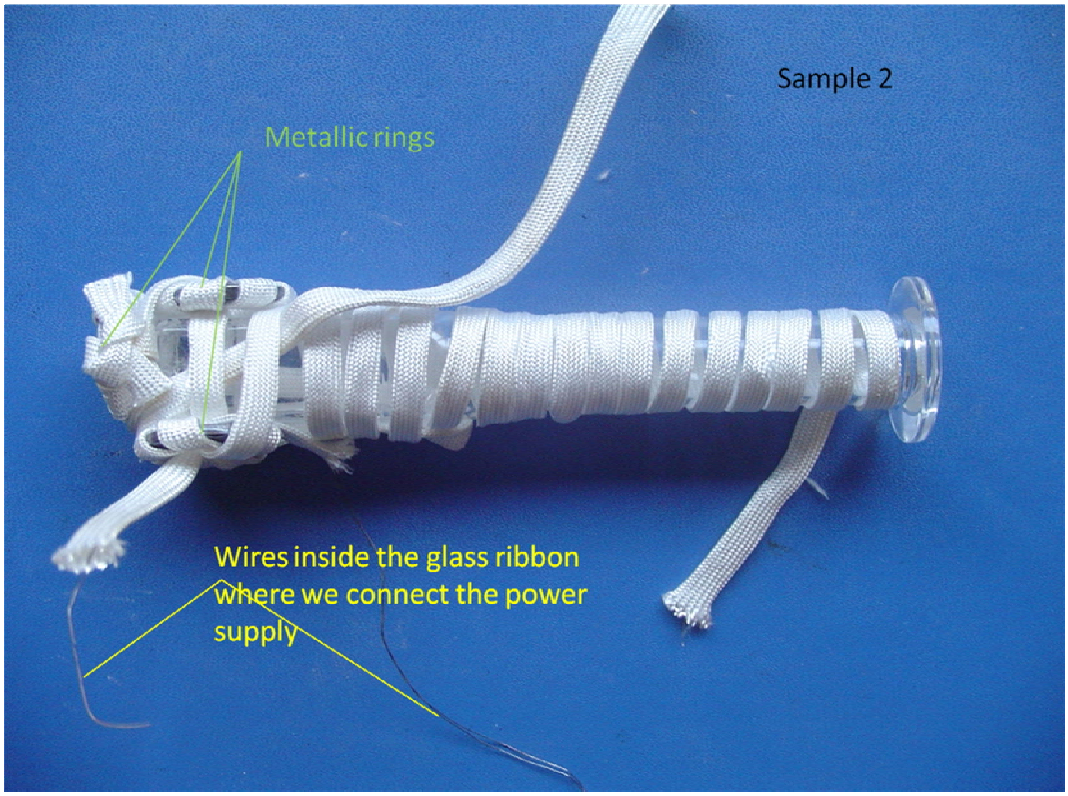

Figure 5.3.d Glass container of PbPc powder with Heater ribbon

The glass container of the PbPc sample was initially evacuated, so that the measured spectra are the Raman "Fingerprint" of lead phthalocyanine molecules in the gas phase, and not any other contaminators (molecules of air etc).

The Raman-Stokes spectra (cm^{-1}) were recorded. Raman scattering is referred to as shift in energy with respect to the excitation laser beam and should be expressed in Δcm^{-1}; for simplicity, it is usually expressed in cm^{-1}. Stokes scattering is produced by the vibration of the molecules that absorb light (photons) of the laser. The absorbing molecules change their vibration frequency. The scattered light (photons) with less energy and lower frequency than those of the laser beam is spectrally analyzed. Since every molecule vibration has a specific Raman frequency, we can identify the vibration modes of molecules with respect to their peaks in the Raman spectra. The spectra are recorded keeping a distance from the Rayleigh line (the elastic scattered light), which is very intense and could damage the CCD. Usually, Raman spectra are recorded up to 100 cm^{-1} from laser beam (and not lower); however, with modern technical equipment, exposure down to 10 cm^{-1} is possible. The intensities of the bands in the Raman spectra are dependent on the nature of the vibration being studied and on instrumentation and sampling factors. Modern instruments can be calibrated to remove the instrumental factors and the intensity to noise ratio can be drastically improved.

The Raman spectrum of PbPc in vapor phase (Graph 12) was recorded under excitation with the 514,5 nm (2,4 eV) line of Ar^+-laser with output power 5,4 W. For mode assignment of the Raman modes of vapor PbPc, we used the results of Density Functional Theory (DFT) calculations of I.M. Kupchak in Ref. [6] and Yuexing Zhang and Xianxi Zhang [8] listed in Table 2, columns 3-5. DFT calculations[25] predict spectra of single molecules in vapor phase as in case of the PbPc molecules studied. It should be noted, that during our Raman experiments with PbPc free molecules, we observed occasionally cosmic rays superposed to the Raman spectrum. Cosmic rays induce highly intensive peaks with a very narrow bandwidth. The peaks assigned to cosmic rays are designated in the Raman spectrum of PbPc in vapor phase (Graph 12).

The Raman bands were fitted with Lorentzians. The fitting results are partially listed in Table 2, column 2, and are given fully in the Appendix (peak position, amplitude, and width). The experimentally recorded Raman spectrum of PbPc in vapor phase ranges from 100 cm^{-1} to 800 cm^{-1}. It consists of 19 peaks with 17 peaks assigned to Raman modes and 2 very narrow peaks, at 753 and 763 cm^{-1}, induced by cosmic rays. Though narrow Raman widths can also be observed on PbPc in vapor phase with low pressure and low temperature, this does not apply in our case. The Raman spectra were acquired shortly after evaporation of the PbPc powder and the PbPc molecules in the gas phase are expected to maintain a relatively high temperature. Most important, except for the very narrow line-width of the peaks at 753 and 763 cm^{-1}, the measured Raman band-widths were in the range 10-30 cm^{-1}. For Raman mode assignment, all of the following factors were simultaneously taken into account

- mode symmetry
- mode frequency
- mode intensity
- mode “coupling” with neighbor modes

A linear shift of mode frequencies accountable for anharmonicity and correlation factors to the same extend for modes of totally different symmetry, as suggested in Ref. [8], seems rather unlikely particularly in case of non-planar molecules as the metal-phthalocyanines.

In Graph 12, the Raman mode frequencies are the fitting results of the spectrum of PbPc in the gas phase measured in our experiment, while mode assignment is in accordance with DFT calculations (Table 2, columns 3-5). For comparison, in Table 2 (columns 6-7), the mode frequencies of the experimental Raman spectra of PbPc powder referred in [6]-[7] are also given. Apparently, a considerable number of Raman modes are in agreement with those identified in PbPc powder. On the other hand, the PbPc is a large molecule with a rich Raman spectrum. It is possible to observe deviations in band frequencies and intensities in case of modifications in the composition of the material.

[25] DFT calculations of solids and liquids can have band shifts due to molecular interactions.

5.4 Results

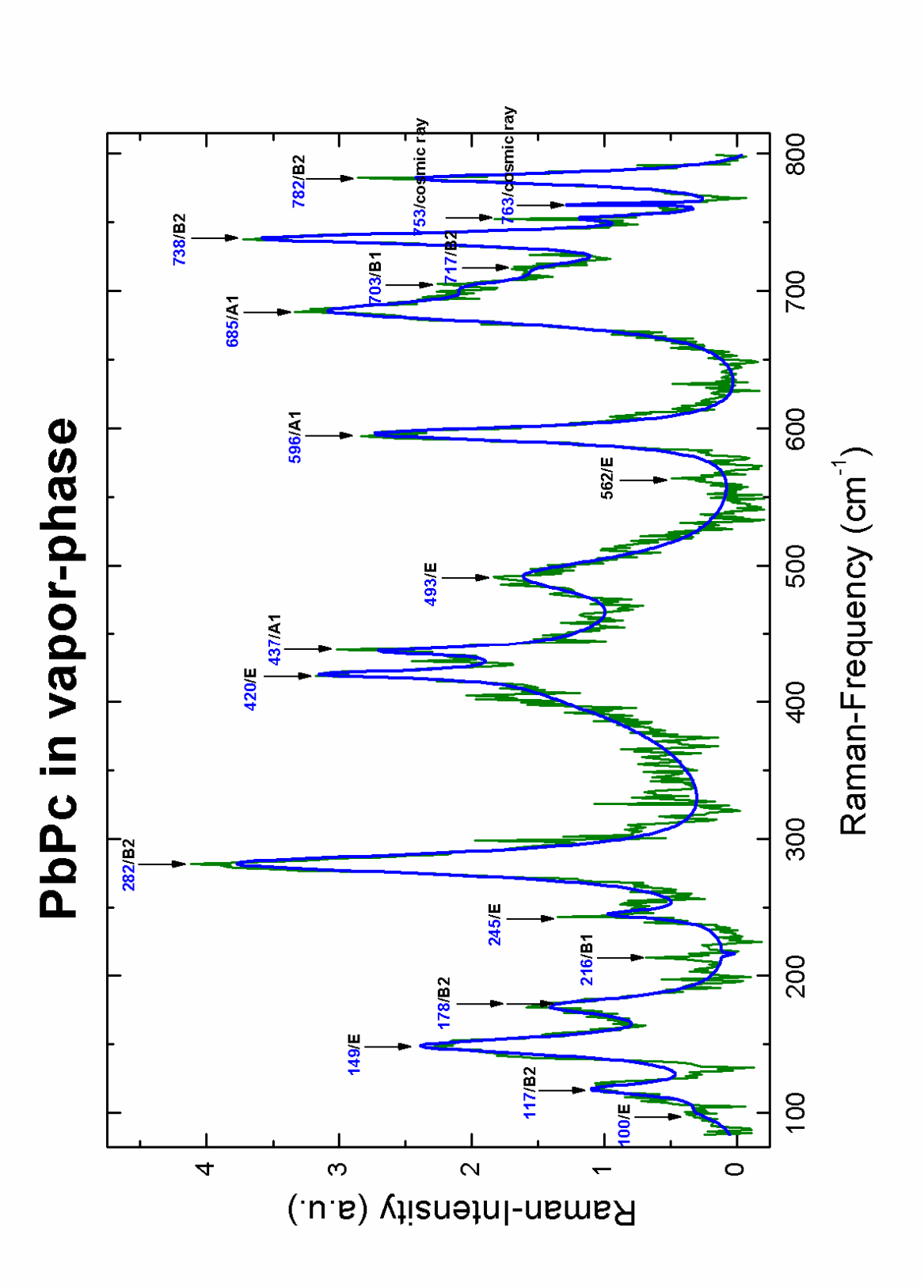

Graph 12 Raman spectrum of PbPc in vapor phase

Table2 : Fitting results of vibrational mode frequencies of PbPc in vapor phase in this work (col.2) in comparison with the results of Density Functional Theory (DFT) and mode assignment by I.M. Kupchak in Ref. [6] including DFT scaled by L.Riele [6] (col.3), DFTcalculations and mode assignment by Y.Zhang & X.Zhang [8] (cols.4-5), and the results of the experimental Raman spectra of PbPc powder Ref. [6] (col. 6) and Ref. [7] (col.7). Abbreviations used in mode assignment: N: nitrogen, H: hydrogen, and C: carbon atom, IPB: in plane bending, OPB: out of plane bending, sy: symmetric, str: stretching, bre: breathing, Ben. exp.: benzene expanding (*753, *763 are very narrow-width peaks assigned to cosmic rays).

Raman peak Nr.	RAMAN SHIFT of PbPc in vapor by fitting	DFT calculations by I.M. Kupchak (scaled DFT by L.Riele)	DFT calculations by Y.Zhang & X.Zhang	Vibrational Mode Assignment by Y.Zhang & X.Zhang	Exp.data PbPc powder by L. Riele	Exp. Data PbPc powder by V. Stamelou
	RAMAN SHIFT (cm^{-1})/ intensity (a.u.)	RAMAN SHIFT (cm^{-1}) (vibrational mode assignment)/ intensity (a.u.)	RAMAN SHIFT (cm^{-1}) (vibrational mode assignment)/ intensity (a.u.)		RAMAN SHIFT (cm^{-1})	RAMAN SHIFT (cm^{-1})
1	100 / 0.2	107 (103) (E) / 5.3	102,97 (E) /5.29	-	-	-
2	117 / 1.0	125 (121) (B_2) / 19.5	121,33(B_2) /19.65	PbN, alternately stretching	-	-
3	149 / 2.3	148 (143) (E) / 0.6	142,67(E) /0.64	-	146	150,151
4	178/ 1.3	165 (159) (B_2) / 10.2	158,63 (B_2) / 10.2	-	169	-
5	216 / 0.3	211 (203) (B_1) / 12.7	203,24(B_1)/ 12.67	-	210	207
6	245 / 0.8	252 (242) (E) / 3.8	241,89 (E)/ 3.802	-	245	-
7	282 /3.8	298 (287) (B_2) /3.8	286,69 (B_2)/ 3,80	-	272	-

8	420 / 1.7	442 (425) (E) / 0.1	424,94(E)/ 0.06	-	-	-
9	437 / 1.3	455 (437) (A_1) / 0.5	437,34(A_1)/ 0.47	CHa OPB, CC OPB	-	-
10	493 / 1.4	512 (492) (E) / 0.2	492,14 (E)/ 0.185	CH CC CN OPB	493	-
11	562 / 0.3	575 (553) (E)/ 0.8	552,61 (E) / 0.75	-	-	566
12	596 / 1.2	585 (563) (A_1) /77.8	562,80 (A_1) / 76.77	Bre., PbN_1 sy. str., CC sy. B	-	-
13	685 / 3.0	671 (645) (A_1) / 351.5	645,00 (A_1) / 351.01	N_2C CC sy. B_2, CN_1 PbN_1 CC str., CH IPB	674	680
14	703 / 1.2	705 (678) (B_1) /38.01	677,98 (B_1) / 37.79	-	708	-
15	717/ 0.9	718 (691) (B2) /15.3	690,57 (B2) / 15.32	-	729	721,722
16	738 / 3.5	760 (731) (B_2) /700.01	730,66 (B_2) / 695.72	N-C sy.B, PbN_1 CC CN str.	742	-
17	*753 / 0.8	768 (738) (A_1) /2.1	737,97 (A_1) /2,10	PbN sy. str., CH OPB, CC OPB	-	-
18	*763 /1.7	794 (764) (E) /0.2	763,64(E) /0.195	Ben. Exp., CH IPB,CC IPB, CC CN PbN str.	769	-
19	782 / 2.6	810-779 (A_1) /91.6	778,63 (A_1) /92.04		-	-

To the notation in Table 2

1. IPB : in-plane bending
2. OPB: out-of–plane bending
3. sy. : symmetrical vibration
4. str. : stretching vibration
5. bre. : breathing mode of the molecule
6. Ben. exp: the benzene expanding
7. N : nitrogen, C : carbon, and H : hydrogen.

- A, B Non-degenerate (single) modes: one set of atom displacements. Symmetric (A) breathing mode or anti-symmetric (B).
- E Doubly degenerate mode. Two sets of atom displacements, symmetric or anti-symmetric.

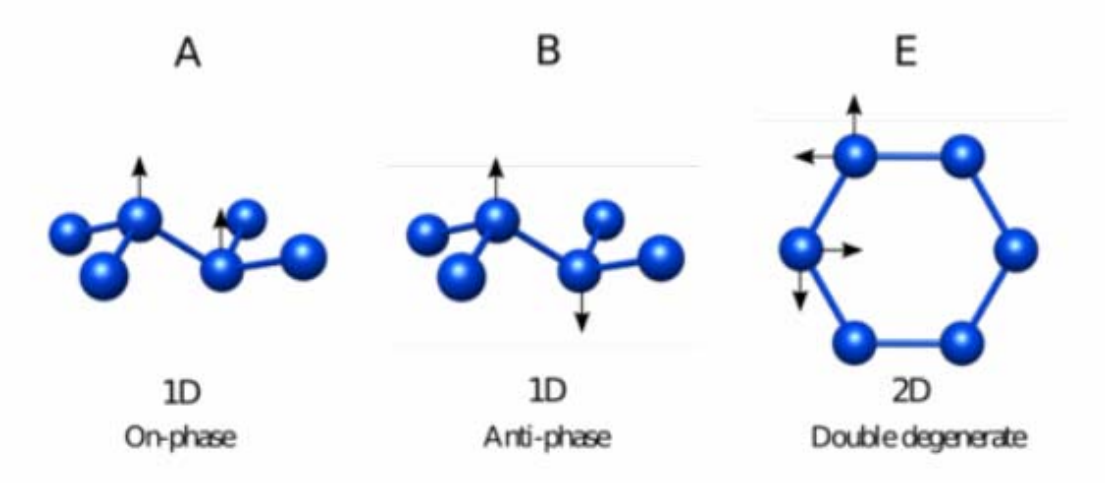

Figure 5.4.1 A,B,E vibrational modes

The PbPc molecule vibrations can be understood in terms of intra-molecular bonding and molecule asymmetry depicted in following Figures 5.4.2-5.4.3. Figure 5.4.2 presents the internal bonds of the atoms in the molecule and their positions. Figure 5.4.3 demonstrates that the PbPc molecule is non planar, since the lead-ion (Pb^{+2}) is larger than the central cavity and lies above the molecule of phthalocyanine. N1 is the nitrogen atom joined to the central metal ion; the Pb-N1 symmetrical stretching vibration is referred to this bond. Similarly, the Pb-N, C-N, C-C, C-H bonds are also involved in mode vibrations denoted in Table 2. Generally, the symbols α, β, γ, δ are indices added to describe that the respective atoms begin as isoindole units from the N1. In Pcs, there are only α and β connections.

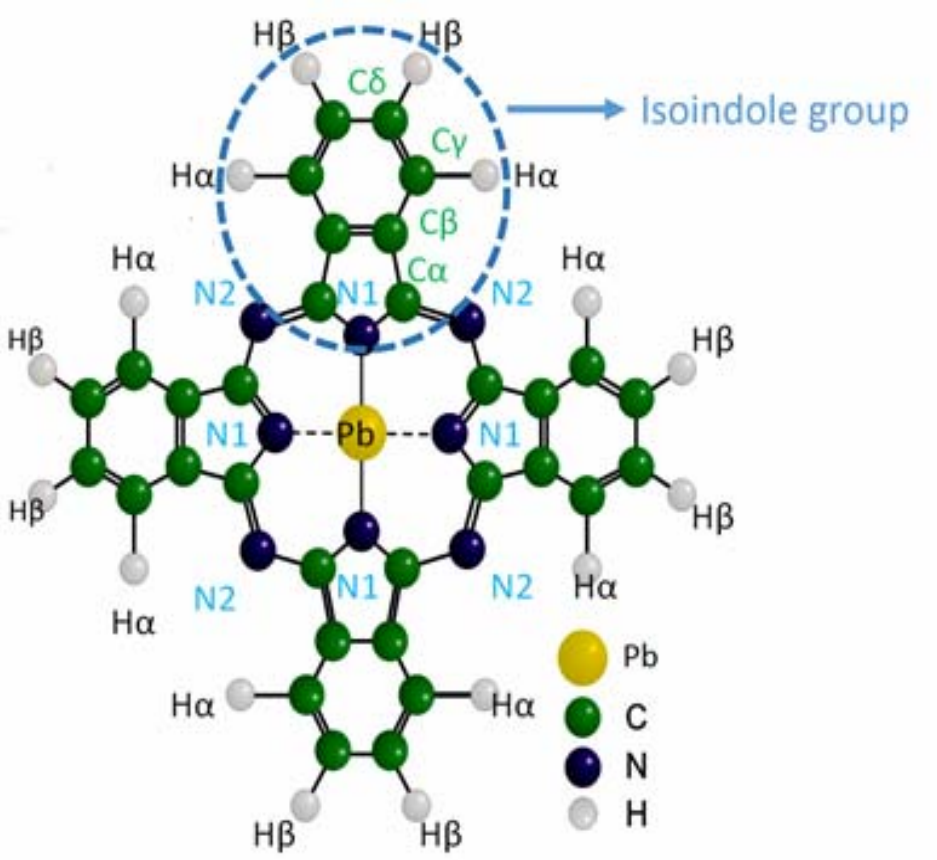

Figure 5.4.2 PbPc molecule and its bonds (top-view)

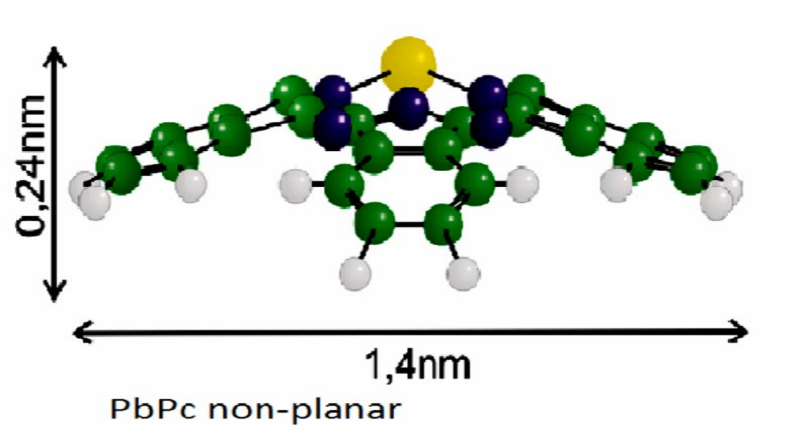

Figure 5.4.3 PbPc molecule and its bonds (side-view) demonstrating that it is a non-planar molecule

E. Bibliography

1. L. M. Peter, *Towards sustainable photovoltaics: the research for new materials*, Royal Society Publications A 369 (2011) 1840-1856
2. N. Papageorgiou, T. Angot, *Physics of ultra-thin phthalocyanine films on semicondutors*, Progress in Surface Science 77 (2004) 139
3. K. Mizoguchi, K. Mizui, *Optoelectronic Properties of Orientation-controlled Lead Phthalocyanine Films*, Japanese Journal of Applied Physics 41 (2002) 6421-6425
4. N. Papageorgiou, Y. Ferro, *Geometry and electronic structure of lead phthalocyanine: Quantum calculations via density-functional theory and photoemission measurements*, Physical Review B 68 (2003) 235105
5. L. Riele, T. Bruhn, *Reconstruction dependent growth of lead phthalocyanine layers on GaAs(001) surfaces*, Physical Review B 84 (2011) 205317
6. L. Riele, Doctoral thesis: *"Raman Scattering: Proving the Controlled Growth of Phthalocyanine on Reconstructed GaAs(001)"*, Tor Vergata, Rome-Italy 2012
7. V. Stamelou, MSc-thesis: *"Investigation of Organic Molecule Layers on Semiconductor Surfaces with Potential Applications in Micro-sensor Technology*", National Technical University of Athens 2009
8. Y. Zhang and X. Zhang, *Comparative density functional theory study of the structures and properties of metallophthalocyanines of group IV B*, Vibrational Spectroscopy 40 (2006) 289–298
9. S.O.Kasap, *Principles of electronic devices*, Ed. Papasotiriou 2006
10. S. Hedegus and A. Luque, *Handbook of Photovoltaic Science and Engineering*, Wiley 2003
11. P. Wurfel, *Physics of solar cells*, second edition, Wiley 2009
12. http://ocw.mit.edu/courses/mechanical-engineering/2-626-fundamentals-of-photovoltaics-fall-2008/lecture-notes/lecture4.pdf MIT open courses
13. http://pveducation.org University of New South Wales
14. W. Shockley, H. J. Queisser, Detailed Balance Limit of Efficiency of p-n Junction Solar Cells, Journal of Applied Physics 32(3) (1961) 510-519
15. pi18-2013-ZSW-WorldrecordCIGS.pdf; M. Powalla, P. Jackson, W. Witte, D. Hariskos, S. Paetel, C. Tschamber, W. Wischmann, *High-efficiency Cu(In,Ga)Se2 cells andmodules*, Solar Energy Materials & Solar Cells 119 (2013) 51–58
16. C. J. Brabec, N. S. Sariciftci, *Plastic solar cells*, Advanced Functional Materials 11 (2001) 15-26

17. H. Hoppe and N. S. Sariciftci, *Organic solar cells: An overview*, Journal of Materials Research 19 (2004) 1924-1945

18. S. Guenes, H. Neugebauer, *Conjugated Polymer-Based Organic Solar Cells*, Chemistry Review 107 (2007) 1324-1338

19. S. Berkley, *The Fabrication and Characterization of Organic Solar Cells*, 2009

20. Heliatek press-release January 16, 2013, http://www.heliatek.com

21. M. Grätzel, *Solar Energy Conversion by Dye-Sensitized Photovoltaic Cells*, Inorg. Chem. 44 (20) (2005) 6841–6851

22. G. Cabailh, I.T. McGovern, *Growth of Metal-Phthalocyanine on GaAs(001):* an NEXAFS study, Proc SPIE 5826 (2005) 37-43

23. P.A. Lane, J. Rostalski, *Electroabsorpton studies of phthalocyanine/perylene solar cells*, Elsevier 2000

24. N.B. McKeown, *Phthalocyanine Materials: Synthesis, Structure and Function, Chemistry of Solid State Materials*, Cambridge University Press 1998

25. M. G. Waltera, A. B. Rudineb, *Porphyrins and phthalocyanines in solar photovoltaic cells*, Journal of Porphyrins Phthalocyanines 14 (2010) 759–792

26. M. Filbian, Doctoral thesis *Electronic properties of novel Phthalocyanine based molecular crystals,* Tor Vergata, Rome-Italy (2007)

27. M.-S. Liao, S. Scheiner, *Electronic structure and bonding in metal phthalo-cyanines*, *Metal= Fe, Co, Ni, Cu, Zn, Mg*, Chemistry and Biochemistry Faculty Publications (2001)

28. R. O. Loutfy ad J. H. Sharp, *Photovoltaic Properties of Metal Free Phthalocyanines*, Journal of Chemistry and Physics 71 (1979) 1211

29. G.H.M. Smith, *High Performance Pigments*, Wiley (2003)

30. W.G. Schmidt, F. Bechstedt, *GaAs (001) surface reconstructions: geometries, chemical bonding and optical properties*, Applied Surface Science, vol. 190 (2002), pg. 264–268

31. G. Turrell and J. Corset, Raman Microscopy, Developments and Applications, Academic Press, London, (1996)

32. E. Smith, G. Dent, *Modern Raman Spectroscopy: A practical approach*, Wiley (2005)

Summary of diploma thesis in Greek

Σύνοψη στα Ελληνικά

Εισαγωγή

Με στόχο την ανάπτυξη χαμηλού κόστους – υψηλής απόδοσης οργανικών φωτοβολταϊκών, στην παρούσα Διπλωματική εργασία επιχειρείται ο έλεγχος των φυσικών ιδιοτήτων (δομικών, οπτικών, ηλεκτρικών) οργανικών φωτοβολταϊκών ημιαγωγών μέσω του προσανατολισμού των μορίων του απορροφητή με επιταξία σε κατάλληλα προσανατολισμένο υπόστρωμα. Συγκεκριμένα, μελετάται η συμπεριφορά του οργανικού μορίου της φθαλοκυανίνης μολύβδου (PbPc) σε δύο διαφορετικά υποστρώματα γαλλίου αρσενικού (GaAs) με επιφανειακές αναδομήσεις:

1) GaAs c(4x4) με πλεόνασμα μορίων αρσενικού (As), και

2) GaAs β2(2x4) στοιχειομετρική (εναλλακτικά, με μικρή περίσσεια μορίων As)

Η φθαλοκυανίνη μολύβδου (PbPc) είναι οργανικό μόριο, με πολύ καλές οπτοηλεκτρονικές ιδιότητες, κατάλληλο για χρήση σε οργανικά φωτοβολταϊκά λεπτών υμενίων ή σε συνδυασμό οργανικών και ανόργανων φωτοβολαϊκών. Χρησιμοποιήθηκαν δύο διαφορετικά υποστρώματα αρσενιούχου γαλλίου (GaAs), ώστε να εξεταστεί, αν υπάρχει αλλαγή-βελτίωση στη συμπεριφορά της φθαλοκυανίνης σε σχέση με τις επιφανειακές αναδομήσεις του αρσενιούχου γαλλίου. Η φθαλοκυανίνη μολύβδου ανήκει στην ομάδα των μεταλλοφθαλοκυανινών, οργανικών υλικών, που αλλάζουν τη μοριακή τους στοίχιση, όταν εναποτίθενται σε διαφορετικά υποστρώματα, ακολουθώντας την κατεύθυνση των επιφανειακών αναδομήσεων του υποστρώματος, ώστε με τον τρόπο αυτό αλλάζει η απορροφητική τους ικανότητα. Η πειραματική μελέτη σε αυτά τα υλικά με βάση τον προσανατολισμό του υποστρώματος μπορεί να υποδείξει, ποιος συνδυασμός επιστρώματος-υποστρώματος είναι πιο αποδοτικός για μελλοντικές τεχνολογικές εφαρμογές. Επίσης, μελετήθηκε η αλληλεπίδραση των δύο υλικών (της φθαλοκυανίνης μολύβδου και του γαλλίου αρσενικού), επειδή θα μπορούσαν να σχηματίζονται χημικοί δεσμοί μεταξύ τους ή να μεταβάλλονται οι χημικοί δεσμοί του μορίου της φθαλοκυανίνης και η δομή της. Η επιταξιακή εναπόθεση οργανικών μορίων σε ανόργανα υποστρώματα είναι, γενικότερα, καινοτόμο αντικείμενο έρευνας λόγω των ποικίλλων ιδιοτήτων που μπορεί να προκύψουν.

Στα πειράματα, που πραγματοποιήθηκαν στα πλαίσια της παρούσας εργασίας, τα μόρια της φθαλοκυανίνης μολύβδου (PbPc) ήταν σε κρυσταλλική μορφή πριν την εναπόθεσή τους στα υποστρώματα GaAs. Η επανόθεση πραγματοποιήθηκε με εξάχνωση και συμπύκνωση των ατμών PbPc επάνω στην επιφάνεια του υποστρώματος. Η ηλεκτρική αγωγιμότητα των μορίων PbPc, όπως γενικά των μεταλλοφθαλοκυανινών, εξαρτάται από τον προσανατολισμό του υποστρώματος. Παράμετροι που επηρεάζουν την κατεύθυνση και τη διάταξη των οργανικών μορίων είναι: το αρχικό κενό στο θάλαμο, η θερμοκρασία του υποστρώματος, το ποσοστό υλικού που εξαχνώνεται, το ποσοστό υλικού που εναποτίθεται, το πάχος του οργανικού υμενίου, κλπ. Η έρευνά μας επικεντρώθηκε στην αλληλεπίδραση του οργανικού μοριακού υμενίου με την επιφάνεια του ανόργανου υποστρώματος και

ιδιαίτερα την κατάσταση που επικρατεί στις πρώτες υπέρλεπτες στρώσεις του οργανικού υμενίου λόγω της ισχυρής αλληλεπίδρασής τους με το υπόστρωμα. Τα υμένια φθαλοκυανίνης μολύβδου εναποτέθηκαν με εξάχνωση στα υποστρώματα του γαλλίου αρσενικού. Το δείγμα ήταν αρχικά σε μορφή σκόνης φθαλοκυανίνης μολύβδου σε δοχείο (σωλήνα) από γυαλί, το οποίο θερμάναμε (ως 565 ^{o}C), ώστε τα μόρια PbPc να είναι μεταβούν στην αέρια φάση. Το πάχος των υμενίων ήταν περί τα 20 nm. Προηγήθηκε δομικός χαρακτηρισμός των υμενίων PbPc στην αέρια φάση, με οπτική μέθοδο (φασματοσκοπία Raman), και στη συνέχεια ακολούθησε ηλεκτρικός χαρακτηρισμός των ηλιακών κυψελών.

Για τον ηλεκτρικό χαρακτηρισμό, καταγράφηκαν οι χαρακτηριστικές καμπύλες ρεύματος-τάσης (I-V) των δομών PbPc/GaAs σε σύγκριση με την I-V του υποστρώματος GaAs.

Για το δομικό χαρακτηρισμό, χρησιμοποιήθηκε φασμασκοπία Raman. Μελετήθηκε η φθαλοκυανίνη μολύβδου σε αέρια φάση. Η φασμασκοπία Raman είναι μη επεμβατική πειραματική μέθοδος που ανιχνεύει τις ταλαντώσεις του μορίου και αναγνωρίζει το χαρακτηριστικό φασματικό του αποτύπωμα. Τα δείγματα μπορούν να εξεταστούν σε μορφή στερεών, υγρών και αερίων, κατά όγκο, σε μικροσκοπικά σωματίδια ή σε επιφανειακές στρώσεις. Καταγράφηκε το φάσμα Raman των ατμών PbPc και ταυτοποιήθηκαν οι τρόποι ταλάντωσης του μορίου στην αέρια φάση. Η ταυτοποίηση των τρόπων ταλάντωσης πραγματοποιήθηκε με βάση θεωρητικούς υπολογισμούς της Πυκνότητας Καταστάσεων (Density Functional Theory των Yuexing Zhang & Xianxi Zhang and I.M. Kupchak). Τα αποτελέσματα συγκλίνουν με εκείνα που αναφέρονται στις Διδακτορικές Διατριβές των L. Riele και Β. Σταμέλου για φθαλοκυανίνη μολύβδου σε σκόνη.

Στη διπλωματική εργασία, παρουσιάζονται αναλυτικά:

Η μέθοδος της φασματοσκοπίας Raman και η μέθοδος του ηλεκτρικού χαρακτηρισμού μέσω καταγραφής καμπυλών ρεύματος-τάσης (I-V) ηλιακών κυψελών, οι πειραματικές διατάξεις όπου λήφθηκαν οι μετρήσεις, τα αποτελέσματα των μετρήσεων και η ερμηνεία τους, και συζητούνται λεπτομερειακά οι αποδόσεις ηλιακών κυψελών PbPc/GaAs και οι δυνατότητες βελτίωσής τους.

Φωτοβολταϊκή τεχνολογία

Η φωτοβολταϊκή τεχνολογία είναι μετατρέπει την ηλιακή ενέργεια σε ηλεκτρικό ρεύμα. Η ηλεκτρική ενέργεια είναι σημαντική για την ανθρωπότητα, εφόσον εξασφαλίζει παροχές, όπως ηλεκτρικό φως, κλιματισμός, διύλιση νερού, και υπηρεσίες, όπως ραδιόφωνο, τηλεόραση, τηλεπικοινωνίες, κλπ.

Η φωτοβολταϊκή τεχνολογία είναι σημαντική αφού χρησιμοποιεί την ηλιακή ενέργεια για την παραγωγή ηλεκτρισμού (ηλεκτρικοί σταθμοί) με τεράστια

αποθέματα και χωρίς ρύπανση του περιβάλλοντος. Η έξαρση της φωτοβολταϊκής τεχνολογίας συμπίπτει με την πετρελαϊκή κρίση[26], το 1970. Τότε, η μελέτη εναλλακτικών πηγών ενέργειας ήταν σε ζήτηση και η έρευνα πάνω σε αυτές αυξήθηκε. Ένας άλλος παράγοντας, που ώθησε την ανθρωπότητα προς τις φιλικές προς το περιβάλλον πηγές ενέργειας, ήταν η επιβαρημένη κατάσταση του φυσικού περιβάλλοντος με την έναρξη του βιομηχανικού αιώνα 1900-2000, ιδιαίτερα η μόλυνση με ραδιενεργά και χημικά κατάλοιπα και η αύξηση της μέσης θερμοκρασίας. Το ενδιαφέρον της ανθρωπότητας για την αύξηση της θερμοκρασίας του περιβάλλοντος διακηρύχθηκε και υπογράφηκε από 191 χώρες με το Πρωτόκολλο του Κιότο, το Δεκέμβριο του 1997, στην Ιαπωνία. Ανάμεσα σε αυτές τις χώρες ήταν όλα τα μέλη της Ευρωπαϊκής ένωσης καθώς και η Ελλάδα. Έτσι το παγκόσμιο ενδιαφέρον στράφηκε σε φιλικές προς το περιβάλλον μορφές ενέργειας.

Παρόλαυτα, ακόμη και σήμερα, στον 21^{ο} αιώνα, το ένα τρίτο της ανθρωπότητας δεν έχει πρόσβαση σε ηλεκτρισμό, άρα και σε υπηρεσίες που προσφέρονται μέσω αυτού, κυρίως υπηρεσίες που αφορούν στην υγεία, όπως το καθαρό νερό. Εκατομμύρια άνθρωποι χάνουν τη ζωή τους από μολυσμένο νερό κι άλλοι υποφέρουν από έλλειψη βασικών ιατρικών υπηρεσιών. Ο αναλφαβητισμός στερεί από εκατομμύρια ανθρώπους την επαφή με νέες ιδέες για τη βελτίωση της ζωής τους. Η ηλεκτρική ενέργεια, σωστά εφαρμοζόμενη, θα μπορούσε να διορθώσει και να βελτιώσει τις ζωές των ανθρώπων σε χώρες του τρίτου κόσμου. Σε κάθε περίπτωση, τα φωτοβολταϊκά συστήματα είναι μια καλή λύση για απομονωμένες αγροτικές ή θαλάσσιες περιοχές.

Εικόνα 1 : Φιλικές προς τον περιβάλλον μορφές ενέργειας

[26] Τον Οκτώβριο του 1973 ξεκίνησε η πετρελαϊκή κρίση, όταν τα μέλη του Οργανισμού Αραβικών χωρών, που εξήγαγαν πετρέλαιο, προκήρυξαν το πετρελαϊκό εμπάργκο στο ΝΑΤΟ.

Πειραματική διάταξη ηλεκτρικού χαρακτηρισμού

Οι πειραματικές μετρήσεις ηλεκτρικού χαρακτηρισμού των δύο διαφορετικών ηλιακών κυψελών φθαλοκυανίνης μολύβδου υπέρλεπτων υμενίων των 20 nm πάνω σε δύο επιφανειακές αναδομήσεις γαλλίου αρσενικού c(4x4) και β2(2x4) πραγματοποιήθηκε στο εργαστήριο του τμήματος Φυσικής του Πανεπιστημίου Tor-Vergata της Ρώμης υπό τη συν-επίβλεψη του καθηγητή Maurizio de Crescendi. Υπολογίσθηκε ο συντελεστής απόδοσης (η) των ηλιακών κυψελών. Επίσης, μετρήθηκαν τα φάσματα κβαντικής απόδοσης. Τα φάσματα μετρήθηκαν σε διάταξη που περιλαμβάνει: φασματική λυχνία Xe (ξένου), μονοχρωμάτορα, κάτοπτρα και συγκεντρωτικούς φακούς για την οδήγηση και εστίαση της δέσμης φωτός, ανακλαστικό μηχανικό διαιρέτη με πτερύγια από αλουμίνιο (Al) και ηλεκτρονικό σύστημα ενίσχυσης και καταγραφής σήματος. Η λυχνία Xe χρησιμοποιήθηκε, επειδή το φάσμα της είναι συγκρίσιμο με το ηλιακό και κατάλληλο για το χαρακτηρισμό ηλιακών κυψελών.

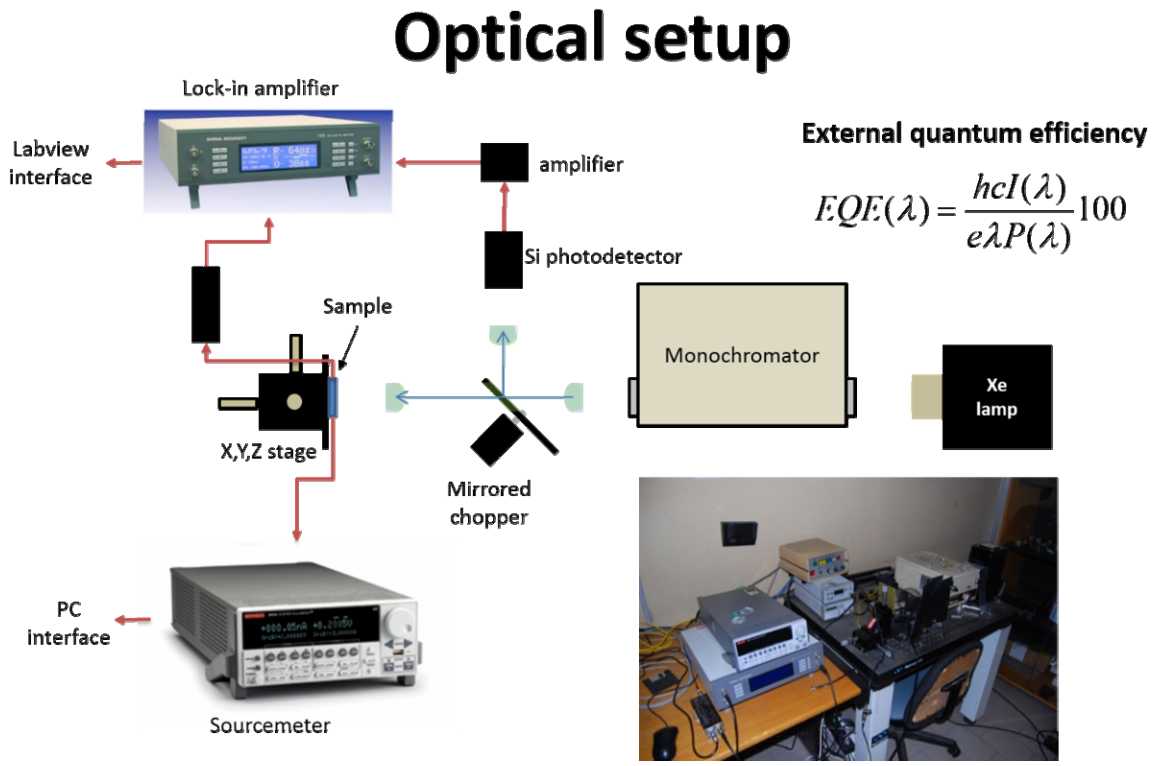

Εικόνα 2: πειραματική διάταξη για τη μέτρηση της κβαντικής απόδοσης ηλιακών κυψελών

Το φως της λυχνίας Xe αναλύεται από το μονοχρωμάτορα με βήμα 5 nm κατά τη σάρωση των μηκών κύματος. Μονοχρωματικό φως 1) εστιάζεται κατά τη διέλευση μέσω του μηχανικού διαιρέτη πάνω στο δείγμα και 2) κατευθύνεται στη φωτοδίοδο (διοδικό ανιχνευτή πυριτίου) κατά την ανάκλαση στα πτερύγια του μηχανικού διαιρέτη. Δηλαδή, ο ανακλαστικός μηχανικός διαιρέτης, φτιαγμένος από αλουμίνιο, επιτρέπει στο φως μία φόρα να περάσει στη φωτοδίοδο από πυρίτιο, ώστε να μετρηθεί η προσπίπτουσα ακτινοβολία και την άλλη φορά να φτάσει στο δείγμα, ώστε το δείγμα να απορροφήσει την ακτινοβολία και να κάνει τη φωτοβολταϊκή μετατροπή. Αυτά τα δύο σήματα συγκρίνονται και δίνουν την κβαντική απόδοση της ηλιακής κυψέλης. Η εξίσωση για τον προσδιορισμό της κβαντικής απόδοσης (EQE = External Quantum Efficiency) δίνεται παρακάτω. Ο δειγματοφορέας είναι δυνατό να μετακινηθεί στις 3 διαστάσεις (x,y,z), ώστε το προσπίπτον φως να μπορεί να εστιαστεί σε διάφορα σημεία του δείγματος. Η φωτοδίοδος είναι φωτοανιχνευτής από πυρίτιο με εύρος φασματικής ανίχνευσης από 190 ως 1100nm.

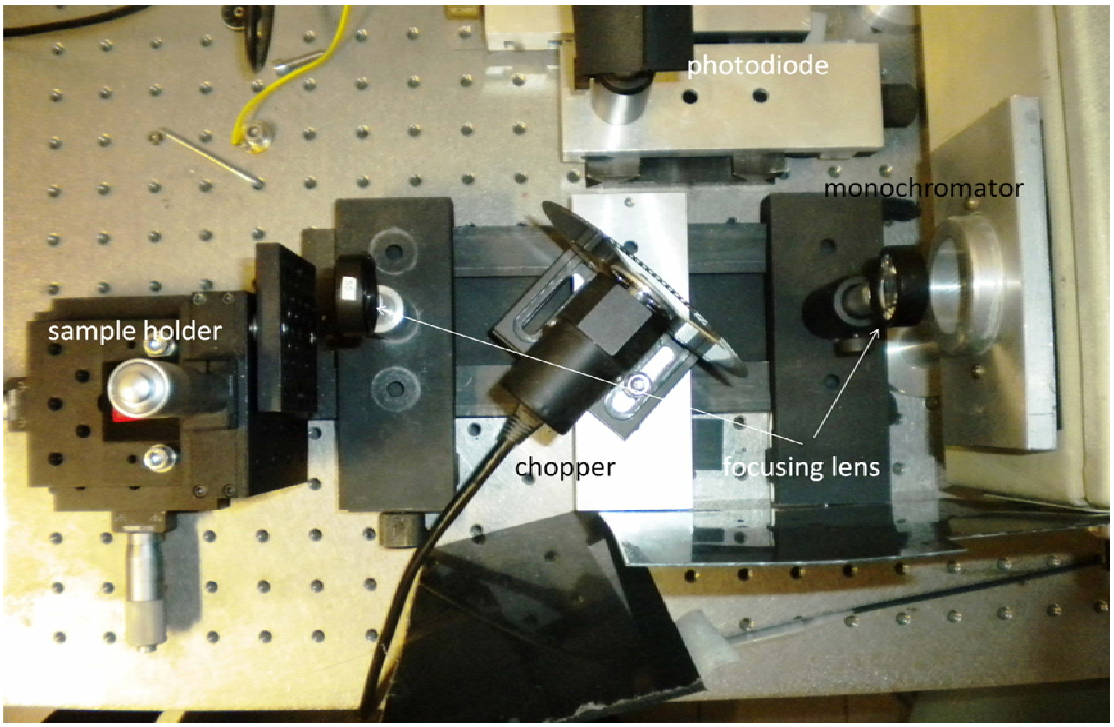

Εικόνα 3: μονοχρωμάτορας, συγκεντρωτικοί φακοί, ανακλαστικός μηχανικός διαιρέτης (chopper) και φωτοδίοδος ανίχνευσης

Το ρεύμα που παρατηρούνταν ως απόκριση από τις ηλιακές κυψέλες ήταν πολύ μικρό και έτσι χρησιμοποιήθηκε ανακλαστήρας-πολλαπλασιαστής για να αυξηθεί και να μπορεί να μετρηθεί από τον ηλεκτρονικό εξοπλισμό. Ο ηλεκτρονικός εξοπλισμός ενισχύει το σήμα και εξασθενεί το θόρυβο που προέρχεται από το διάχυτο φωτισμό και τα ηλεκτρονικά του εργαστηρίου. Το ρεύμα που μετρήθηκε ήταν της τάξης των μΑ.

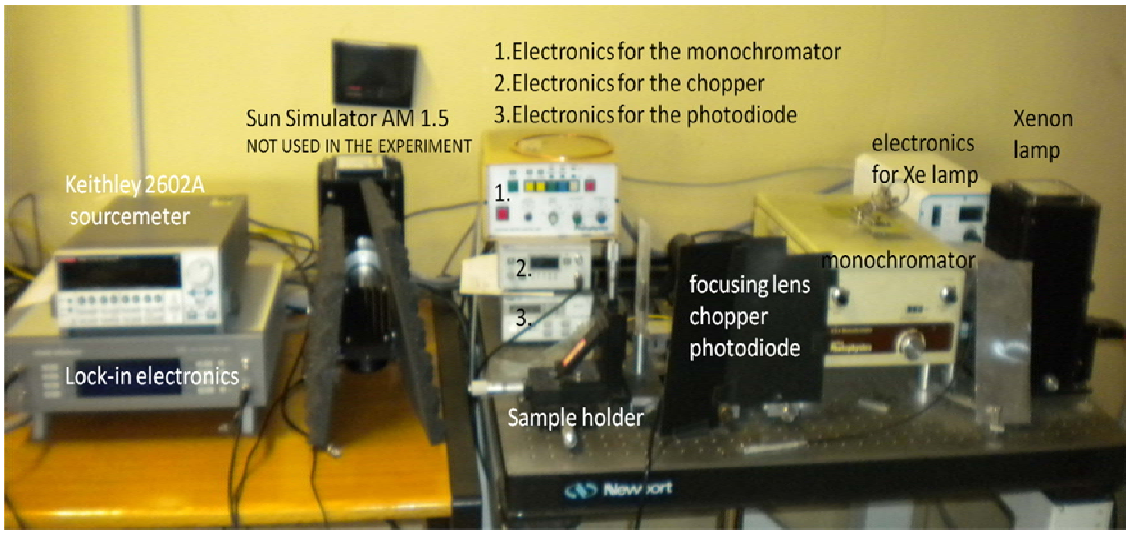

Εικόνα 4: εξοπλισμός του εργαστηρίου ηλεκτρικού χαρακτηρισμού

Η πειραματική διάταξη, που περιγράφηκε, μετράει συγχρόνως τη χαρακτηριστική καμπύλη ρεύματος – τάσης (I-V) των ηλιακών κυψελών και την κβαντική απόδοσή τους (EQE). Με την EQE καθορίζεται η οπτική απόκριση της κάθε ηλιακής κυψέλης (η απορρόφησή της) για κάθε μήκος κύματος, ενώ με την καμπύλη ρεύματος- τάσης οι παράμετροι που προσδιορίζονται είναι

1. Το ρεύμα βραχυκύκλωσης της ηλιακής κυψέλης (short circuit current, Isc)
2. Η τάση ανοιχτού κυκλώματος (open circuit voltage, Voc)
3. Το σημείο μέγιστης ισχύος (maximum power point, MPP)

Σημειώνεται, ότι χρησιμοποιήθηκαν μεταλλικά ηλεκτρόδια Ag υπό μορφή ρινισμάτων από άργυρο σε διάλυμα ακετόνης για το δείγμα PbPc/GaAs β2(2x4). Ο άργυρος χρησιμοποιήθηκε, επειδή έχει καλή αγωγιμότητα, ώστε το φωτορεύμα να είναι βέλτιστο. Η κηλίδα φωτός, κατά την εστίαση πάνω στα δείγματα, είχε μέγεθος 0,5x3 mm2. Χρησιμοποιήθηκαν, επίσης, δυο διαφορετικοί δειγματοφορείς για μετρήσεις παράλληλα και κάθετα στα λεπτά υμένια των ηλιακών κυψελών ώστε να ανιχνευθούν δύο διαφορετικές ροές ρεύματος.

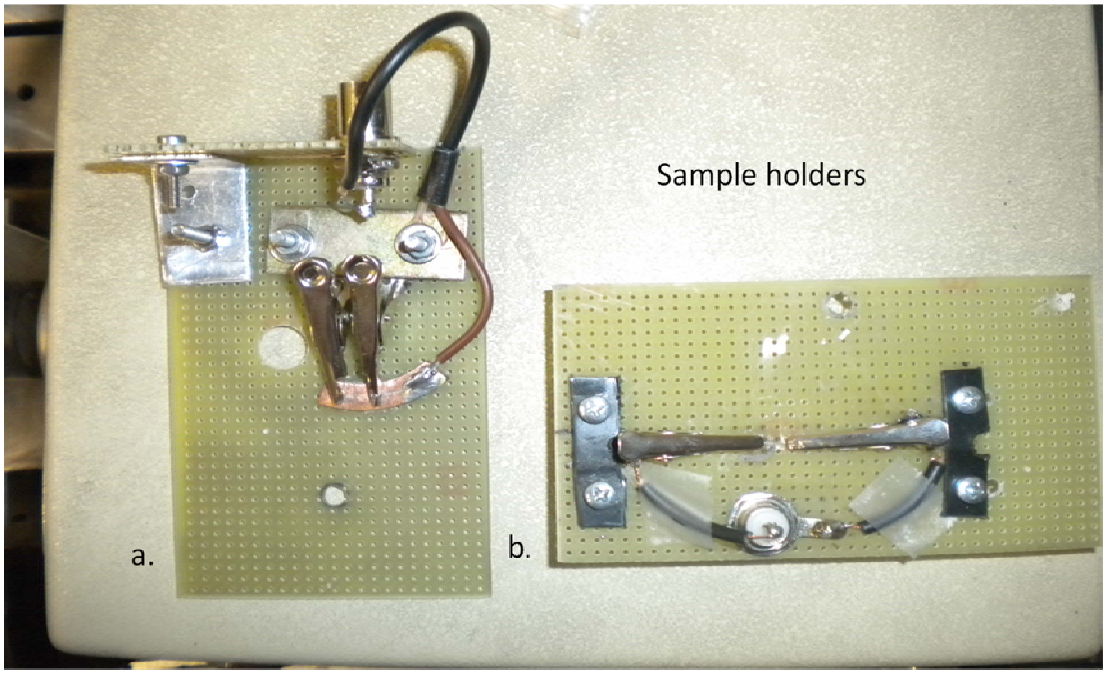

Εικόνα 5: οι δύο διαφορετικοί δειγματοφορείς που χρησιμοποιήθηκαν για τη μέτρηση του φωτορεύματος παράλληλα και κάθετα στις στρώσεις ηλιακών κυψελών PbPc/GaAs.

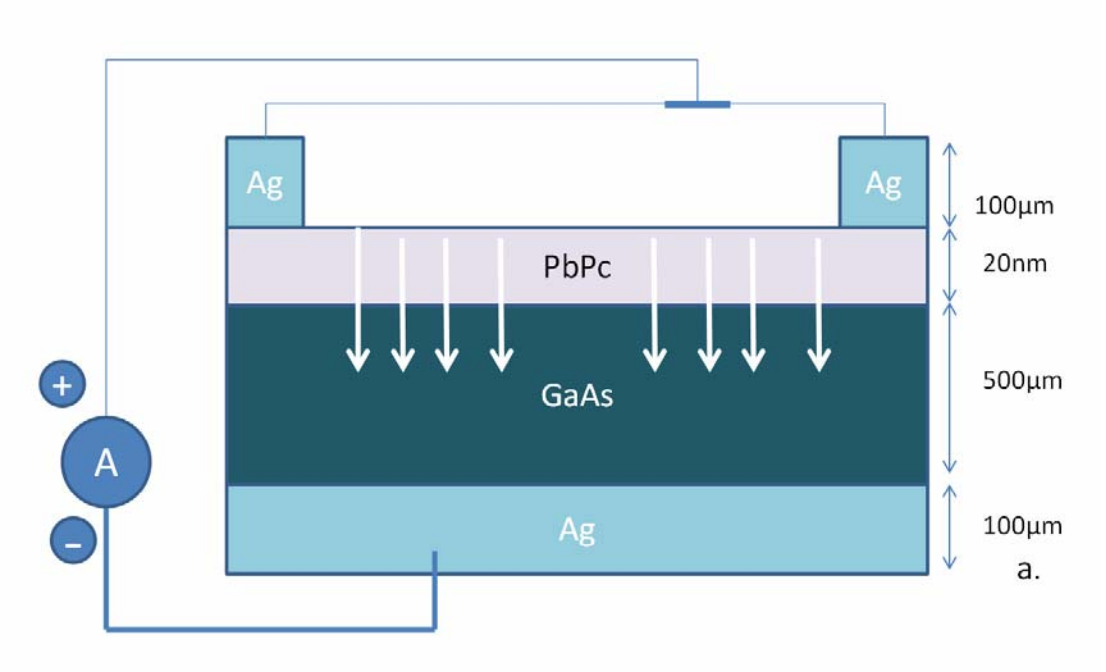

Εικόνα 6: μέτρηση της ροής ρεύματος κάθετα στα λεπτά υμένια PbPc/GaAs

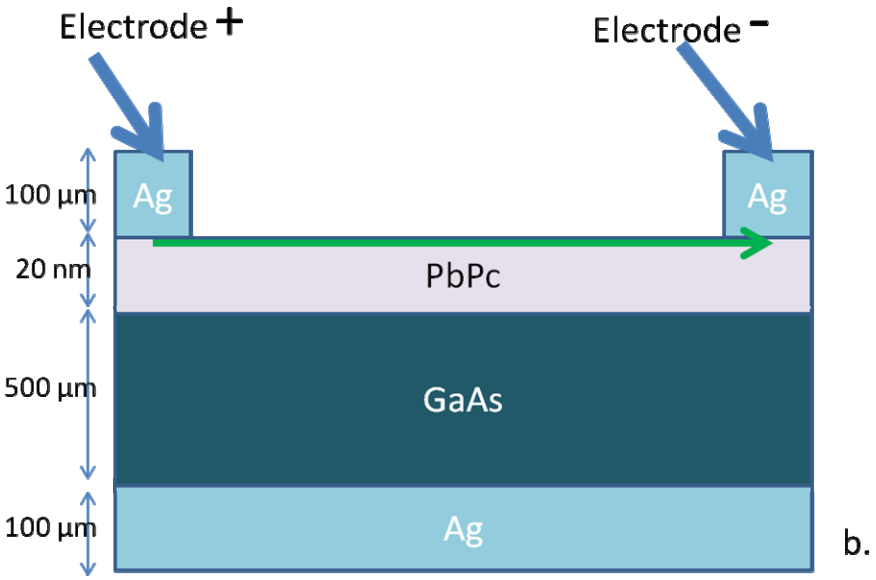

Εικόνα 7: μέτρηση της ροής ρεύματος παράλληλα στα λεπτά υμένια PbPc/GaAs

Στην κάθετη διαμόρφωση, το ρεύμα μετράται ανάμεσα στα πάνω και κάτω (front-to-back) ηλεκτρόδια της ηλιακής κυψέλης, όπως φαίνεται στην εικόνα 6, ενώ στην παράλληλη διαμόρφωση, το ρεύμα συλλέγεται μόνο από τα πάνω ηλεκτρόδια.

Το GaAs είναι δότης (n-type), ενώ η PbPc είναι δέκτης ηλεκτρονίων (p-type).

Η απόδοση μετατροπής (IPCE = Internal Power Conversion Efficiency) ορίζεται ως:

IPCE(%)=ηλεκτρόνια που δημιουργούνται/ φωτόνια που προσπίπτουν

IPCE(%)=100 * hcI(λ) / λ P(λ)

όπου I(λ) το φωτόρευμα, P(λ) η πυκνότητα ισχύος της λυχνίας Xe από 0,5 έως 3,0 $mWcm^{-2}$ (σε όλο το εύρος του φάσματος φωτός που μετρούσαμε).

Μετρήσεις λήφθηκαν υπό σκότος και με ακτινοβόληση, ώστε να προσδιοριστεί η απόδοση μετατροπής των ηλιακών κυψελών.

Γενικά, οι ηλιακές κυψέλες μετρήθηκαν σε 'κανονικοποιημένες' - κανονικές συνθήκες (Standard Test Conditions), δηλαδή: θερμοκρασία 25˚C, πυκνότητα ακτινοβολίας 1000 W/m^2 και μάζα αέρος 1.5 (AM1.5). Αυτές οι συνθήκες αντιστοιχούν σε μια αίθρια ημέρα με ήλιο και μέτρηση σε γωνία πρόσπτωσης της ηλιακής ακτινοβολίας $41,81^o$ πάνω από τον ορίζοντα.

Αρχικά μετρήθηκαν οι I-V του γαλλίου αρσενικού για να συγκριθούν, στη συνέχεια, με τις I-V ηλιακών κυψελών με επίστρωση φθαλοκυανίνης μολύβδου. Η απόκριση στο GaAs είναι μικρή αλλά αναμενόμενη, εφόσον μετρούμε μόνο το υπόστρωμα. Το υπόστρωμα σχηματίζει επαφή schottky με τα ηλεκτρόδια του αργύρου και δίνει ένα ασθενές σήμα που αποκλίνει από το μηδενικό (η καμπύλη στο 3^o τεταρτημόριο, στη μέτρηση χωρίς φωτισμό, δεν ταυτίζεται με τον άξονα y).

Στις ηλιακές κυψέλες πρέπει να έχουμε ωμικές επαφές μεταξύ ηλεκτροδίων και υλικού, ώστε το ρεύμα να ρέει χωρίς αντιστάσεις.

Η μέγιστη ισχύς, που μετρήθηκε στο υπόστρωμα, ήταν Pmax= 0,341nW.

Οι καμπύλες των ηλιακών κυψελών PbPc/GaAs c(4x4) και PbPc/GaAs β2(2x4) συγκρινόμενες με αυτές του υποστρώματος θα μας δείξουν πόσο αποδοτικές είναι οι ηλιακές κυψέλες και κατά πόσο η επίστρωση 20nm PbPc οδηγεί σε ηλιακές κυψέλες με ικανοποιητική απόδοση.

Αποτελέσματα- Γραφήματα

Οι καμπύλες ρεύματος- τάσης (I-V), που μετρήθηκαν, είναι οι ακόλουθες:

a. Υπόστρωμα GaAs

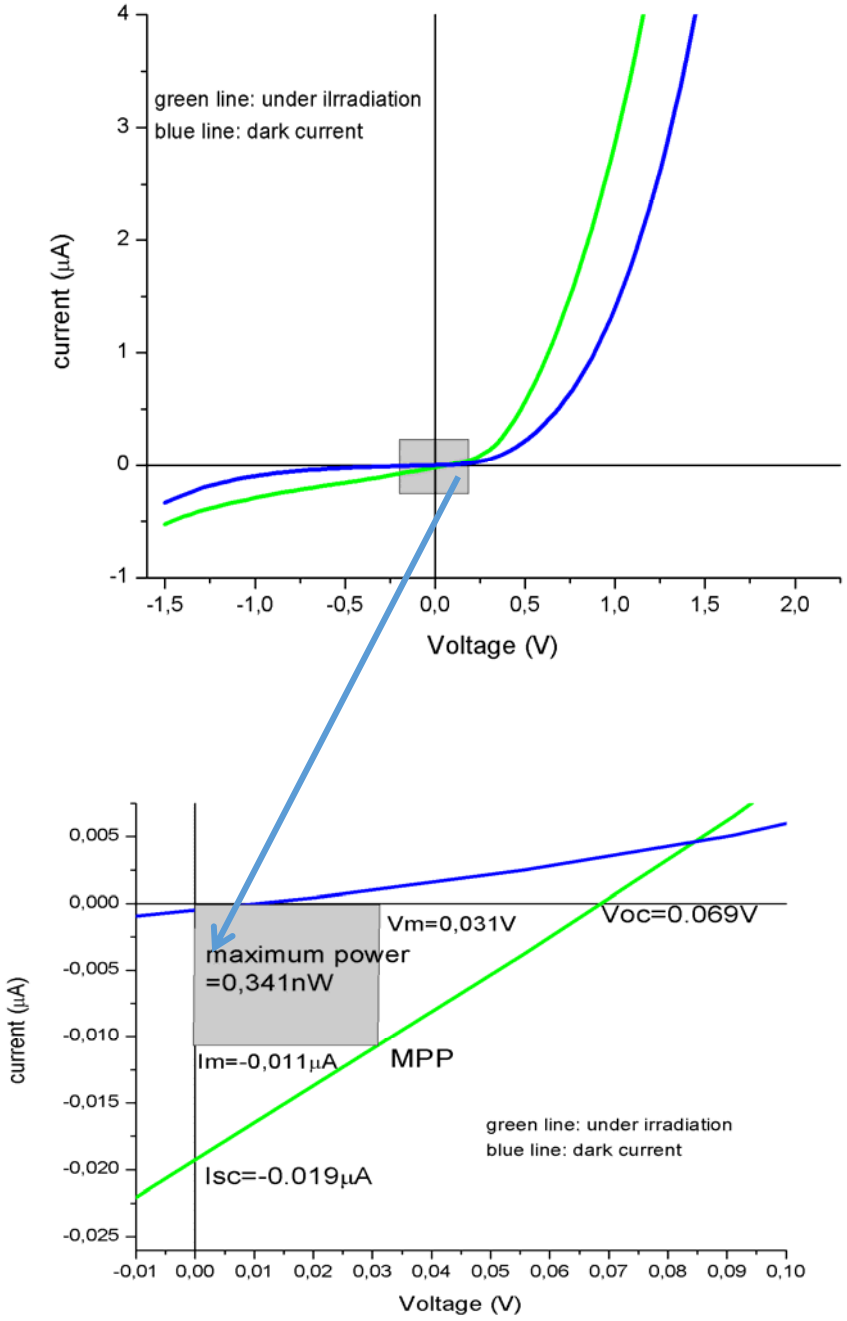

Γραφήματα 1, 2. Υπόστρωμα GaAs: μετρήσεις I-V υπό σκότος (μπλε καμπύλη) και με ακτινοβόληση (πράσινη καμπύλη).

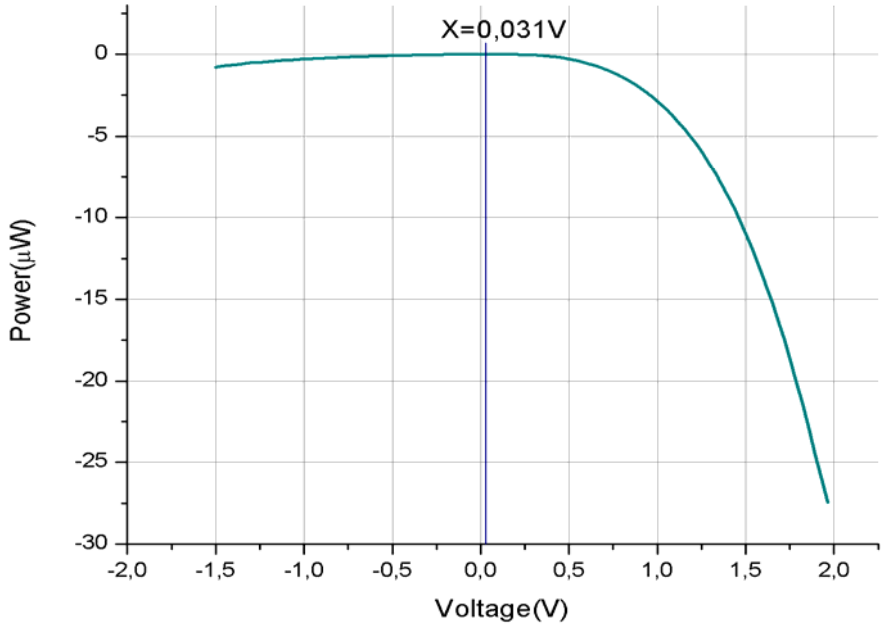

Γράφημα 3. Υπόστρωμα GaAs: χαρακτηριστική καμπύλη απόδοσης ισχύος - τάσης με μέγιστο τάσης Vm=0,031V

b. PbPc/ GaAs β2(2x4)

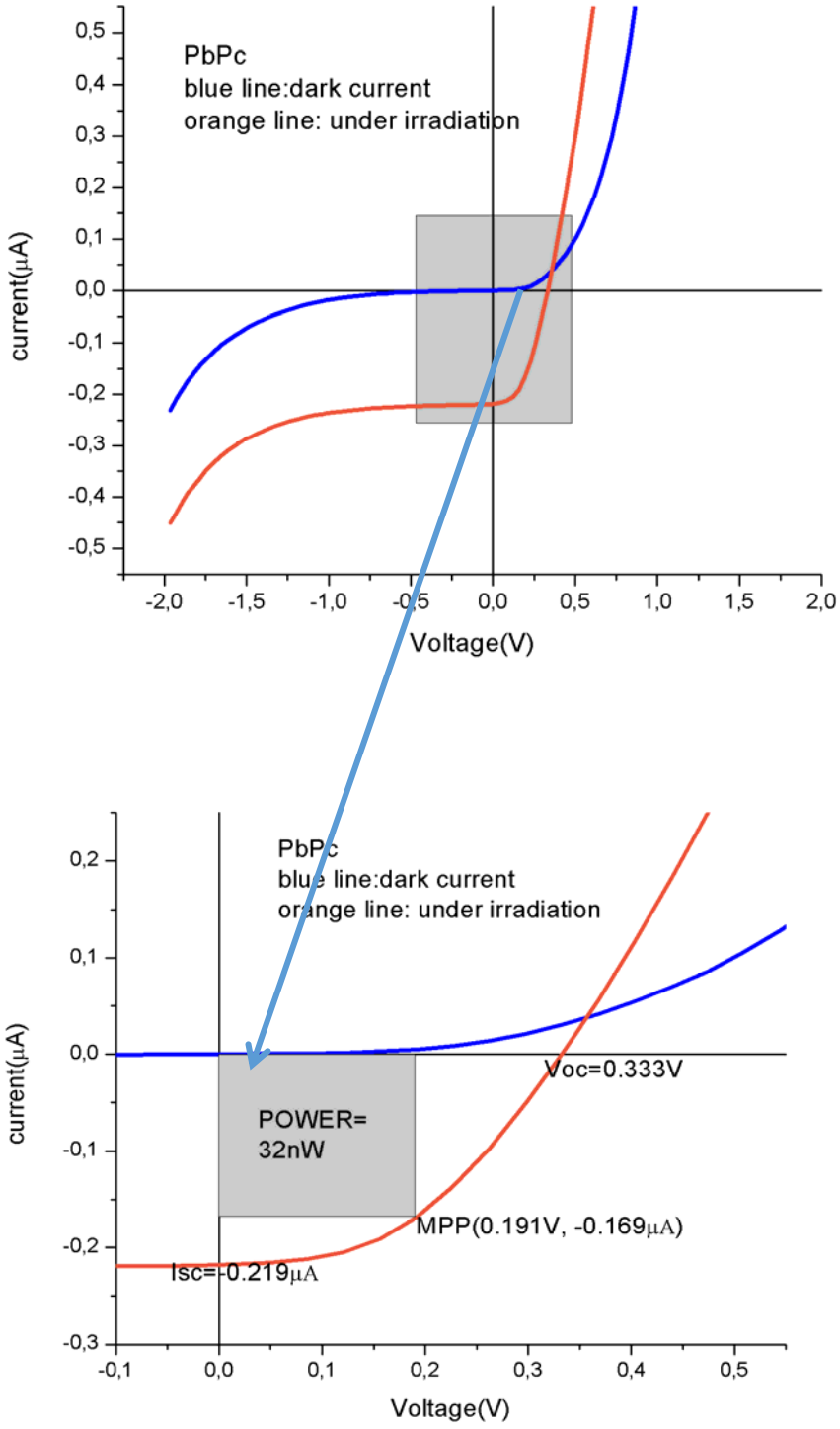

Γραφήματα 4,5. Ηλιακή κυψέλη PbPc/GaAs β2(2x4): μετρήσεις I-V υπό σκότος (μπλε καμπύλη) και με ακτινοβόληση (πορτοκαλί καμπύλη).

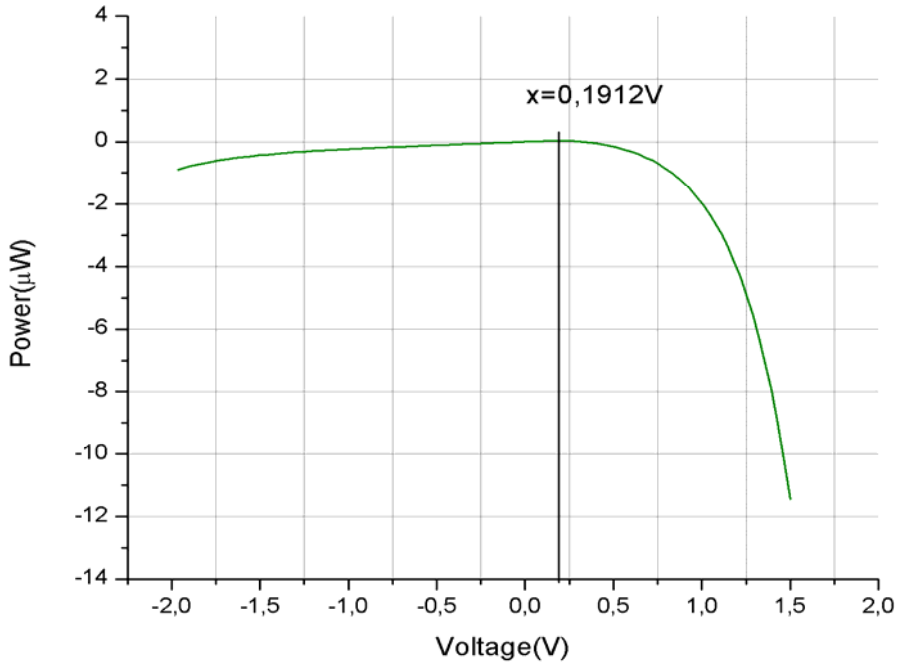

Γράφημα 6. Ηλιακή κυψέλη PbPc/GaAs β2(2x4): χαρακτηριστική καμπύλη απόδοσης ισχύος - τάσης με μέγιστο τάσης στα Vm =0,1912V

Η καμπύλη υπό σκότος περνά από το σημείο (0,0). Από την καμπύλη υπό ακτινοβόληση, σε μηδενική τάση προσδιορίζεται το ρεύμα βραχυκύκλωσης, ενώ μηδενικό ρεύμα αντιστοιχεί στην τάση ανοικτού κυκλώματος. Το ρεύμα βραχυκύκλωσης Isc και η τάση ανοιχτού κυκλώματος Voc είναι δύο σημαντικές παράμετροι που χαρακτηρίζουν μια ηλιακή κυψέλη και απεικονίζονται στα γραφήματα. Από το ορθογώνιο (σκιασμένο στο γράφημα), υπολογίζονται το ρεύμα και η τάση του σημείου μέγιστης ισχύος (MPP). Το εμβαδόν του ορθογωνίου δίνει τη μέγιστη ισχύ. Η μέγιστη ισχύς του υποστρώματος GaAs είναι 0,34nW, ενώ η μέγιστη ισχύς της ηλιακής κυψέλης PbPc/GaAs β2(2x4) είναι 32 nW, δηλαδή δύο τάξεις μεγέθους μεγαλύτερη.

c. PbPc/GaAs c(4x4)-Au

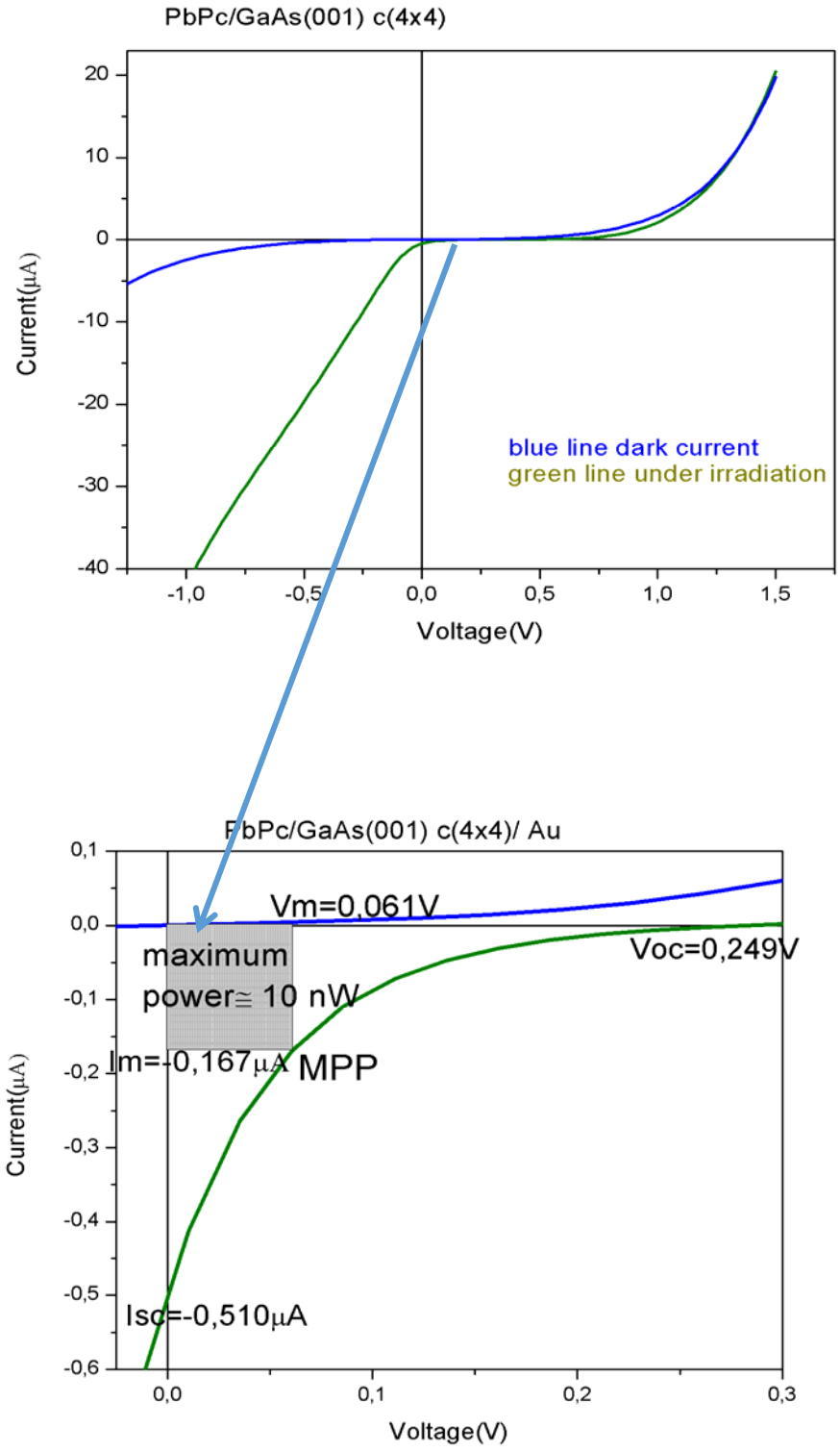

Γράφημα 7, 8. Ηλιακή κυψέλη PbPc/GaAs c(4x4)-Au: μετρήσεις I-V υπό σκότος (μπλε καμπύλη) και με ακτινοβόληση (πράσινη καμπύλη).

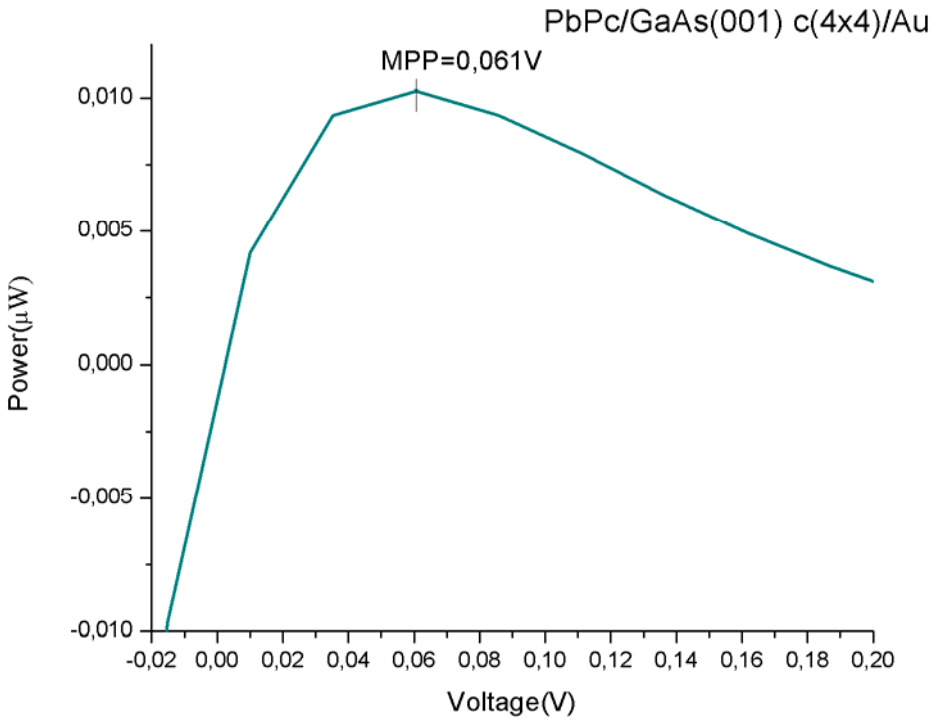

Γράφημα 9. Ηλιακή κυψέλη PbPc/GaAs c(4x4)-Au: χαρακτηριστική καμπύλη απόδοσης ισχύος - τάσης με μέγιστο τάσης Vm= 0,061V

Οι μετρήσεις I-V σε ηλιακή κυψέλη PbPc/GaAs c(4x4) που πραγματοποιήθηκαν κάθετα στις στρώσεις της κυψέλης υποδεικνύουν, ότι η κυψέλη έχει σημαντικά μικρότερη απόδοση. Ενδέχεται η αναδόμηση της επιφάνειας GaAs c(4x4) να έχει οδηγήσει ανασταλτικά στη φωτοβολταϊκή μετατροπή ή η κυψέλη να είναι βραχυκυκλωμένη. Επειδή για την αύξηση της αγωγιμότητας της κυψέλης χρησιμοποιήθηκαν ηλεκτρόδια από χρυσό (Au), ενδέχεται η εξάχνωση του χρυσού να οδήγησε σε βραχυκύκλωμα της κυψέλης. Από τη μέτρηση υπό σκότος (μπλε καμπύλη), διαπιστώνουμε, ότι για αρνητικές τιμές τάσης (-1,25V) η χαρακτηριστική καμπύλη I-V παρουσιάζει σημαντική απόκλιση σε έντονα αρνητικές τιμές ρεύματος (-0,5μA) συγκριτικά με τις αντίστοιχες τιμές της κυψέλης PbPc/GaAs β2(2x4) (-1,25V, -0,05 μA). Επιπλέον, η κυψέλη υπό σκότος παρουσιάζει ελάχιστο ρεύμα στην έξοδό της, παρότι εφαρμόζεται τάση 1,5V. Σημειώνεται, ότι η μέτρηση με ακτινοβόληση (πράσινη καμπύλη) δείχνει συμπεριφορά διπλής διόδου που οδηγεί σε μικρή τιμή του παράγοντα πλήρωσης (Fill Factor) και της απόδοσης η.

Ο παράγοντας πλήρωσης FF (fill factor) και η απόδοση η (efficiency) του υποστρώματος GaAs, της φθαλοκυανίνης μολύβδου PbPc σε υπόστρωμα γαλλίου αρσενικού GaAs β2(2x4) (PbPc/GaAs β2(2x4)) και της φθαλοκυανίνης μολύβδου PbPc σε υπόστρωμα γαλλίου αρσενικού GaAs c(4x4) (PbPc/GaAs β2(2x4)) υπολογίστηκαν από τους παρακάτω τύπους:

$$FF=\frac{I_m V_m}{I_{SC} V_{OC}} \qquad \eta=FF\frac{I_{sc} V_{oc}}{P_S}$$

όπου Im, Vm το ρεύμα και η τάση του σημείου μέγιστης ισχύος, Isc, Voc το ρεύμα βραχυκύκλωσης και η τάση ανοιχτού κυκλώματος, χαρακτηριστικά των ηλιακών κυψελών, και Ps η ισχύς της πηγής φωτός. Για τη λυχνία Xe, που χρησιμοποιήθηκε, ήταν 21 mW.

Πίνακας 1: παράγοντας πλήρωσης (Fill Factor) και απόδοση (η)

Pinc=21mW *I(μA), V(V)*	*Fill Factor %*	*η (efficiency)%*
1.GaAs ***Im=-0,011 Vm=0,031*** ***Isc=-0,019 Voc=0,068***	***26,4***	***0,016* x10^{-4}**
2.PbPc/GaAs β2(2x4) ***Im=-0,191 Vm=0,169*** ***Isc=-0,219 Voc=0,333***	***44,3***	***1,537* x10^{-4}**
3.PbPc/GaAs c(4x4) ***Im=-0 ,167 Vm=0,061*** ***Isc=-0,510 Voc=0,249***	***8,0***	***0,485* x10^{-4}**

Σύμφωνα με τα αποτελέσματα των μετρήσεων, ο μέγιστος παράγοντας πλήρωσης και η μέγιστη απόδοση παρατηρούνται στην ηλιακή κυψέλη της φθαλοκυανίνης μολύβδου σε υπόστρωμα γαλλίου αρσενικού β2(2x4) (PbPc/GaAs β2(2x4)). Συγκρίνοντας τις δύο κυψέλες PbPc/GaAs β2(2x4) και PbPc/GaAs c(4x4), διαπιστώνουμε, ότι ο παράγοντας πλήρωσης εμφανίζεται κατά 67,8% αυξημένος και η απόδοση κατά 95,1 %. Η σχετική αύξηση υπολογίζεται από τον τύπο:

$$\frac{f_2 - f_1}{f_1}100$$

Η απόδοση της κυψέλης PbPc/GaAs β2(2x4) είναι 1,537 x10^{-4} %, ενώ τα οργανικά φωτοβολταϊκά στοιχεία παρουσιάζουν ελάχιστη απόδοση περίπου 3,0%. Βελτιώσεις μπορούν να γίνουν με επιλογή κατάλληλου συνδυασμού μεταλλικών συλλεκτών (Ωμικών επαφών) και με αύξηση του πάχους του απορροφητή. Είναι σκόπιμο να γίνει μεγαλύτερης έκτασης έρευνα σε αυτούς τους συνδυασμούς ηλιακών κυψελών.

d. Κβαντική απόδοση ηλιακών κυψελών φθαλοκυανίνης μολύβδου σε διαφορετικές αναδομήσεις γαλλίου αρσενικού

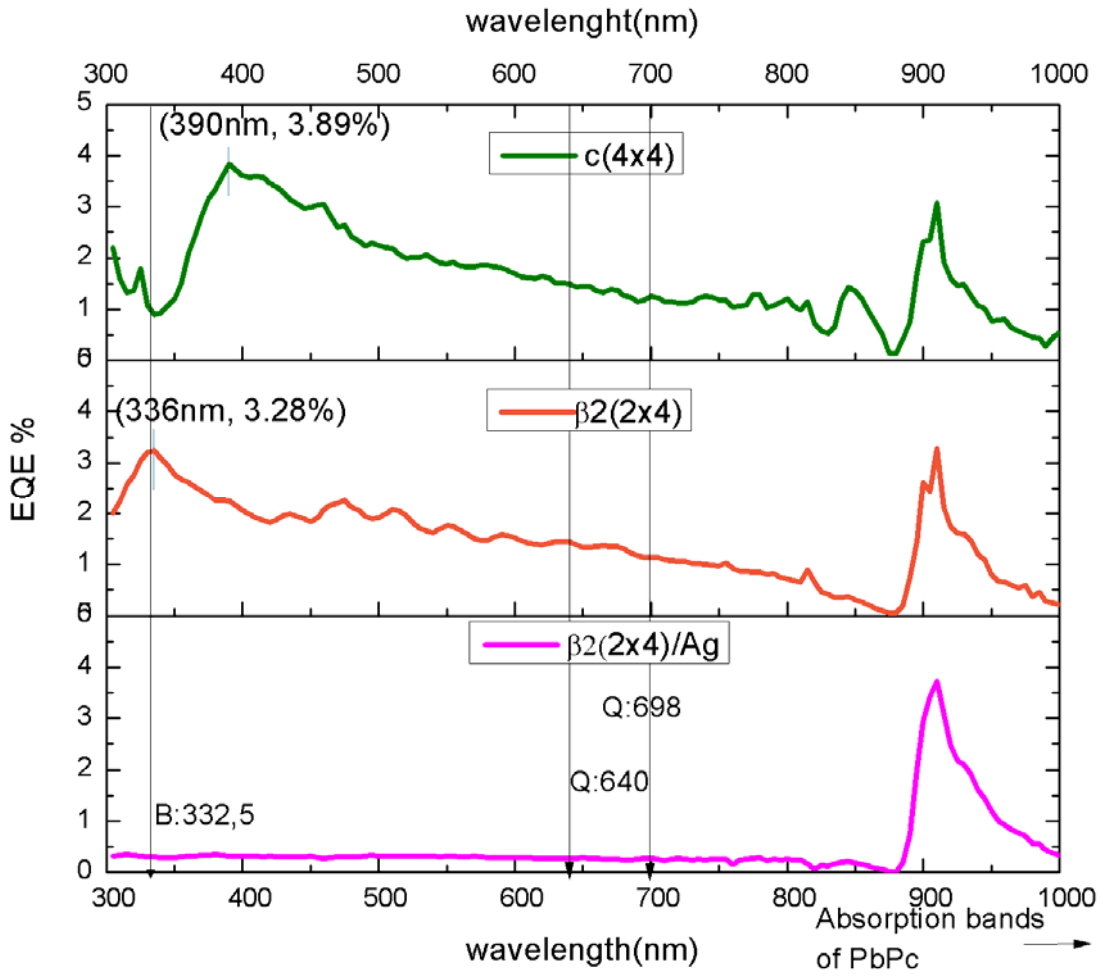

Γράφημα 10. κβαντική απόδοση ηλιακών κυψελών PbPc σε υποστρώματα GaAs β2(2x4) και GaAs c(4x4)

Η κβαντική απόδοση (EQE =External Quantum Efficiency) περιγράφει τον αριθμό των ηλεκτρονίων που δημιουργούνται από τον αριθμό των προσπιπτόντων φωτονίων

$$EQE = \frac{\alpha\rho\iota\theta\mu\acute{o}\varsigma\ \eta\lambda\varepsilon\kappa\tau\rho o\nu\acute{\iota}\omega\nu}{\alpha\rho\iota\theta\mu\acute{o}\varsigma\ \phi\omega\tau o\nu\acute{\iota}\omega\nu} 100$$

Οι τύποι που συσχετίζουν την ενέργεια με το μήκος κύματος της ακτινοβολίας (και αντιστρόφως) είναι

λ (Å) =12400/E(eV) και E=hν=hc/λ

όπου c=3x10^{8}m/s ταχύτητα φωτός στο κενό και h=6,626x10^{-34}Js=4,136eVs η σταθερά Planck.

Στα φάσματα EQE, η ζώνη στα 900-1000nm, στο υπέρυθρο (λ>700nm), οφείλεται στην εκπομπή της λυχνίας Xe. Για το λόγο αυτό, υπάρχει και στα τρία φάσματα. Το ενεργειακό χάσμα του GaAs παρατηρείται, στο φάσμα PbPc/GaAs c(4x4) στα 871,34nm.

Με σύγκριση των φασμάτων PbPc/GaAs c(4x4) και PbPc/GaAs β2(2x4), διαπιστώνουμε, ότι το διαφορετικό υπόστρωμα, δηλαδή, οι διαφορετικές επιφανειακές αναδομήσεις του υποστρώματος GaAs, επηρεάζουν τη φωτοαπόκριση των κυψελών. Το μέγιστο της κβαντικής απόδοσης της κυψέλης με επιφανειακή αναδόμηση c(4x4) εμφανίζεται σε μήκος κύματος λ=390nm και ενέργεια E=3,18 eV, ενώ για την ηλιακή κυψέλη με επιφανειακή αναδόμηση υποστρώματος β2(2x4) είναι μετατοπισμένο στην υπεριώδη περιοχή λ=336 nm και ενέργεια E=3,69 eV. Το μέγιστο της κβαντικής απόδοσης (EQE) της φθαλοκυανίνης, και στα δύο δείγματα, είναι (3,5±0,5)%. Αυτό υποδεικνύει, ότι και τα δύο δείγματα έχουν την ίδια φωτοαπόκριση και παράγουν τον ίδιο περίπου αριθμό ηλεκτρονίων κατά την ακτινοβόληση με την ίδια ισχύ, αλλά τα φαινόμενα μεταφοράς και συλλογής των φορέων παρουσιάζουν σημαντικές διαφορές με αποτέλεσμα σημαντική μείωση του συντελεστή απόδοσης της κυψέλης PbPc/GaAs c(4x4). Σημειώνεται, ότι η φθαλοκυανίνη μολύβδου συνεισφέρει με απορρόφηση στην υπεριώδη περιοχή, ενώ η απόκριση στο ορατό οφείλεται στο αρσενιούχο γάλλιο.

Το τρίτο φάσμα, στο γράφημα 10, αντιστοιχεί σε ηλιακή κυψέλη με επιφανειακή αναδόμηση υποστρώματος β2(2x4), όπου η προσθήκη αργυρού στα ηλεκτρόδια για να βελτιωθεί η απόδοση της ηλιακής κυψέλης οδήγησε σε «σκίαση» του απορροφητή. Παρατηρείται, ότι δεν έχουμε δημιουργία φωτορεύματος, εφόσον η προσθήκη αργύρου δεν επιτρέπει στο φως να φτάσει τη φωτοενεργή ένωση (p-n junction).

Σημειώνεται, ότι στα φάσματα κβαντικής απόδοσης PbPc/GaAs δεν εμφανίζονται κορυφές που μπορούν να αποδοθούν στην Q-ζώνη απορρόφησης της φθαλοκυανίνης μολύβδου, παρόλο που είναι πιο ισχυρή από τη B ζώνη.

Το φάσματα απορρόφησης των φθαλοκυανινών παρουσιάζονται στην ακόλουθη Εικόνα 8 :

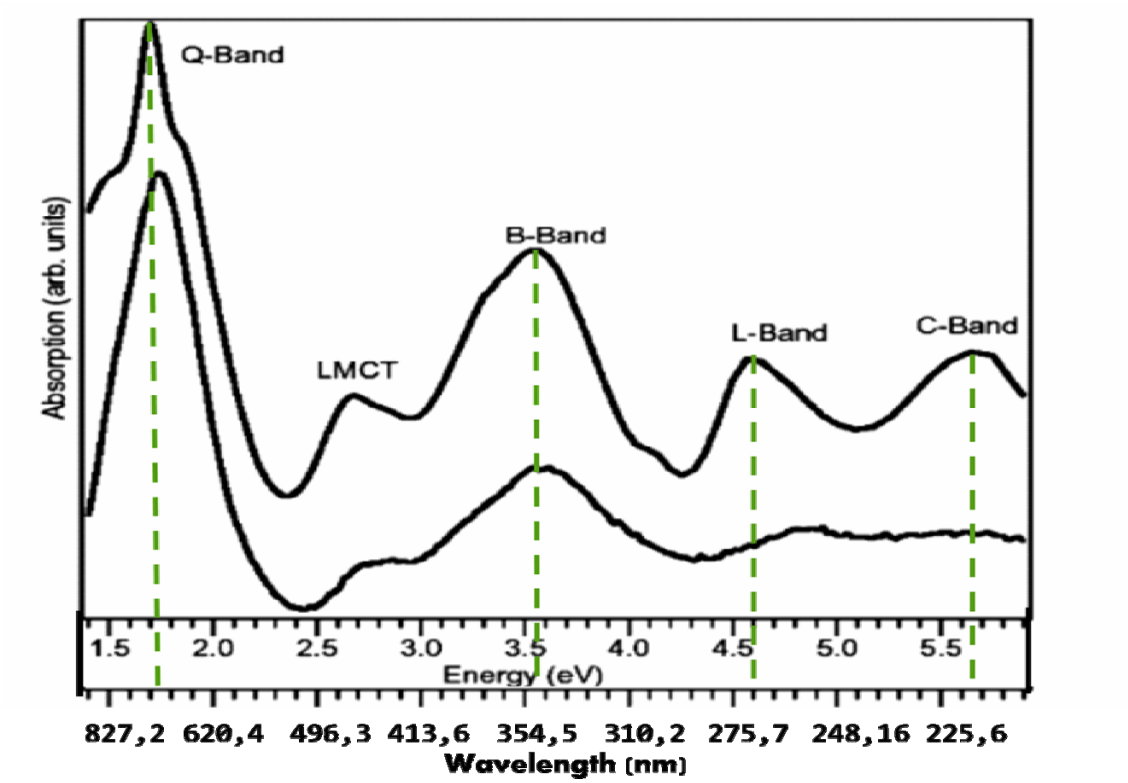

Εικόνα 8: Φάσματα φθαλοκυανινών: ζώνες απορρόφησης φθαλοκυανινών στο υπέρυθρο και ορατό φάσμα (άνω) και φάσμα απωλειών λόγω απορρόφησης (κάτω). Τα φάσματα αντιπροσωπεύουν συνολικά την οικογένεια των φθαλοκυανινών, εκτός από την κορυφή LMCT που είναι χαρακτηριστική για κάθε φθαλοκυανίνη.

Οπτικός χαρακτηρισμός των ελεύθερων μορίων PbPc με φασμασκοπία Raman

Πειραματική διάταξη Raman

Το φασματόμετρο Raman (Dilor spectrometer) περιλαμβάνει laser ιόντων αργού, φακούς και κάτοπτρα για την οδήγηση και εστίαση της δέσμης στο δείγμα, ανιχνευτή CCD, πολύ ευαίσθητο στην ανίχνευση φωτός και με ψύξη σε χαμηλή θερμοκρασία για την ελαχιστοποίηση του θορύβου. Για τη λήψη των φασμάτων Raman φθαλοκυανίνης μολύβδου (PbPc) στην αέρια φάση, εξαχνώθηκε σκόνη PbPc. Το δείγμα ήταν σε γυάλινο σωλήνα, υπό κενό $8x10^{-3}$ mbar, περιτυλιγμένο με Ωμική σπείρα από ίνες γυαλιού, που είχε μέσα σύρμα από βολφράμιο, ως θερμαντικό στοιχείο. Με την παροχή ηλεκτρικού ρεύματος, ήταν δυνατή η αύξηση της θερμοκρασίας στο σύρμα ως τη θερμοκρασία εξάχνωσης (περίπου 570 ^{o}C), ώστε τα μόρια της φθαλοκυανίνης να είναι σε αέρια φάση και, ως εκ τούτου, ελεύθερα. Σημειώνεται, ότι το γυαλί από χαλαζία του δειγματοφορέα έχει θερμοκρασία αποσκλήρυνσης περί 580 ^{o}C. Για τη μέτρηση της θερμοκρασίας του δείγματος, χρησιμοποιήθηκαν θερμοστοιχεία νικελίου χρωμίου και νικελίου αλουμινίου.

Γενική άποψη της πειραματικής διάταξης, που χρησιμοποιήθηκε για τη λήψη των φασμάτων Raman, παρουσιάζεται στην Εικόνα 9, ενώ λεπτομέρειες με το δειγματοφορέα PbPc και την εστίαση της δέσμης παρουσιάζονται στις Εικόνες 10-11, που ακολουθούν.

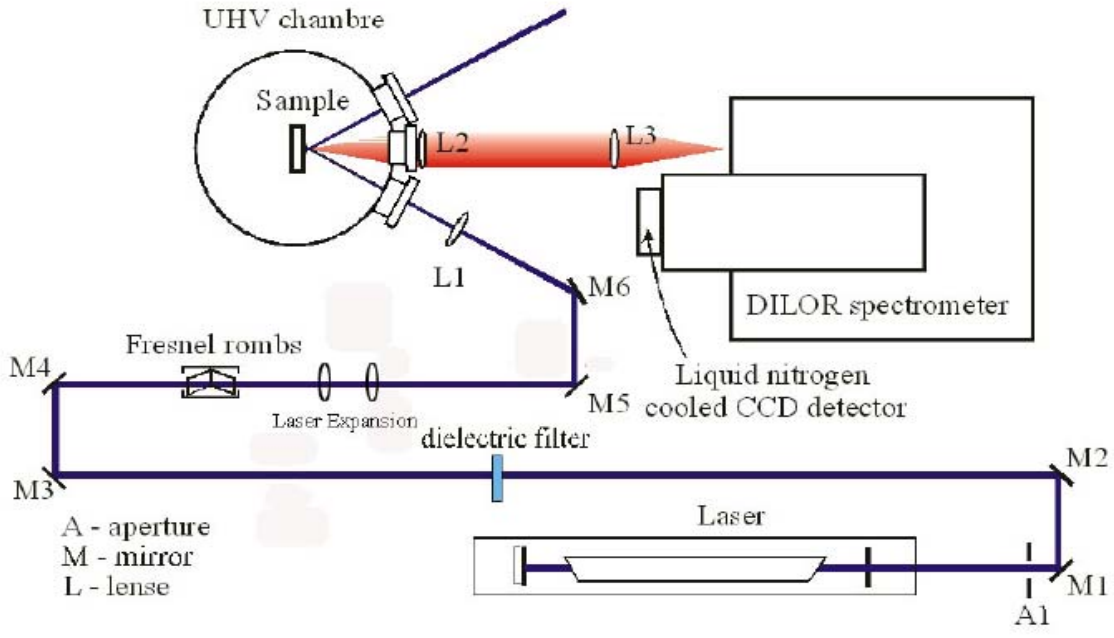

Εικόνα 9: φασματόμετρο Raman

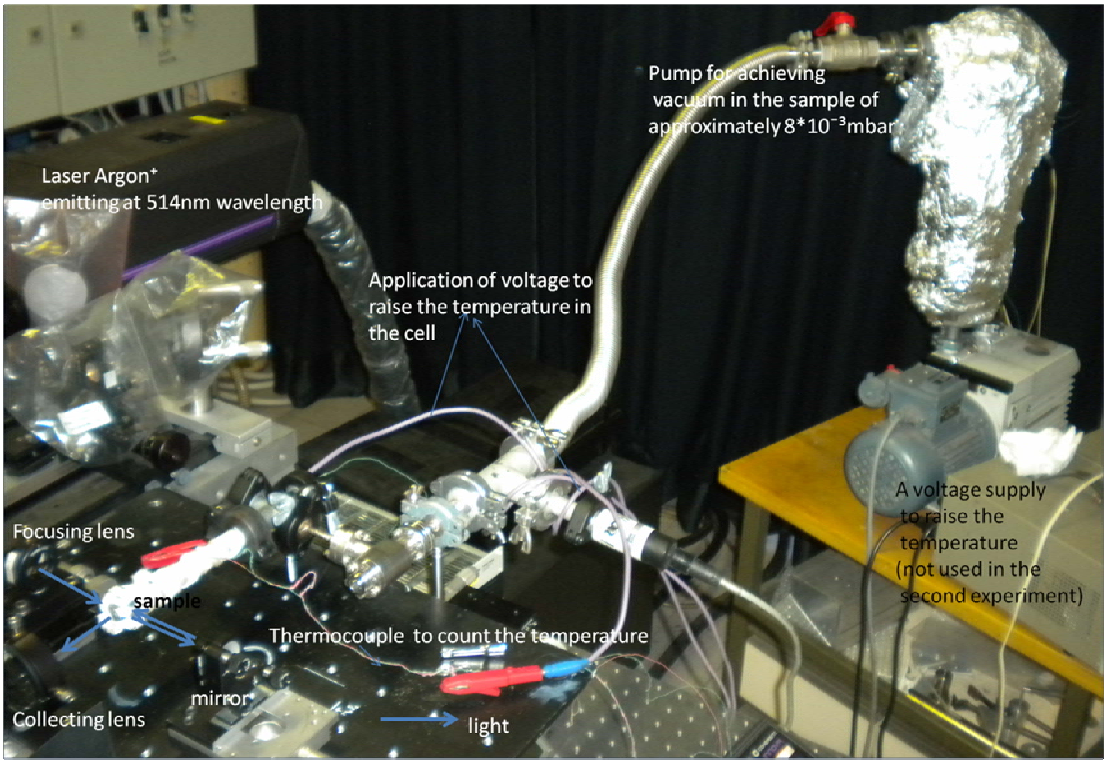

Εικόνα 10: φασματόμετρο Raman με δειγματοφορέα PbPc

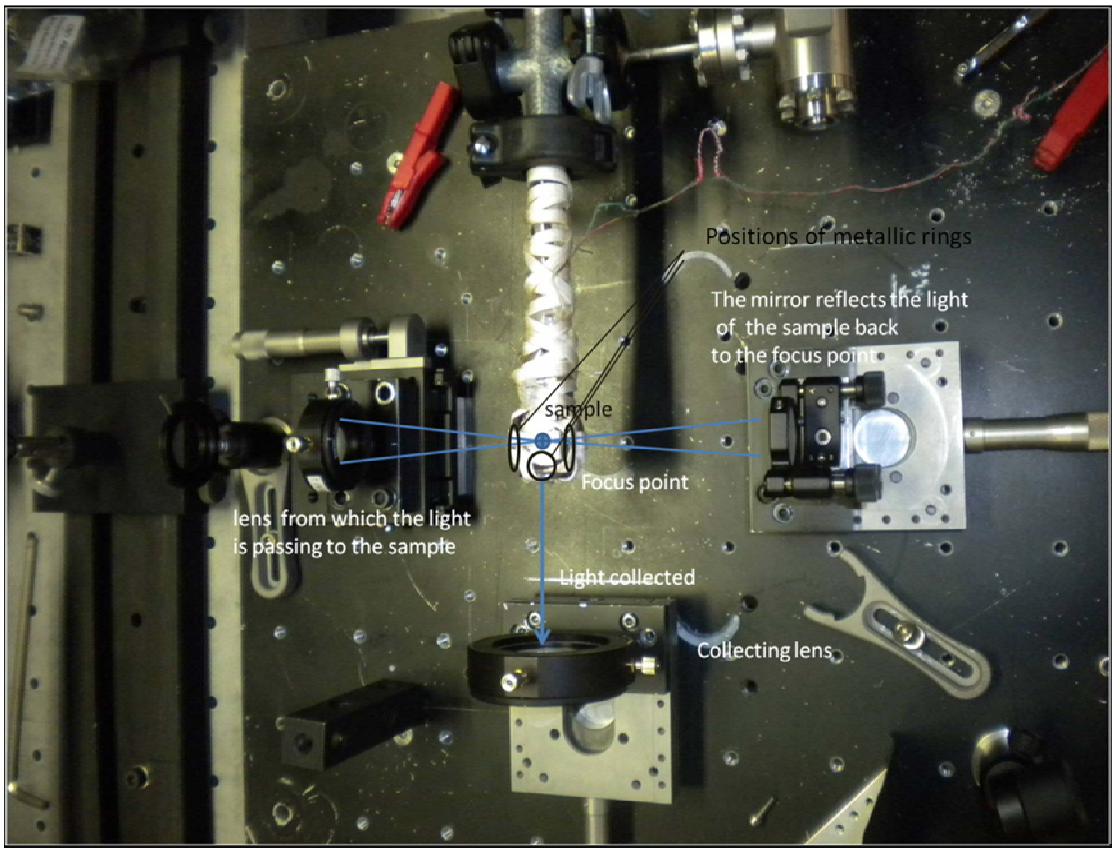

Εικόνα 11: οπτική διαδρομή της δέσμης μέσω του δείγματος (τα μεταλλικά δαχτυλίδια χρησιμοποιήθηκαν για να αυξηθεί η θερμοκρασία στην περιοχή των οπτικών παραθύρων).

Αναλυτικά, η πειραματική διάταξη Raman περιλαμβάνει:

1. Ar^+-laser[27] συντονισμένο σε μήκος κύματος 514,5 nm (πράσινο). Τα laser ιόντων αργού εκπέμπουν σε 12 μήκη κύματος από το υπεριώδες, μέσω του ορατού, ως το υπέρυθρο: 351,1 nm, 363,8 nm, 454,6 nm, 457,9 nm, 465,8 nm, 476,5 nm, 488,0 nm, 496,5 nm, 501,7 nm , 514.5 nm, 528,7 nm, 1092,3 nm με πιο συχνά χρησιμοποιούμενα μήκη κύματος τα 514,5 και 488,0 nm.
2. Φακούς και κάτοπτρα για την ευθυγράμμιση της δέσμης καθώς και για την εξασφάλιση της εστίασης της δέσμης στο δείγμα, μετά από αλλεπάλληλες ανακλάσεις, έτσι ώστε να αυξηθεί η ένταση του σήματος, η οποία είναι χαμηλή, επειδή το δείγμα είναι στην αέρια φάση.
3. Ανιχνευτής συζευγμένων φορτίων (CCD), ο οποίος ψύχεται με υγρό άζωτο. Η σκέδαση Raman έχει πολύ χαμηλό σήμα και, ως εκ τούτου, είναι απαραίτητο να ελαχιστοποιηθεί το υπόβαθρο θορύβου.

Για το δείγμα, χρησιμοποιήθηκαν δύο διαφορετικοί δειγματοφορείς από γυαλί, εκ των οποίων, το ένα από χαλαζία πολύ καλής κρυσταλλικής ποιότητας. Το γυαλί, όπως το νερό, είναι ισχυροί απορροφητές της υπέρυθρης ακτινοβολίας και ασθενείς σκεδαστές στη φασματοσκοπία Raman, ιδιότητες, οι οποίες τα καθιστούν κατάλληλα για τις μετρήσεις στην παρούσα εργασία.

Η ομοιογένεια του δείγματος είναι πολύ σημαντική, ώστε κάθε σημείο εστίασης να παράγει τα ίδια αποτελέσματα. Για το λόγο αυτό, είναι απαραίτητη η ομοιόμορφη θέρμανση του δείγματος που εξασφαλίστηκε με το θερμαντικό στοιχείο, τα μεταλλικά δαχτυλίδια γύρω από τα οπτικά παράθυρα, και τη συμπληρωματική θέρμανση με το πιστόλι θερμότητας. Με τη συμπληρωματική θέρμανση αντιμετωπίστηκε ένα πρόβλημα που προκύπτει από την προσκόλληση των μορίων PbPc στα παράθυρα για οπτικές μετρήσεις λόγω διαφοράς θερμοκρασίας ως προς την αέρια φάση.

Κατά την μελέτη της αέριας φάση των μορίων της PbPc είναι επίσης σημαντικό, ο αριθμός των μορίων σε αέρια φάση ανά μονάδα όγκου να είναι σχετικά μικρός. Για το σκοπό αυτό, ο δειγματοφορέας, που χρησιμοποιήθηκε, ήταν γυάλινος σωλήνας με σχετικά μεγάλο μήκος, όπως φαίνεται στην ακόλουθη Εικόνα 12. Ο σωλήνας ήταν υπό κενό, ώστε να μετράται αποκλειστικά η σκέδαση Raman των μορίων φθαλοκυανίνης μολύβδου στην αέρια φάση, και όχι προσμίξεων ή ρυπαντών.

[27] Το Ar^+-laser εφευρέθηκε το 1964 από τον William Bridges στο Hughes Aircraft και ανήκει στην οικογένεια των laser ιόντων που χρησιμοποιούν ευγενές αέριο ως ενεργό μέσο.

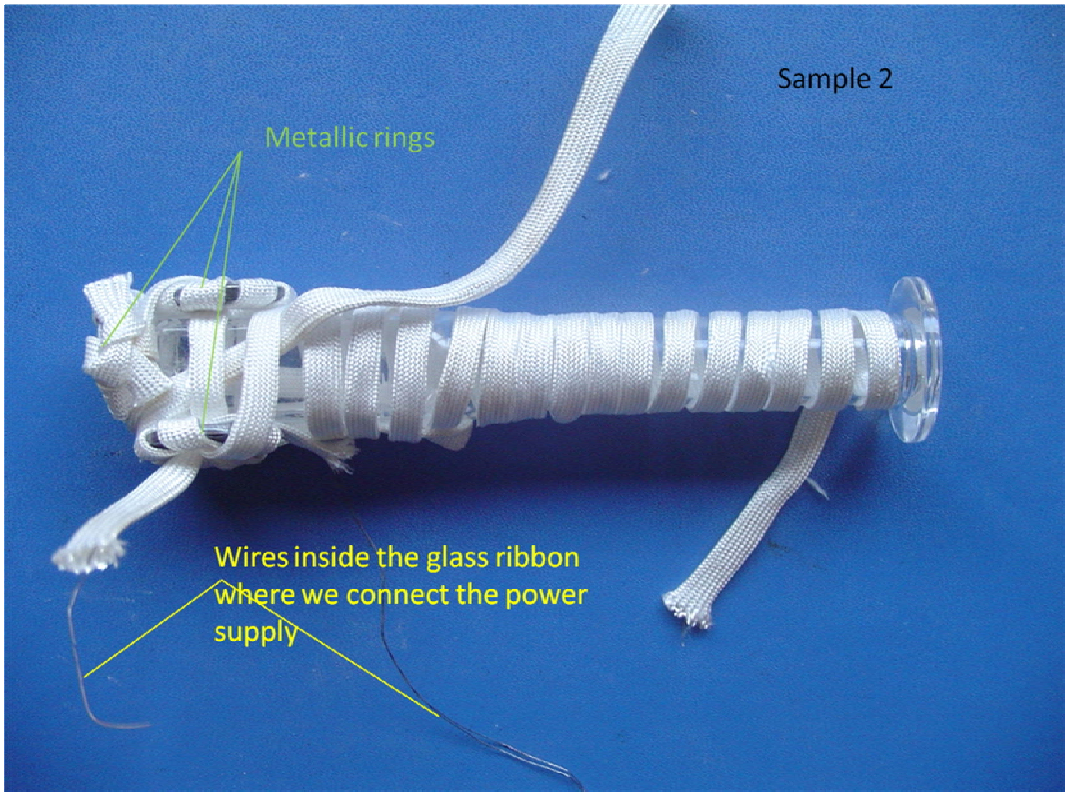

Εικόνα 12: γυάλινος δειγματοφορέας της σκόνης PbPc η οποία εξαχνώνεται με τάση εφαρμοζόμενη στο σύρμα βολφραμίου από το θερμαντικό στοιχείο

Αποτελέσματα

Η διέγερση της σκέδασης Raman μορίων φθαλοκυανίνης μολύβδου σε αέρια φάση πραγματοποιήθηκε με ακτινοβολία Ar^{+}-laser μήκους κύματος 514,5 nm και ισχύος εξόδου 5,4 W. Το φάσμα Raman PbPc στην αέρια φάση παρουσιάζεται στο Γράφημα 11.

Στο φάσμα, απεικονίζεται: η ένταση του σκεδαζόμενου φωτός ως συνάρτηση της μετατόπισης Raman-Stokes (cm^{-1}). Η σκέδαση Stokes εμφανίζεται σε συχνότητα χαμηλότερη από τη συχνότητα της δέσμης laser που χρησιμοποιείται για τη διέγερση. Η καταγραφή της σκέδασης Raman παρουσιάζεται μόνο ως φάσμα Stokes (και όχι αντι-Stokes) επειδή είναι σημαντικά υψηλότερης έντασης.

Κάθε ταλάντωση του μορίου PbPc έχει μια συγκεκριμένη συχνότητα Raman. Συνεπώς, από τις κορυφές που υπάρχουν στο φάσμα, είναι δυνατό να προσδιοριστεί ο τρόπος ταλάντωσης του μορίου. Το φάσμα λήφθηκε 100 cm^{-1} από τη γραμμή Rayleigh του ελαστικά σκεδαζόμενου φωτός, επειδή αυτή είναι πολύ έντονη και θα μπορούσε να καταστρέψει το CCD, αλλά και επειδή το φάσμα PbPc περιλαμβάνει τις περισσότερες από τις χαρακτηριστικές ταλαντώσεις του μορίου σε κυματαριθμούς άνω των 200 cm^{-1}. Οι εντάσεις των ζωνών στο φάσμα Raman εξαρτώνται από τη φύση της ταλάντωσης, που μελετάται. Για τη βελτίωση του

λόγου σήματος προς θόρυβο, χρησιμοποιήθηκε ενισχυτής εγκλείδωσης συχνότητας (lock-in), ώστε να ελαχιστοποιούνται οι παράγοντες οπτικού και ηλεκτρονικού θορύβου.

Η ταυτοποίηση των τρόπων ταλάντωσης του μορίου PbPc έγινε με βάση υπολογισμούς της Πυκνότητας Καταστάσεων (DFT =Density Functional Theory). Οι υπολογισμοί DFT[28] χαρακτηρίζουν ελεύθερα μόρια, όπως στο πείραμα για τα μόρια της PbPc σε αέρια φάση.

Για την επεξεργασία του φάσματος PbPc και τον προσδιορισμό των χαρακτηριστικών συχνοτήτων Raman χρησιμοποιήθηκε το πρόγραμμα Datlab. Οι τρόποι ταλάντωσης του μορίου και οι αντίστοιχες συχνότητες και εντάσεις των ζωνών Raman έχουν καταχωρηθεί στον Πίνακα 2.

Το φάσμα Raman, στην περιοχή 100-800 cm^{-1}, παρουσιάζει 19 κορυφές, από τις οποίες οι 17 ταυτοποιήθηκαν με δονήσεις του μορίου. Οι κορυφές στα 753 και 763 cm^{-1} θεωρήθηκαν, ότι οφείλονται σε κοσμικές ακτίνες λόγω του εξαιρετικά μικρού εύρους τους. Μικρού εύρους κορυφές μπορεί να παρατηρηθούν σε αέρια με χαμηλή πίεση και χαμηλή θερμοκρασία. Αυτό όμως θα οδηγούσε σε στενές κορυφές σε όλο το φάσμα, ενώ στη συγκεκριμένη περίπτωση το εύρος των ζωνών PbPc κυμαίνεται από 10 ως 30 cm^{-1}. Τα κριτήρια που λήφθηκαν υπόψη για την ταυτοποίηση των κορυφών ήταν τα ακόλουθα:

- Η συμμετρία των τρόπων ταλάντωσης του μορίου
- Η συχνότητα στην οποία εμφανίζονται οι κορυφές
- Η ένταση των κορυφών
- Η ενδεχόμενη αλληλεπίδραση γειτονικών ταλαντώσεων

Όπως παρουσιάζεται στον παρακάτω Πίνακα 2, υπάρχουν διαφορές στις εντάσεις των κορυφών σε σύγκριση με εκείνες που αναμένονται με βάση τις θεωρητικές προβλέψεις της DFT. Μια πιθανή εξήγηση δίνεται από το γεγονός, ότι η PbPc είναι ένα μεγάλο μόριο με ένα πλούσιο φάσμα Raman και, ως εκ τούτου, είναι δυνατό να παρατηρηθούν διαφορές στις συχνότητες και στις εντάσεις, εάν υπάρχουν ακόμα και μικρές διαφορές στη σύνθεση του υλικού.

[28] Φάσματα των υπολογισμών DFT σε στερεά και υγρά μπορούν να εμφανίζουν μετατοπίσεις ζωνών που οφείλονται σε μοριακές αλληλεπιδράσεις

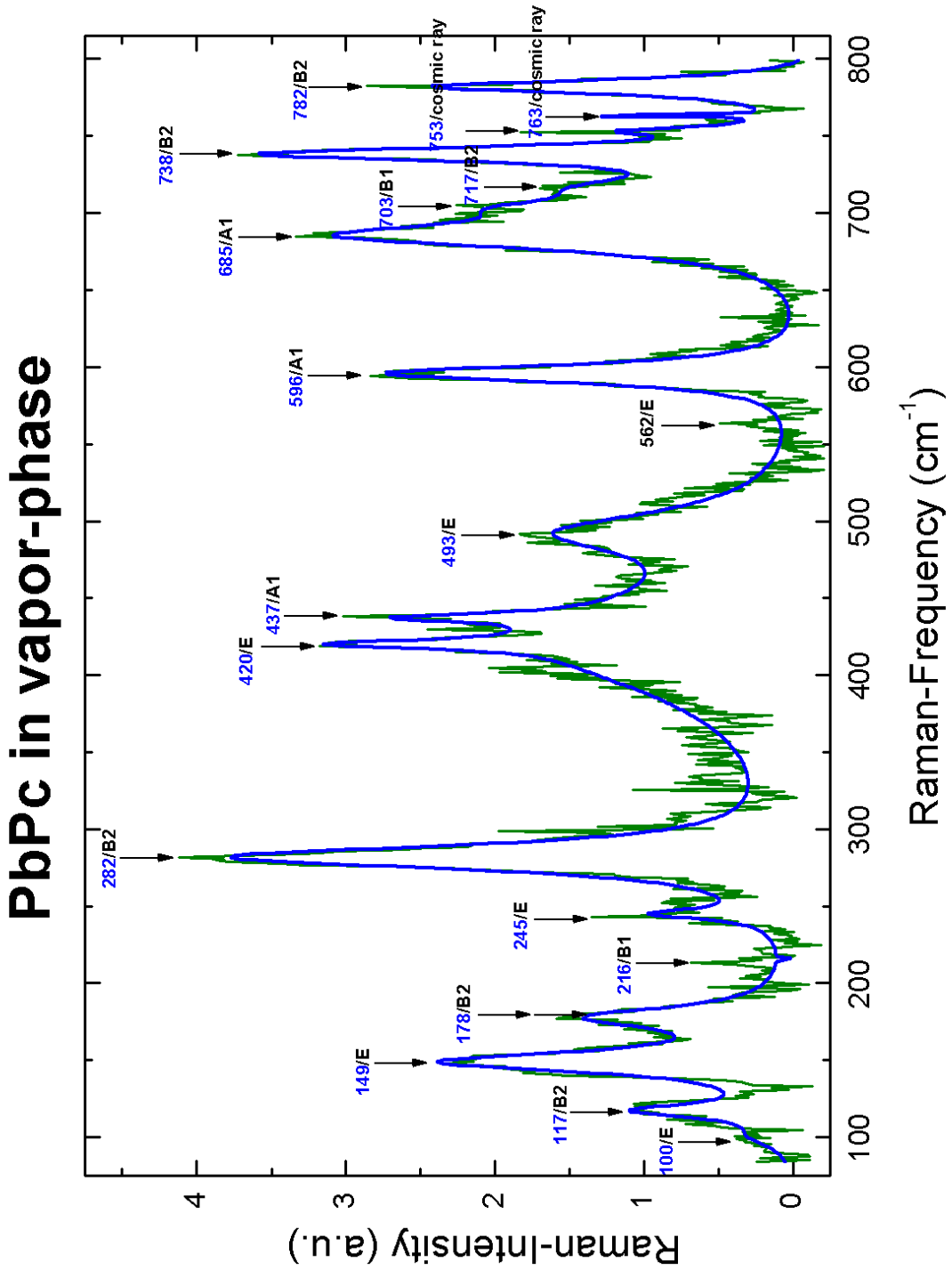

Γράφημα 11. Φάσμα φθαλοκυανίνης μολύβδου (PbPc) στην αέρια φάση (σημειώνονται: συχνότητες Raman (cm^{-1}) / τρόποι ταλάντωσης)

Πίνακας 2: Συχνότητες και εντάσεις των κορυφών Raman μορίων PbPc στην αέρια, φάση σύμφωνα με τα αποτελέσματα της παρούσας εργασίας (στήλη $2^{η}$), και σύγκριση με θεωρητικά προβλεπόμενες συχνότητες και εντάσεις των αντίστοιχων τρόπων ταλάντωσης (στήλες 3-5) και με τις συχνότητες φασμάτων Raman PbPc σε σκόνη (στήλες 6-7).

Raman peak Nr.	RAMAN SHIFT of PbPc in vapor by fitting	DFT calculations by I.M. Kupchak (scaled DFT by L.Riele)	DFT calculations by Y.Zhang & X.Zhang	Vibrational Mode Assignment by Y.Zhang & X.Zhang	Exp.data PbPc powder by L. Riele	Exp. Data PbPc powder by V. Stamelou
	RAMAN SHIFT (cm^{-1})/ intensity (a.u.)	RAMAN SHIFT (cm^{-1}) (vibrational mode assignment)/ intensity (a.u.)	RAMAN SHIFT (cm^{-1}) (vibrational mode assignment)/ intensity (a.u.)		RAMAN SHIFT (cm^{-1})	RAMAN SHIFT (cm^{-1})
1	100 / 0.2	107 (103) (E) / 5.3	102,97 (E) /5.29	-	-	-
2	117 / 1.0	125 (121) (B_2) / 19.5	121,33(B_2) /19.65	PbN, alternately stretching	-	-
3	149 / 2.3	148 (143) (E) / 0.6	142,67(E) /0.64	-	146	150,151
4	178/ 1.3	165 (159) (B_2) / 10.2	158,63 (B_2) / 10.2	-	169	-
5	216 / 0.3	211 (203) (B_1) / 12.7	203,24(B_1)/ 12.67	-	210	207
6	245 / 0.8	252 (242) (E) / 3.8	241,89 (E)/ 3.802	-	245	-
7	282 /3.8	298 (287) (B_2) /3.8	286,69 (B_2)/ 3,80	-	272	-

8	420 / 1.7	442 (425) (E) / 0.1	424,94(E)/ 0.06	-	-	-
9	437 / 1.3	455 (437) (A_1) / 0.5	437,34(A_1)/ 0.47	CHa OPB, CC OPB	-	-
10	493 / 1.4	512 (492) (E) / 0.2	492,14 (E)/ 0.185	CH CC CN OPB	493	-
11	562 / 0.3	575 (553) (E)/ 0.8	552,61 (E) / 0.75	-	-	566
12	596 / 1.2	585 (563) (A_1) /77.8	562,80 (A_1) / 76.77	Bre., PbN_1 sy. str., CC sy. B	-	-
13	685 / 3.0	671 (645) (A_1) / 351.5	645,00 (A_1) / 351.01	N_2C CC sy. B_2, CN_1 PbN_1 CC str., CH IPB	674	680
14	703 / 1.2	705 (678) (B_1) /38.01	677,98 (B_1) / 37.79	-	708	-
15	717/ 0.9	718 (691) (B2) /15.3	690,57 (B2) / 15.32	-	729	721,722
16	738 / 3.5	760 (731) (B_2) /700.01	730,66 (B_2) / 695.72	N-C sy.B, PbN_1 CC CN str.	742	-
17	*753 / 0.8	768 (738) (A_1) /2.1	737,97 (A_1) /2,10	PbN sy. str., CH OPB, CC OPB	-	-
18	*763 /1.7	794 (764) (E) /0.2	763,64(E) /0.195	Ben. Exp., CH IPB,CC IPB, CC CN PbN str.	769	-
19	782 / 2.6	810-779 (A_1) /91.6	778,63 (A_1) /92.04		-	-

Στον Πίνακα 2, χρησιμοποιούνται οι συντομεύσεις:

N= άζωτο, H= υδρογόνο, C= άνθρακας,
IPB= ταλάντωση κάμψης στο επίπεδο του μορίου,
OPB= ταλάντωση κάμψης κάθετα στο επίπεδο του μορίου,
sy. str.= συμμετρική εκτατική ταλάντωση,
Bre.= απόλυτα συμμετρική ταλάντωση («αναπνοή»),
Ben. Exp.= επεκτατική ταλάντωση αρωματικού δακτυλίου.

Το μόριο της φθαλοκυανίνης μολύβδου με τους δεσμούς μεταξύ των ατόμων του απεικονίζεται παραστατικά στην Εικόνα 13, ώστε να καταστεί κατανοητό, σε ποιο δεσμό λαμβάνει χώρα η κάθε ταλάντωση, αν είναι εντοπισμένη ή αν αναφέρεται σε όλο το μόριο, και τι ταλάντωση είναι.

Συμβολίζονται με: N1 το άζωτο, το προσδεδεμένο στο κεντρικό κατιόν του μολύβδου Pb, N2 το άζωτο, το συνδεδεμένο με άνθρακα C, H το υδρογόνο. Καθώς απομακρυνόμαστε από το κεντρικό κατιόν Pb, τα άτομα των ισοϊνδολικών μονάδων έχουν ως δείκτες μικρά γράμματα της αλφαβήτου α,β,γ,δ.

Το μόριο δεν είναι επίπεδο, εφόσον το κατιόν του μολύβδου Pb^{+2} είναι μεγαλύτερο της κοιλότητας της φθαλοκυανίνης και προεξέχει από το μόριο, όπως φαίνεται στην παρακάτω Εικόνα 14.

Ο συμβολισμός των τρόπων ταλάντωσης προέρχεται από τη θεωρία ομάδων. Α είναι (απόλυτα) συμμετρικός τρόπος ταλάντωσης του μορίου (breathing mode), Β αντισυμμετρικός τρόπος, ενώ Ε είναι διπλά εκφυλισμένη κατάσταση με συμμετρική ή αντι-συμμετρική δόνηση.

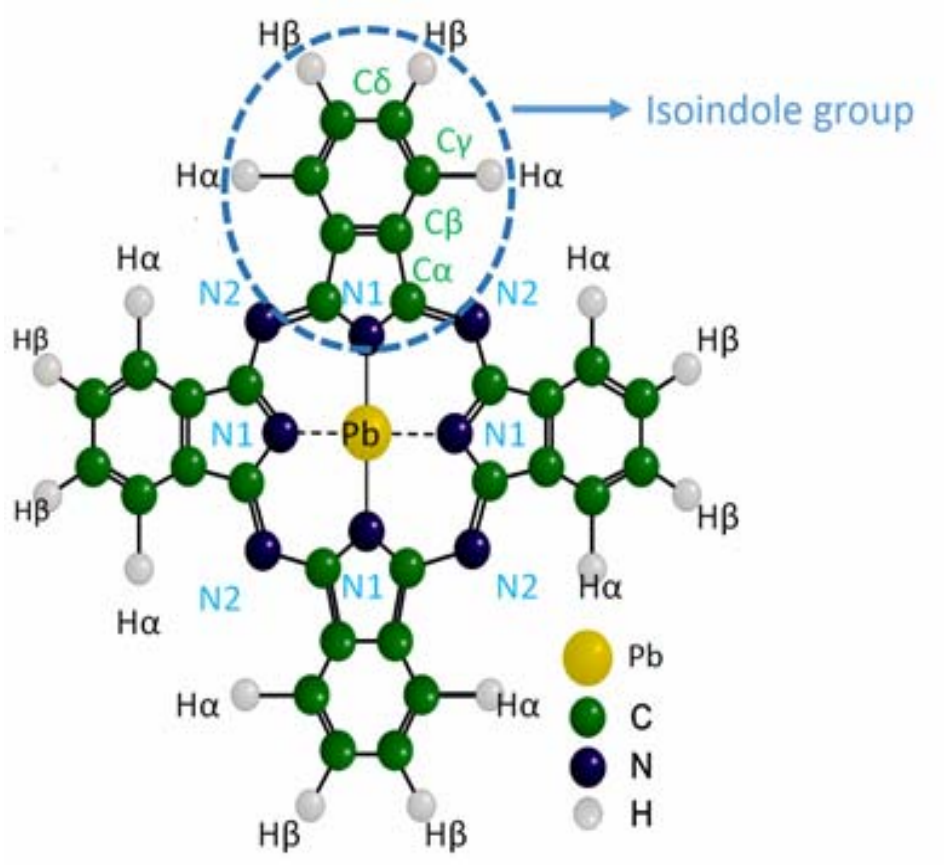

Εικόνα 13: Το μόριο της φθαλοκυανίνης μολύβδου

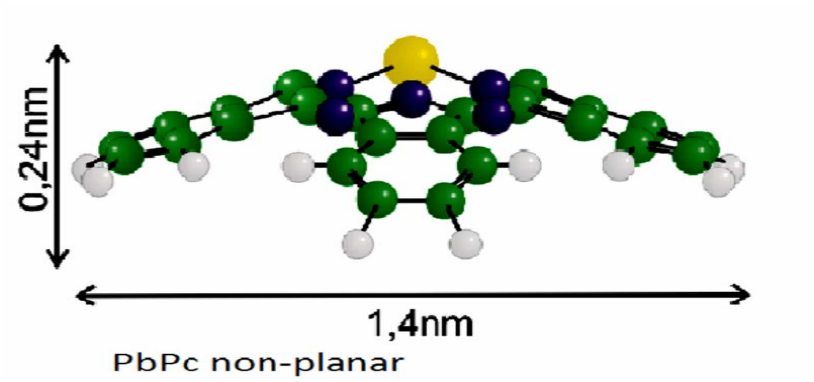

Εικόνα 14: μη επίπεδο μόριο PbPc

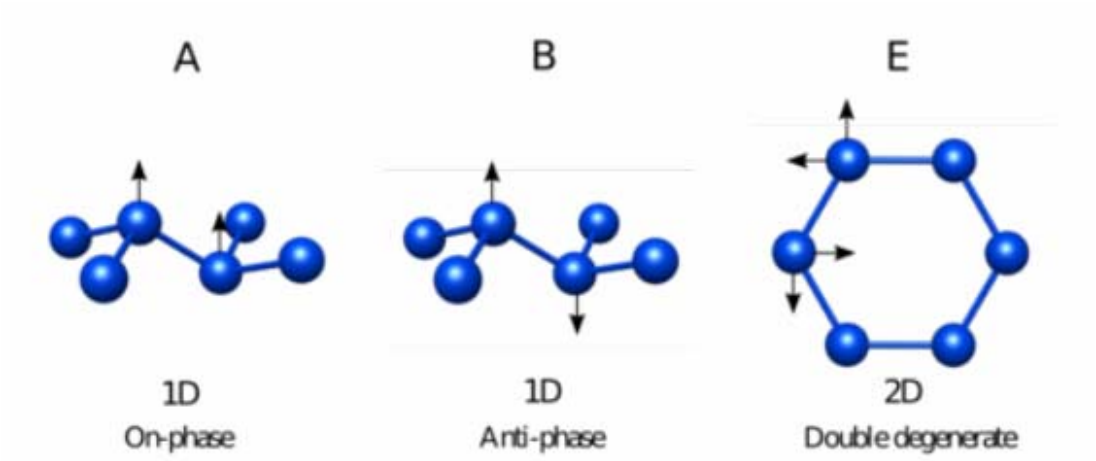

Εικόνα 15: A,B,E τρόποι ταλάντωσης

G. APPENDIX

Fitting Results of Raman-spectrum of PbPc in vapor-phase

Peak 1			
Position:	100,29 cm^{-1}	± 8,06 cm^{-1}	
Amplitude:	0,21 a.u	± 0,18 a.u	
Width:	16,12 cm^{-1}	± 2,77 cm^{-1}	
Peak 2			
Position:	117,15 cm^{-1}	± 1,26 cm^{-1}	
Amplitude:	0,97 a.u	± 0,22 a.u	
Width:	10,34 cm^{-1}	± 4,43 cm^{-1}	
Peak 3			
Position:	148,83 cm^{-1}	± 0,60 cm^{-1}	
Amplitude:	2,31 a.u	± 0,17 a.u	
Width:	15,85 cm^{-1}	± 2,06 cm^{-1}	
Peak 4			
Position:	177,72 cm^{-1}	± 1,10 cm^{-1}	
Amplitude:	1,28 a.u	± 0,18 a.u	
Width:	16,45 cm^{-1}	± 3,88 cm^{-1}	
Peak 5			
Position:	215,65 cm^{-1}	± 1,20 cm^{-1}	
Amplitude:	0,30 a.u		estimated value
Width:	0,35 cm^{-1}	± 3,72 cm^{-1}	
Peak 6			
Position:	244,90 cm^{-1}	± 1,23 cm^{-1}	
Amplitude:	0,76 a.u	± 0,23 a.u	
Width:	8,07 cm^{-1}	± 3,74 cm^{-1}	
Peak 7			
Position:	281,83 cm^{-1}	± 0,38 cm^{-1}	
Amplitude:	3,76 a.u	± 0,15 a.u	
Width:	18,79 cm^{-1}	± 1,23 cm^{-1}	
Peak 8			
Position:	420,47 cm^{-1}	± 3,26 cm^{-1}	
Amplitude:	1,72 a.u	± 0,16 a.u	
Width:	8,75 cm^{-1}		estimated value

Peak 9			
Position:	437,37 cm^{-1}	± 0,68 cm^{-1}	
Amplitude:	1,27 a.u	± 0,26 a.u	
Width:	6,83 cm^{-1}	± 2,53 cm^{-1}	
Peak 10			
Position:	492,73 cm^{-1}	± 1,51 cm^{-1}	
Amplitude:	1,36 a.u	± 0, 12 a.u	
Width:	31,94 cm^{-1}	± 5,50 cm^{-1}	
Peak 11			
Position:	562,00 cm^{-1}		estimated value
Amplitude:	0,30 a.u		estimated value
Width:	0,35 cm^{-1}		estimated value
Peak 12			
Position:	595,79 cm^{-1}	± 0,42 cm^{-1}	
Amplitude:	2,84 a.u	± 0,17 a.u	
Width:	13,62 cm^{-1}	± 1,34 cm^{-1}	
Peak 13			
Position:	685,10 cm^{-1}	± 0,87 cm^{-1}	
Amplitude:	2,99 a.u	± 0,24 a.u	
Width:	21,24 cm^{-1}	± 2,44 cm^{-1}	
Peak 14			
Position:	702,81 cm^{-1}	± 2,33 cm^{-1}	
Amplitude:	1,18 a.u	± 0,38 a.u	
Width:	17,57 cm^{-1}	± 8,78 cm^{-1}	
Peak 15			
Position:	716,53 cm^{-1}	± 2,85 cm^{-1}	
Amplitude:	0,91 a.u	± 0,35 a.u	
Width:	17,80 cm^{-1}	± 9,62 cm^{-1}	
Peak 16			
Position:	738,24 cm^{-1}	± 0,34 cm^{-1}	
Amplitude:	3,53 a.u	± 0,20 a.u	
Width:	11,28 cm^{-1}	± 1,31 cm^{-1}	
Peak 17			
Position:	753,26 cm^{-1}	± 0,92 cm^{-1}	
Amplitude:	0,84 a.u	± 0,27 a.u	
Width:	5,56 cm^{-1}	± 3,02 cm^{-1}	

Peak 18		
Position:	763,17cm^{-1}	± 0,17 cm^{-1}
Amplitude:	1,70 a.u	± 1,70 a.u
Width:	1,06 cm^{-1}	± 1,15 cm^{-1}
Peak 19		
Position:	7,82 cm^{-1}	± 0,39 cm^{-1}
Amplitude:	2,64 a.u	± 0,20 a.u
Width:	10,60 cm^{-1}	± 1,28 cm^{-1}

ΒΙΟΓΡΑΦΙΚΟ ΣΗΜΕΙΩΜΑ

Βιογραφικό σημείωμα	15-12-2014
Ονοματεπώνυμο	Κωνσταντίνα Ρούσση
Ημερομηνία Γέννησης	29/03/1986
Διεύθυνση	Μακεδονίας 90, Αθήνα 15669 (Παπάγου)
Τηλέφωνο	6986231665
E-mail	nadiaralou@hotmail.gr

Σπουδές

2003-2014	Φοιτήτρια ΕΜΠ, Σχολή Εφαρμοσμένων Μαθηματικών και Φυσικών Επιστημών
2013	Εργασία στο μάθημα Φυσική του Περιβάλλοντος: Όζον και υπεριώδης ακτινοβολία
2012-2013	Erasmus scholar στο πανεπιστήμιο Tor Vergata της Ρώμης, Διπλωματική εργασία στη «Φωτοβολταϊκή Τεχνολογία Οργανικών Ημιαγωγών»
2003	Απόφοιτη Πειραματικού Σχολείου Πανεπιστημίου Αθηνών (Λίαν καλώς, 17.7)

Επαγγελματική εμπειρία	Πρακτική άσκηση στα ΕΛΤΑ (2011, 6μηνη), διδασκαλία μαθηματικών και φυσικής

Ξένες Γλώσσες	1. Αγγλικά (Advanced: grade B), 2. Γαλλικά (Delf 1), 3. Ιταλικά